A PHASED ARRAY ANTENNA OF SWITCHED-BEAM ELEMENTS

PHAISAN NGAMJANYAPORN

A THESIS SUBMITTED IN PARTIAL FULFILLMENT OF
THE REQUIREMENT FOR THE DEGREE OF
DOCTOR OF ENGINEERING IN ELECTRICAL ENGINEERING
SCHOOL OF GRADUATE STUDIES
KING MONGKUT'S INSTITUTE OF TECHNOLOGY LADKRABANG
2005

ISBN 974-15-1444-1

หัวข้อวิทยานิพนธ์	สายอากาศแถวลำดับแบบปรับเฟสของอิลิเมนต์แบบสวิตช์ลำคลื่น
นักศึกษา	นายไพศาล งามจรรยาภรณ์
รหัสนักศึกษา	44060005
ปริญญา	วิศวกรรมศาสตรดุษฎีบัณฑิต
สาขาวิชา	วิศวกรรมไฟฟ้า
พ.ศ.	2548
อาจารย์ผู้ควบคุมวิทยานิพนธ์	ศ.ดร.โมไนย ไกรฤกษ์

บทคัดย่อ

วิทยานิพนธ์นี้นำเสนอสายอากาศแถวลำดับแบบปรับเฟสของอิลิเมนต์แบบสวิตช์ลำคลื่น โดยสายอากาศที่นำเสนอนี้จะเป็นสายอากาศแถวลำดับที่สามารถสวิตช์ลำคลื่นได้โดยอาศัยวงจรเลื่อนเฟสและสามารถเปลี่ยนทิศทางของนัลล์ได้ด้วยการใช้อิลิเมนต์เป็นสายอากาศแพตช์เดี่ยวที่สวิตช์ลำคลื่นได้ในสองทิศทางโดยใช้สวิตช์ความถี่วิทยุ สายอากาศแถวลำดับที่นำเสนอเป็นแถวลำดับวงกลม 4 อิลิเมนต์และมีรัศมีของแถวลำดับเท่ากับครึ่งความยาวคลื่น วงจรเลื่อนเฟสถูกออกแบบเพื่อใช้ในการสวิตช์ลำคลื่นของแถวลำดับไปในทิศทาง 45° 135° 225° และ 315° คุณลักษณะของสายอากาศถูกวิเคราะห์ด้วยโปรแกรม IE3D ซึ่งใช้วิธีการโมเมนต์วิเคราะห์ปัญหาคลื่นแม่เหล็กไฟฟ้า แล้วจึงสร้างและทดสอบสายอากาศ สายอากาศที่นำเสนอนี้มีค่าอัตราส่วนคลื่นนิ่งน้อยกว่า 2:1 และให้แบบรูปการแพร่กระจายคลื่นหกสิบสี่แบบที่ทิศทางของนัลล์เปลี่ยนแปลงได้ สมรรถนะของสายอากาศสวิตช์ลำคลื่นในการรับสัญญาณถูกประเมินด้วยค่าสัมประสิทธิ์สหสัมพันธ์และค่าอัตราขยายไดเวอร์ซิตี ซึ่งผลเชิงทฤษฎีให้ค่าสัมประสิทธิ์สหสัมพันธ์ต่ำสุดเท่ากับ 0.37 และค่าอัตราขยายไดเวอร์ซิตีเท่ากับ 8 เดซิเบล และการยกระดับอัตราส่วนสัญญาณต่อสัญญาณแทรกสอดทำได้ด้วยอิลิเมนต์แบบสวิตช์ลำคลื่นที่จะเปลี่ยนทิศทางของนัลล์เพื่อช่วยกำจัดสัญญาณแทรกสอด ซึ่งสามารถยกระดับอัตราส่วนสัญญาณต่อสัญญาณแทรกสอดได้มากกว่า 10 เดซิเบล นอกจากนี้ได้เสนอการประยุกต์ใช้งานของสายอากาศในระบบการสื่อสารแบบหลายอินพุตหลายเอาต์พุต และการประยุกต์ใช้เป็นสายอากาศสำหรับระบบสายอากาศแถวลำดับแบบปรับตัวที่ใช้อัลกอริทึมการมอดุลัสคงที่ โดยจากผลวิเคราะห์เบื้องต้นพบว่าการใช้สายอากาศสวิตช์ลำคลื่นในระบบการสื่อสารแบบหลายอินพุตหลายเอาต์พุตนั้นสามารถเพิ่มความจุของช่องสัญญาณได้ด้วยสายอากาศที่มีขนาดกะทัดรัดกว่า สำหรับการประยุกต์ใช้ในระบบสายอากาศแถวลำดับแบบปรับตัวที่ใช้อัลกอริทึมการมอดุลัสคงที่นั้น สายอากาศสวิตช์ลำคลื่นสามารถช่วยให้คุณสมบัติการลู่เข้าของอัลกอริทึมการมอดุลัสคงที่ดีขึ้นโดยใช้สัญญาณรับสูงสุดที่ได้จากสายอากาศสวิตช์ลำคลื่นเป็นค่าเริ่มต้นให้กับระบบ

Thesis	A Phased Array Antenna of Switched-Beam Elements
Student	Mr. Phaisan Ngamjanyaporn
Student ID.	44060005
Degree	Doctor of Engineering
Programme	Electrical Engineering
Year	2005
Thesis Advisor	Prof. Dr. Monai Krairiksh

ABSTRACT

This thesis presents a new switched-beam antenna called a phased array antenna of switched-beam elements. It is a phased array antenna in which the main beam can be steered using phase shifters and the null pattern can be varied by switching beam patterns of individual array elements. The switched-beam elements are single patch antennas which employ RF switches to switch the beam in two directions. Four switched-beam elements are arranged in a circular array with the radius of 0.5λ. The phase shifters are designed to steer the beam of the array antenna in directions of 45°, 135°, 225° and 315°. The characteristics of the individual antenna elements and the array are analyzed utilizing the IE3D Simulator based on Moment Method. Next, the array antenna is fabricated and tested. The phased array antenna of switched-beam elements shows the VSWR of less than 2:1 over the desired frequency band. Sixty-four radiation patterns with changeable null directions are available. For the switched-beam antenna, the correlation coefficient and diversity gain are evaluated to determine an improvement in the received signal. The theoretical investigation shows the lowest correlation coefficient of 0.37 and diversity gain of 8 dB. The signal-to-interference ratio (SIR) improvement is accomplished by using the switched-beam elements which change the null direction to eliminate the interfering signal. Using this method the SIR can be improved more than 10 dB. In addition, the prospective applications of the switched-beam antenna such as antenna for multiple-input multiple-output (MIMO) communication system and antenna for Constant Modulus Algorithm (CMA) adaptive array antenna are described. The preliminary results show that using the switched-beam antenna in MIMO system the channel capacity can be increased. For the CMA adaptive array antenna, the switched-beam antenna provides the improved convergence property of CMA by using the knowledge of the maximum received signal of the switched-beam antenna as an initial value in an iterative procedure.

ACKNOWLEDGEMENTS

This thesis could not be completed without the assistance of many persons to whom I would like to express my appreciation.

First, I would like to thank my advisor, Professor Monai Krairiksh, who has given me many helpful suggestions and useful advice during the undertaken research. My appreciation is also shown to Associated Professor Sompol Kosulvit and Assistant Professor Chuwong Phongcharoenpanich for their helpful discussions.

I would like to acknowledge Associated Professor Prayoot Akkaraekthalin of Faculty of Engineering, King Mongkut's Institute of Technology North Bangkok (KMITNB) for providing access to the IE3D simulator to carry out simulation required in this research, and the Philips Electronics (Thailand) Co., Ltd. for contributing the BAP51-02 PIN diodes which were used in the development of the switched beam array antenna.

I would like to thank Mr. Suwan Janin, who offered the antenna fabrication and measurement facilities, and my colleagues in Wireless Communication Laboratory for their friendship and kindness.

I wish to thank Professor Marek E. Bialkowski of the School of Information Technology and Electrical Engineering, the University of Queensland, Australia for giving me an invaluable opportunity to be a visiting scholar in his laboratory.

I am grateful to the Thailand Research Fund (TRF) which provided financial assistance to the undertaken project through the Royal Golden Jubilee Ph.D. Program (Grant No. PHD/0071/2545). Also, the partial support offered by the National Electronics and Computer Technology Center (NECTEC), the National Science and Technology Development Agency (NSTDA), Thailand, under Contract No. 17/2545 is acknowledged.

Special thanks go to Ms. Wanlika Buasomboon for her patience, understanding and cheerfulness during a long period of my Ph.D. course.

Finally, I am very grateful to my parents, who have perpetually supported and motivated me throughout my life.

Phaisan Ngamjanyaporn

TABLE OF CONTENTS

TABLE OF CONTENTS (continued)

TABLE OF CONTENTS (continued)

LIST OF TABLES

LIST OF FIGURES

LIST OF FIGURES (continued)

LIST OF FIGURES (continued)

LIST OF FIGURES (continued)

LIST OF FIGURES (continued)

CHAPTER 1
INTRODUCTION

1.1 Historical notes on switched-beam antennas

In modern wireless communications, the performance of the system can be seriously degraded by multipath fading and co-channel interference. The multipath fading is caused by the different path lengths with different arrival angles that arise from the transmitted signal impinging on objects in the environment, while the co-channel interference is due undesired co-channel signals from other base stations or user terminals. To overcome or reduce these problems, the switched-beam antenna can be an effective solution. There are many switch-beam antennas proposed for wireless communication systems. A four-beam switched array antenna which uses the 90° hybrid couplers and switching input terminals of hybrid couplers to carry out the beam switching was proposed [1]. Several switched-beam antennas employing switched parasitic elements were proposed in [2] – [7]. The circular switched monopole array was proposed by Sibille et al. [2]. In the presented solutions, beam switching is achieved through switching the active monopole, acting as a radiator, whereas other monopoles, passive monopoles, are connected to reactive loads serving as scatterers. In particular, Yagi concept was utilized in the switched parasitic elements array antenna. The planar microstrip Yagi array antenna was introduced by Huang [3], and later an electronically steerable Yagi-Uda microstrip patch antenna array was developed and described by Gray et al. [4]. Four Yagi-Uda antennas forming the array antenna were located along a radial direction from a single reflector patch. By switching the four elements, the main beam of the array was steerable. In [5], a five-element Yagi-Uda antenna was introduced. The beam was switched in the forward and backward directions by driving the center patch and switching shorted and opened parasitic patches to act as reflectors or directors. The monopole array structure was also proposed for antenna diversity by employing the Yagi concept [6]. The switched parasitic antennas were also presented in [7]. As an alternative solution, an electronically steerable passive array radiator (ESPAR) antenna was designed [8]. A monopole, active radiator, surrounded by monopoles, parasitic elements, loaded with variable reactance at the bottom was proposed to switch beam by varying the reactance of parasitic elements.

An antenna offering a discrete number of different beams can be accomplished by employing phased array techniques. The phase shifter is used to shift phase of excitation for each element to form beam in a desired direction. Minimum bit phase shifter is preferred for realizing less complicated phased array antennas. A dividing/phasing network using 1-bit phase shifters for a compact switched-beam array antenna was described in [9], and a compact phased array antenna using 1-bit phase shifters to achieve four-beam switching was presented in [10].

It should be noted that the preceding works were intended to switch the main beam. Each of the above-quoted switched-beam antennas was able to switch main beam successfully to track a mobile user. However, the desired user tracking is insufficient to maintain good performance of a wireless communication system when the beam points in the direction close to interference direction. In order to improve the performance of such a system, a switched-beam antenna with the changeable null pattern should be employed to eliminate the interference.

1.2 Purpose and scope of the thesis

In this thesis, a new switched-beam antenna is proposed to improve the performance of a wireless communication system, which operates in the presence of co-channel interference. The proposed antenna offers not only the capability of tracking the desired signal, but also offers the changeable null pattern to suppress the interference.

The proposed antenna, called a phased array antenna of switched-beam elements, is a phased array antenna which steers the beam with the use of phase shifters. In addition, by employing switched-beam elements as the array elements it is able to change the null pattern. First, two types of switched-beam antennas, a switched-beam single patch antenna and a flat four-beam compact phased array antenna, are investigated to form foundations for designing a phased array antenna of switched-beam elements. These array antennas are described in Chapter 2. In the next step, the phased array antenna of switched-beam elements is designed and developed by combining the design principles of the flat four-beam compact phased array antenna and switched-beam single patch antennas, which are used as the array elements. The VSWR and radiation patterns of the phased array antenna of switched-beam elements are presented in Chapter 3. Chapter 4 addresses the performance of the phased array antenna of switched-beam elements when it is used in a wireless communication system. The received signal improvement is

evaluated in terms of correlation coefficient and diversity gain. The interference suppression is investigated experimentally in a multipath environment. New applications of the phased array antenna of switched-beam elements are described in Chapter 5. This antenna is investigated in the context of a multiple-input multiple-output (MIMO) communication system and when applied in the Constant Modulus Algorithm (CMA) adaptive array antenna system. The preliminary results concerning these investigations are reported. Finally, Chapter 6 summarizes the results presented in earlier chapters. This chapter also describes future directions which stem from the accomplished work.

CHAPTER 2
FOUNDATION OF A PHASED ARRAY ANTENNA OF SWITCHED-BEAM ELEMENTS

2.1 Introduction

The design and development of a phased array antenna of switched-beam elements is initiated with considering first a switched-beam single patch antenna [11] and a flat four-beam compact phased array antenna [10]. The switched-beam single patch antenna is a patch antenna whose beam can be switched in two directions by using PIN diodes. The flat four-beam compact phased array antenna is a switched-beam array antenna which uses four omnidirectional elements and 1-bit phase shifters to generate four beams. In order to obtain a phased array antenna of switched-beam elements the omnidirectional element is replaced by the switched-beam single patch antenna. The purpose of employing switched-beam elements is to obtain interference suppression capability. In this chapter, the design and development of the switched-beam single patch antenna and the flat four-beam compact phased array antenna, which are the foundation of a phased array antenna of switched-beam elements, is presented.

2.2 A Switched-Beam Single Patch Antenna

A single patch antenna is introduced that is capable of switching the beam in azimuth direction. This antenna element is excited at higher mode to obtain the radiation pattern that has null normal to the patch and maximum in azimuth direction. The radiation pattern of the antenna will be switched in azimuth with the use of PIN diodes. The antenna operation, PIN diode models and the antenna results are described in this section.

2.2.1. Antenna operation

Since a switched-beam single patch antenna is purposely designed to switch the radiation pattern in azimuth direction, in this context the radiation pattern that has null normal to the patch and maximum in azimuth direction is desirable. Therefore, the antenna is excited at the higher modes of TM^z_{200} and TM^z_{020}, as shown in Fig. 2.1(a) and 2.1(b), to provide the mentioned radiation pattern switched to x and y directions,

respectively. The radiated fields of the antenna operating at these two modes are analyzed.

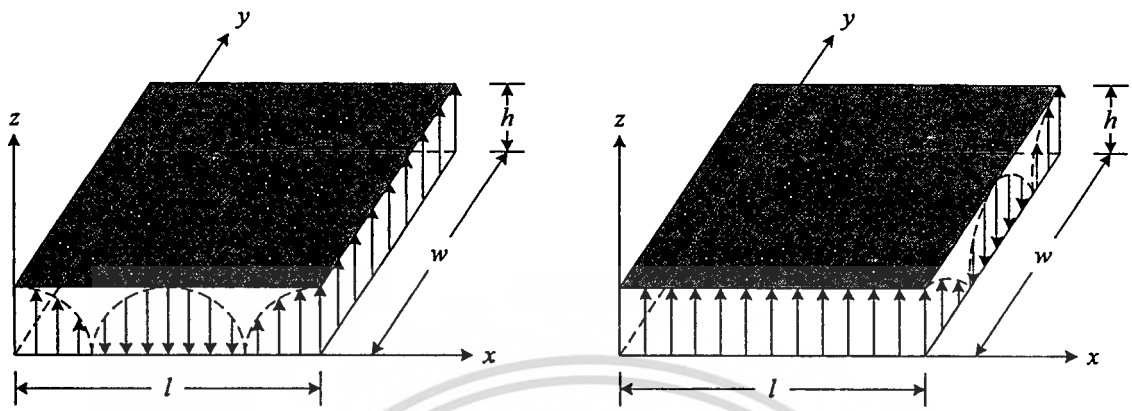

Fig. 2.1 Field configurations for the microstrip patch: (a) TM^z_{200}, (b) TM^z_{020}.

By using the cavity model [12], the microstrip patch antenna is modeled as a dielectric loaded cavity bounded by electric conductors at top and bottom walls of the cavity and by magnetic walls along the perimeter of the cavity. The field configuration within the cavity can be found using the vector potential approach [13]. Considering the TM^z mode shown in Fig. 2.1, the vector potential A_z must satisfy the wave equation of

$$\nabla^2 A_z + k^2 A_z = 0. \tag{2.1}$$

The solution is written as

$$\begin{aligned} A_z = &[A_1 \cos(k_x x) + B_1 \sin(k_x x)] \cdot [A_2 \cos(k_y y) + B_2 \sin(k_y y)] \\ &\cdot [A_3 \cos(k_z z) + B_3 \sin(k_z z)] \end{aligned} \tag{2.2}$$

where k_x, k_y, k_z are the wave numbers along the x, y, z directions, respectively. These wave numbers will be determined subject to the boundary conditions. The electric and magnetic fields within the cavity are related to the vector potential A_z by

$$E_x = -j\frac{1}{\omega\mu\varepsilon}\left(\frac{\partial^2 A_z}{\partial x \partial z}\right) \tag{2.3a}$$

$$E_y = -j\frac{1}{\omega\mu\varepsilon}\left(\frac{\partial^2 A_z}{\partial y \partial z}\right) \tag{2.3b}$$

$$E_z = -j\frac{1}{\omega\mu\varepsilon}\left(\omega^2\mu\varepsilon + \frac{\partial^2}{\partial z^2}\right)A_z \tag{2.3c}$$

$$H_x = \frac{1}{\mu}\left(\frac{\partial A_z}{\partial y}\right) \tag{2.3d}$$

$$H_y = -\frac{1}{\mu}\left(\frac{\partial A_z}{\partial x}\right) \tag{2.3e}$$

$$H_z = 0 \tag{2.3f}$$

subject to the boundary conditions of

$$E_x(0 \le x' \le l, 0 \le y' \le w, z' = 0) = E_x(0 \le x' \le l, 0 \le y' \le w, z' = h) = 0 \tag{2.4a}$$

$$H_x(0 \le x' \le l, y' = 0, 0 \le z' \le h) = H_x(0 \le x' \le l, y' = w, 0 \le z' \le h) = 0 \tag{2.4b}$$

$$H_y(x' = 0, 0 \le y' \le w, 0 \le z' \le h) = H_y(x' = l, 0 \le y' \le w, 0 \le z' \le h) = 0 \tag{2.4c}$$

The primed coordinates (x', y', z') are used to denote the fields within the cavity.

By applying the boundary conditions $E_x(0 \le x' \le l, 0 \le y' \le w, z' = 0) = 0$ and $E_x(0 \le x' \le l, 0 \le y' \le w, z' = h) = 0$, it can be found that $B_3 = 0$ and

$$k_z = \left(\frac{p\pi}{h}\right), \quad p = 0, 1, 2, \ldots \tag{2.5}$$

Then, applying the boundary conditions $H_x(0 \le x' \le l, y' = 0, 0 \le z' \le h) = 0$ and $H_x(0 \le x' \le l, y' = w, 0 \le z' \le h) = 0$, it can be found that $B_2 = 0$ and

$$k_y = \left(\frac{n\pi}{w}\right), \quad n = 0, 1, 2, \ldots \tag{2.6}$$

Finally, applying the boundary conditions $H_y(x'=0,0\le y'\le w,0\le z'\le h)=0$ and $H_y(x'=l,0\le y'\le w,0\le z'\le h)=0$, it can be found that $B_1=0$ and

$$k_x=\left(\frac{m\pi}{l}\right),\quad m=0,1,2,... \tag{2.7}$$

Therefore, the vector potential A_z within the cavity is

$$\begin{aligned} A_z &= A_1\cos(k_x x')A_2\cos(k_y y')A_3\cos(k_z z') \\ &= A_{mnp}\cos(k_x x')\cos(k_y y')\cos(k_z z') \end{aligned} \tag{2.8}$$

where A_{mnp} represents the amplitude coefficients of each *mnp* mode. The wave numbers k_x, k_y and k_z are equal to

$$\left.\begin{aligned} k_x &= \left(\frac{m\pi}{l}\right), \quad m=0,1,2,... \\ k_y &= \left(\frac{n\pi}{w}\right), \quad n=0,1,2,... \\ k_z &= \left(\frac{p\pi}{h}\right), \quad p=0,1,2,... \end{aligned}\right\} \; m=n=p\neq 0 \tag{2.9}$$

where m, n, p represent the number of half-cycle field variations along the x, y, z directions. Since the wave numbers k_x, k_y and k_z are subject to the constraint equation

$$k_x^2+k_y^2+k_z^2=\left(\frac{m\pi}{l}\right)^2+\left(\frac{n\pi}{w}\right)^2+\left(\frac{p\pi}{h}\right)^2=k_r^2=\omega_r^2\mu\varepsilon \tag{2.10}$$

the resonant frequency for the cavity is given by

$$(f_r)_{mnp}=\frac{1}{2\pi\sqrt{\mu\varepsilon}}\sqrt{\left(\frac{m\pi}{l}\right)^2+\left(\frac{n\pi}{w}\right)^2+\left(\frac{p\pi}{h}\right)^2} \tag{2.11}$$

Substituting (2.8) into (2.3a) – (2.3f), the electric and magnetic fields within the cavity are written as

$$E_x = -j\frac{k_x k_z}{\omega\mu\varepsilon} A_{mnp} \sin(k_x x')\cos(k_y y')\cos(k_z z') \tag{2.12a}$$

$$E_y = -j\frac{k_y k_z}{\omega\mu\varepsilon} A_{mnp} \cos(k_x x')\sin(k_y y')\cos(k_z z') \tag{2.12b}$$

$$E_z = -j\frac{(k^2 - k_z^2)}{\omega\mu\varepsilon} A_{mnp} \cos(k_x x')\cos(k_y y')\cos(k_z z') \tag{2.12c}$$

$$H_x = -\frac{k_y}{\mu} A_{mnp} \cos(k_x x')\sin(k_y y')\cos(k_z z') \tag{2.12d}$$

$$H_y = \frac{k_x}{\mu} A_{mnp} \sin(k_x x')\cos(k_y y')\cos(k_z z') \tag{2.12e}$$

$$H_z = 0 \tag{2.12f}$$

After obtaining the electric and magnetic fields within the cavity, the equivalent electric and magnetic current densities, $\mathbf{J}_s$ and $\mathbf{M}_s$, are formed as the source of radiation, and the radiated **E** and **H** fields are determined.

The equivalent current density is obtained using the Field Equivalent Principle (Huygen's Principle). Since the microstrip patch is modeled as a dielectric-loaded cavity with perfectly conducting electric walls (top and bottom) and four perfectly conducting magnetic walls (sidewalls), the four sidewalls represent four narrow apertures by which the fields radiated. The microstrip patch is represented by an equivalent electric current density $\mathbf{J}_t$ at the top surface of the patch to account for the presence of the patch. There is also a current density $\mathbf{J}_b$ at the bottom of the patch, which is not needed for this model. The four side apertures are represented by the equivalent electric current density $\mathbf{J}_s$ and equivalent magnetic current density $\mathbf{M}_s$, as shown in Fig. 2.2(a), each represented by

$$\mathbf{J}_s = \hat{\mathbf{n}} \times \mathbf{H}_a \tag{2.13}$$

$$\mathbf{M}_s = -\hat{\mathbf{n}} \times \mathbf{E}_a \tag{2.14}$$

where $\mathbf{E}_a$ and $\mathbf{H}_a$ are the electric and magnetic fields at the apertures. $\hat{\mathbf{n}}$ is normal vector. For microstrip patch with very small height-to-width ratio, since the current density $\mathbf{J}_t$ at

the top of the patch is much smaller than the current density $\mathbf{J}_b$ at the bottom of the patch, it will be assumed it is negligible and it will be set to zero. Also, the tangential magnetic fields along the edges of the microstrip patch are very small, ideally zero. Therefore, the corresponding equivalent electric current density $\mathbf{J}_s$ will be very small, and it will be set to zero. Thus, there is only the equivalent magnetic current density $\mathbf{M}_s$ along the side periphery of the cavity radiating in the presence of the ground plane, as shown in Fig. 2.2(b). The presence of ground plane can be taken into account by image theory which will double the equivalent magnetic current density. Therefore, the equivalent magnetic current density will be finally given as

$$\mathbf{M}_s = -2\hat{\mathbf{n}} \times \mathbf{E}_a \tag{2.15}$$

around the side periphery of the patch radiating into free space, as shown in Fig. 2.2(c).

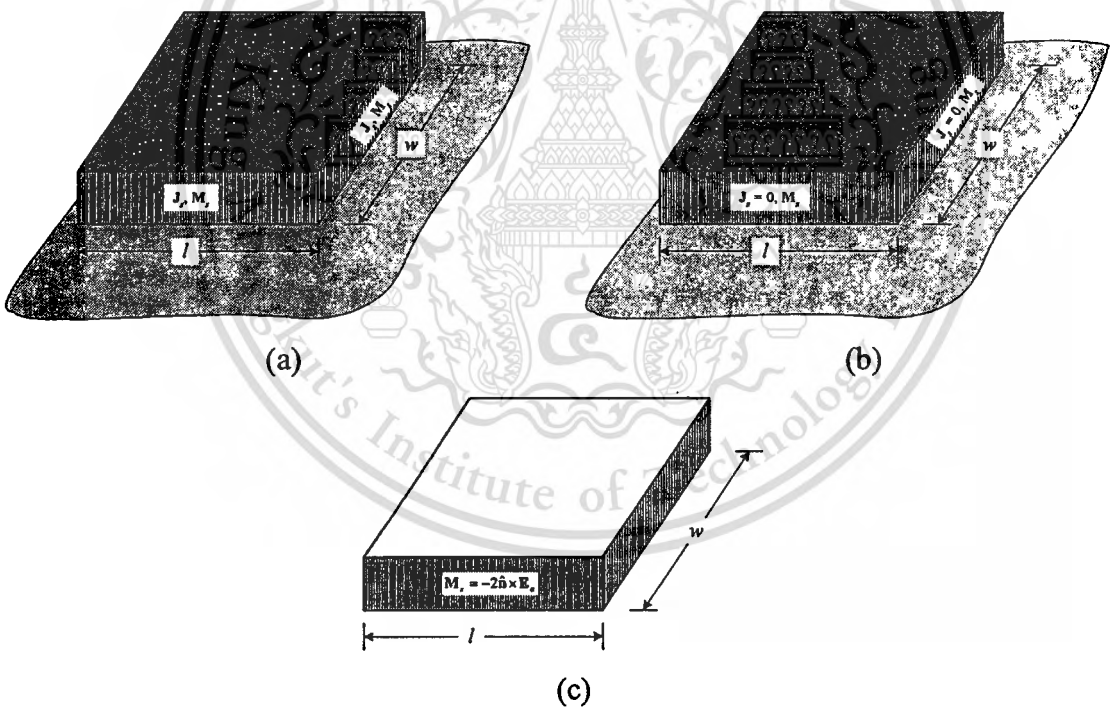

Fig. 2.2 Equivalent current densities on four sides of microstrip patch: (a) $\mathbf{J}_s$, $\mathbf{M}_s$ with ground plane, (b) $\mathbf{J}_s = 0$, $\mathbf{M}_s$ with ground plane, (c) $\mathbf{M}_s$ without ground plane.

In order to find the fields radiated from an aperture, the fields are determined using the geometries shown in Fig. 2.3, and the radiation equations of the **E** and **H** fields are written as

$$E_r = 0 \tag{2.16a}$$

$$E_\theta = -j\frac{ke^{-jkr}}{4\pi r}(L_\phi + \eta N_\theta) \tag{2.16b}$$

$$E_\phi = j\frac{ke^{-jkr}}{4\pi r}(L_\theta - \eta N_\phi) \tag{2.16c}$$

$$H_r = 0 \tag{2.16d}$$

$$H_\theta = j\frac{ke^{-jkr}}{4\pi r}(N_\phi - \frac{L_\theta}{\eta}) \tag{2.16e}$$

$$H_\phi = -j\frac{ke^{-jkr}}{4\pi r}(N_\theta + \frac{L_\phi}{\eta}) \tag{2.16f}$$

where N_θ, N_ϕ, L_θ and L_ϕ are obtained from

$$N_\theta = \iint_S [J_x \cos\theta\cos\phi + J_y \cos\theta\sin\phi - J_z \sin\theta]e^{jkr'\cos\psi}ds' \tag{2.17a}$$

$$N_\phi = \iint_S [-J_x \sin\phi + J_y \cos\phi]e^{jkr'\cos\psi}ds' \tag{2.17b}$$

$$L_\theta = \iint_S [M_x \cos\theta\cos\phi + M_y \cos\theta\sin\phi - M_z \sin\theta]e^{jkr'\cos\psi}ds' \tag{2.17c}$$

$$L_\phi = \iint_S [-M_x \sin\phi + M_y \cos\phi]e^{jkr'\cos\psi}ds' \tag{2.17d}$$

The geometries of aperture lied on the *yz*-plane, *xz*-plane and *xy*-plane are shown in Fig. 2.3(a), 2.3(b) and 2.3(c), respectively.

For the TM^z_{200} mode, Fig. 2.1(a), the electric and magnetic field components will be reduced to

$$E_z = -j\frac{\left(\frac{2\pi}{l}\right)^2}{\omega\mu\varepsilon}A_{200}\cos\left(\frac{2\pi}{l}x'\right) = E_0\cos\left(\frac{2\pi}{l}x'\right) \tag{2.18}$$

$$H_y = \frac{2\pi}{\mu l}A_{200}\sin\left(\frac{2\pi}{l}x'\right) = H_0\sin\left(\frac{2\pi}{l}x'\right) \tag{2.19}$$

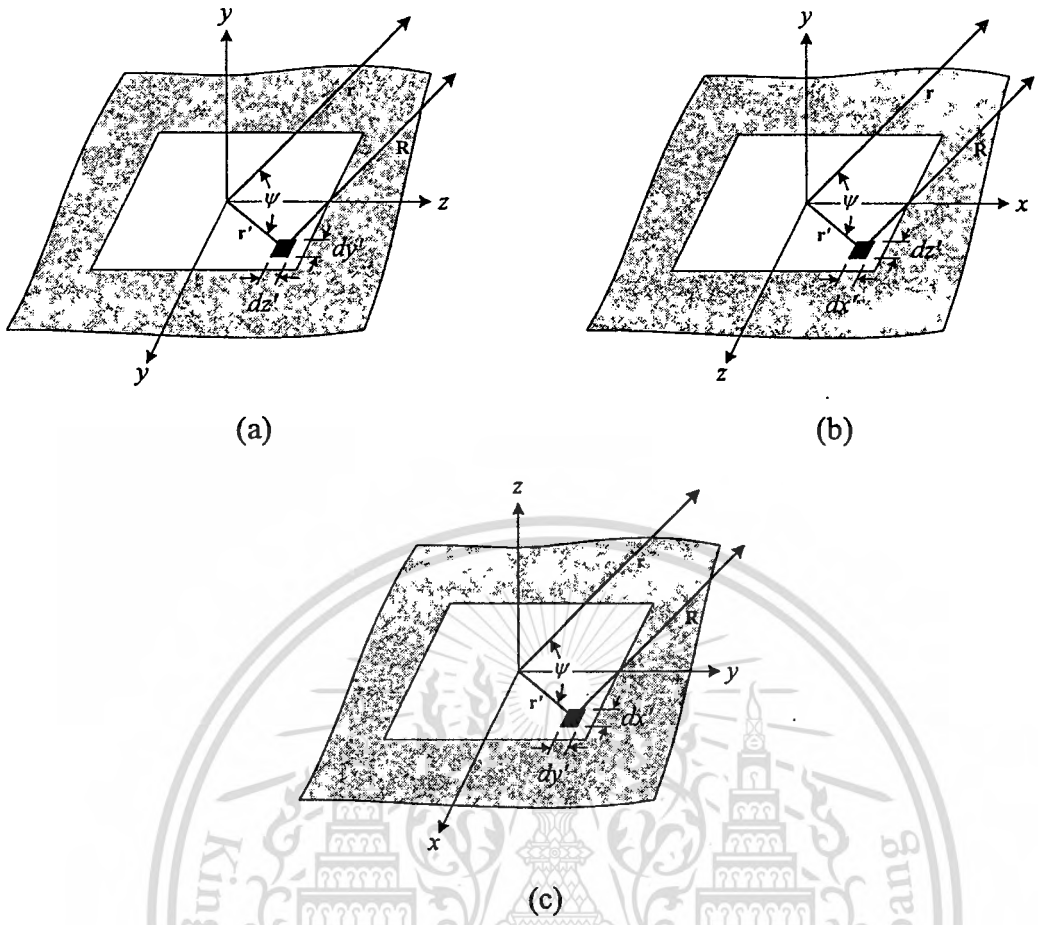

Fig. 2.3 Coordinate positions used for the solution of fields radiated through aperture: (a) on the *yz*-plane, (b) on the *xz*-plane, (c) on the *xy*-plane.

The equivalent magnetic current density exists along the aperture of width w and height h (in the *yz*-plane), so $\hat{\mathbf{n}} = \hat{a}_x$ and (2.15) is written as

$$\mathbf{M}_s = -2\hat{\mathbf{n}} \times \mathbf{E}_a = -2\hat{a}_x \times E_z \hat{a}_z = -2E_0 \cos\left(\frac{2\pi}{l}x'\right)\hat{a}_y \tag{2.20}$$

The equivalent magnetic current density M_y component is obtained. Substituting the M_y component into (2.17c) and (2.17d), the L_θ and L_ϕ components can be worked out. Thus, the far-zone electric fields radiated by each aperture can be found as

$$E_r = 0 \tag{2.21a}$$

$$E_\theta = -j\frac{2khwE_0 e^{-jkr}}{4\pi r}\cos\phi\frac{\sin(Y)}{Y}\frac{\sin(Z)}{Z} \tag{2.21b}$$

$$E_\phi = j\frac{2khwE_0e^{-jkr}}{4\pi r}\cos\theta\sin\phi\frac{\sin(Y)}{Y}\frac{\sin(Z)}{Z} \tag{2.21c}$$

where $Y = \frac{kw\sin\theta\sin\phi}{2}$ and $Z = \frac{kh\cos\theta}{2}$.

The total electric field for the patch antenna is derived from the total electric field for the two apertures separated by a distance l along the x direction. The array factor for two elements of (2.22) is used.

$$AF_x = 2\cos\left[\frac{1}{2}(kl\cos\theta\cos\phi)\right] \tag{2.22}$$

Consequently, the total electric fields for the patch antenna are written as (2.23a) and (2.23b) for the E_θ and E_ϕ components, respectively.

$$E_\theta = -j\frac{khwE_0e^{-jkr}}{\pi r}\cos\phi\left[\frac{\sin\left(\frac{kw\sin\theta\sin\phi}{2}\right)}{\frac{kw\sin\theta\sin\phi}{2}}\right]\left[\frac{\sin\left(\frac{kh\cos\theta}{2}\right)}{\frac{kh\cos\theta}{2}}\right] \times\cos\left[\frac{1}{2}(kl\cos\theta\cos\phi)\right] \tag{2.23a}$$

$$E_\phi = j\frac{khwE_0e^{-jkr}}{\pi r}\cos\theta\sin\phi\left[\frac{\sin\left(\frac{kw\sin\theta\sin\phi}{2}\right)}{\frac{kw\sin\theta\sin\phi}{2}}\right]\left[\frac{\sin\left(\frac{kh\cos\theta}{2}\right)}{\frac{kh\cos\theta}{2}}\right] \times\cos\left[\frac{1}{2}(kl\cos\theta\cos\phi)\right] \tag{2.23b}$$

In the E-plane, the $E_\phi = 0$ and the E_θ component is expressed as

$$E_\theta = -j\frac{khwE_0e^{-jkr}}{\pi r}\cos\phi\left[\frac{\sin\left(\frac{kh\cos\theta}{2}\right)}{\frac{kh\cos\theta}{2}}\right]\cos\left[\frac{1}{2}(kl\cos\theta)\right] \tag{2.24}$$

For the TM^z_{020} mode, Fig. 2.1(b), the electric and magnetic field components will be reduced to

$$E_z = -j\frac{\left(\frac{2\pi}{w}\right)^2}{\omega\mu\varepsilon}A_{020}\cos\left(\frac{2\pi}{w}y'\right) = E_0\cos\left(\frac{2\pi}{w}y'\right) \tag{2.25}$$

$$H_x = -\frac{2\pi}{\mu w}A_{020}\sin\left(\frac{2\pi}{w}y'\right) = H_0\sin\left(\frac{2\pi}{w}y'\right) \tag{2.26}$$

The equivalent magnetic current density exists along the aperture of width l and height h (in the xz-plane), so $\hat{\mathbf{n}} = \hat{a}_y$ and (2.15) is written as

$$\mathbf{M}_s = -2\hat{\mathbf{n}}\times\mathbf{E}_a = -2\hat{a}_y\times E_z\hat{a}_z = 2E_0\cos\left(\frac{2\pi}{w}y'\right)\hat{a}_x \tag{2.27}$$

From (2.27), the L_θ and L_ϕ components are given by substituting the M_x component into (2.17c) and (2.17d). Then, the expressions for far-zone electric fields radiated by the aperture of (2.16a) – (2.16c) can be written as

$$E_r = 0 \tag{2.28a}$$

$$E_\theta = -j\frac{2khlE_0e^{-jkr}}{4\pi r}\sin\phi\frac{\sin(X)}{X}\frac{\sin(Z)}{Z} \tag{2.28b}$$

$$E_\phi = -j\frac{2khlE_0e^{-jkr}}{4\pi r}\cos\theta\cos\phi\frac{\sin(X)}{X}\frac{\sin(Z)}{Z} \tag{2.28c}$$

where $X = \frac{kl\sin\theta\cos\phi}{2}$ and $Z = \frac{kh\cos\theta}{2}$.

According to the two-element array, the array factor for the two apertures separated by a distance w along the y direction is given as

$$AF_y = 2\cos\left[\frac{1}{2}(kw\cos\theta\sin\phi)\right] \tag{2.29}$$

Consequently, the total electric fields for the patch antenna are written as (2.30a) and (2.30b) for the E_θ and E_ϕ components, respectively.

$$E_\theta = -j\frac{khwE_0e^{-jkr}}{\pi r}\sin\phi\left[\frac{\sin\left(\frac{kl\sin\theta\cos\phi}{2}\right)}{\frac{kl\sin\theta\cos\phi}{2}}\right]\left[\frac{\sin\left(\frac{kh\cos\theta}{2}\right)}{\frac{kh\cos\theta}{2}}\right] \times\cos\left[\frac{1}{2}(kw\cos\theta\sin\phi)\right] \tag{2.30a}$$

$$E_\phi = -j\frac{khwE_0e^{-jkr}}{\pi r}\cos\theta\cos\phi\left[\frac{\sin\left(\frac{kl\sin\theta\cos\phi}{2}\right)}{\frac{kl\sin\theta\cos\phi}{2}}\right]\left[\frac{\sin\left(\frac{kh\cos\theta}{2}\right)}{\frac{kh\cos\theta}{2}}\right] \times\cos\left[\frac{1}{2}(kw\cos\theta\sin\phi)\right] \tag{2.30b}$$

In the E-plane, the $E_\phi = 0$ and the E_θ component is expressed as

$$E_\theta = -j\frac{khwE_0e^{-jkr}}{\pi r}\sin\phi\left[\frac{\sin\left(\frac{kh\cos\theta}{2}\right)}{\frac{kh\cos\theta}{2}}\right]\cos\left[\frac{1}{2}(kw\cos\theta)\right] \tag{2.31}$$

The E-plane patterns of the patch antenna excited at the modes of TM^z_{200} and TM^z_{020} are plotted in Fig. 2.4(a) and 2.4(b), respectively.

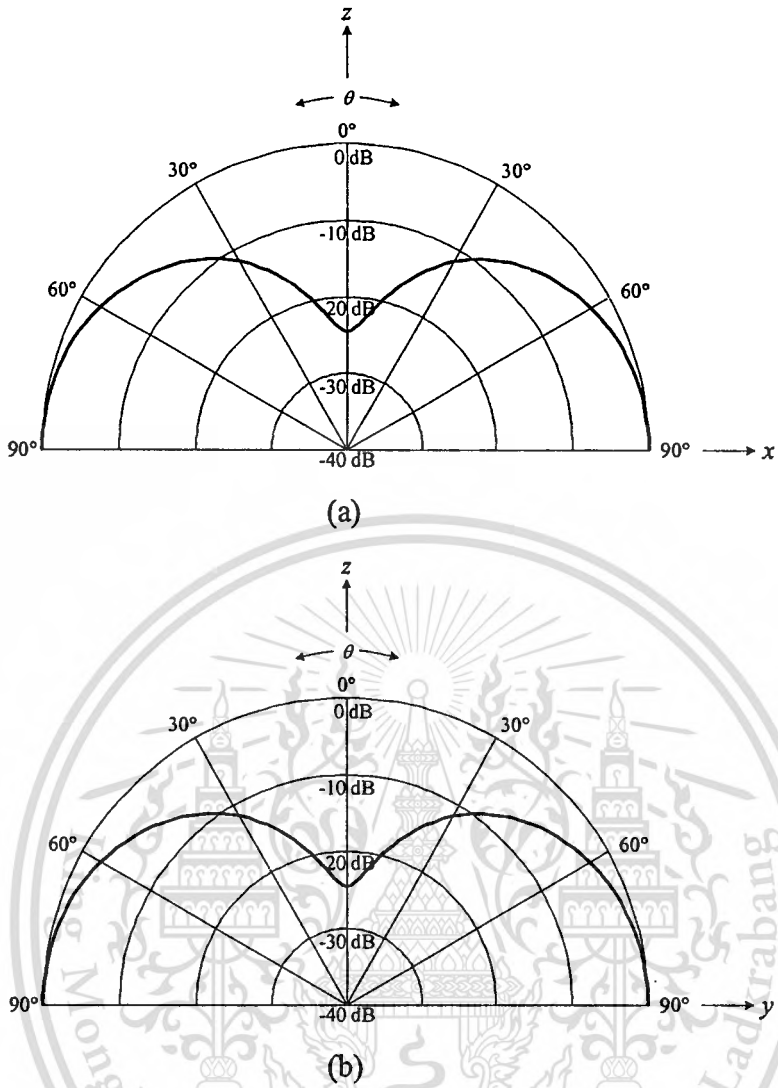

Fig. 2.4 The *E*-plane patterns of the patch antenna: (a) TM^{z}_{200}, (b) TM^{z}_{020}.

In order to properly utilize this antenna operation, the symmetric structure of a square patch ($w = l$) is chosen to obtain identical radiation patterns for two switching states. A square patch antenna with the size of one wavelength in dielectric (λ_d) is used to support the TM^{z}_{200} and TM^{z}_{020} modes. Two PIN diodes are placed on each edge at the position of null of field distribution to cut off radiation from these edges, as shown in Fig. 2.5, so that the antenna operation can be changed between the TM^{z}_{200} and TM^{z}_{020} modes by switching the PIN diodes. When the forward bias is applied, the PIN diodes on the front and rear edges (the edges parallel to *x*-axis) are shorted. The patch operates in the TM^{z}_{200} and radiates in *x* direction. Alternatively, when the reverse bias is applied, the PIN diodes on the left and right edges (the edges parallel to *y*-axis) are shorted. The patch

operates in the TM^{z}_{020} and radiates in y direction. Therefore, it should be noted that the physical configuration of the antenna is fixed but the radiation pattern is switched by suitable biasing of the PIN diodes.

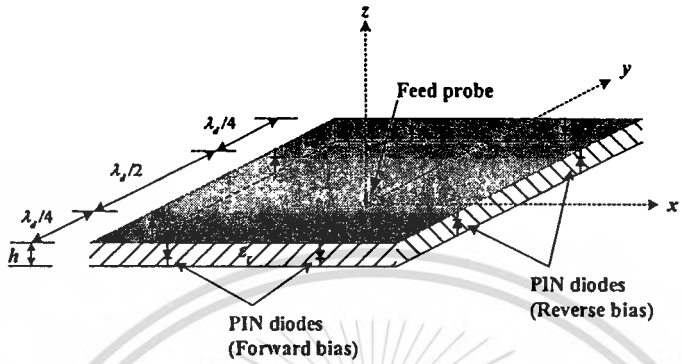

Fig. 2.5 Configuration of the switched-beam single patch antenna.

2.2.2. PIN diode models

In this section, an equivalent circuit model of PIN diode is described which will be used in the antenna simulation. The physical structure of PIN diode is shown in Fig. 2.6(a). It consists of a high-resistivity semiconductor or I (intrinsic) layer between two highly doped P and N regions. Fig. 2.6(b) and 2.6(c) show the equivalent circuits for ON-state and OFF-state diodes, respectively [14].The package inductance L_p and capacitance C_p are dependent on the type of package used, and will appear in both ON- and OFF-states. For the ON-state diode, the resistance R_f, representing the forward biased resistance, is in the range of 0.2 – 5.0 Ω. For the OFF-state diode, the capacitance C_j and the resistance R_s represent the junction capacitance and the sum of P-layer, N-layer and contact resistance, respectively. The capacitance C_j typically ranges from 0 to 1 pF and the resistance R_s is in the range of 5 kΩ.

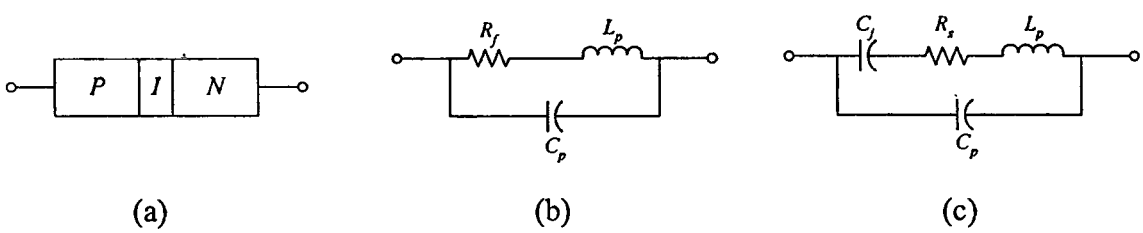

Fig. 2.6 A PIN diode: (a) physical layout, (b) equivalent circuit for ON-state diode, (c) equivalent circuit for OFF-state diode.

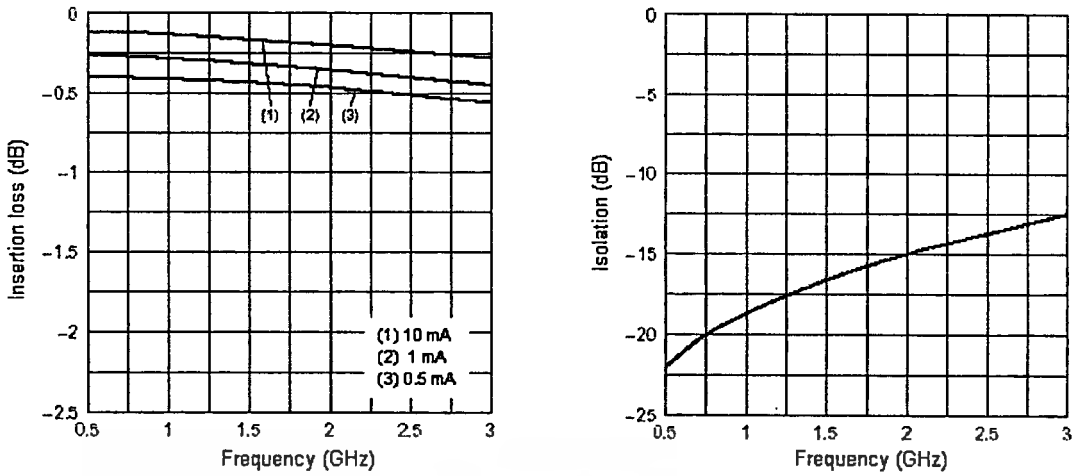

(a) (b)

Fig. 2.7 Characteristics of the Philips BAP51-02 PIN diode: (a) insertion loss of forward biased diode, (b) isolation of zero biased diode.

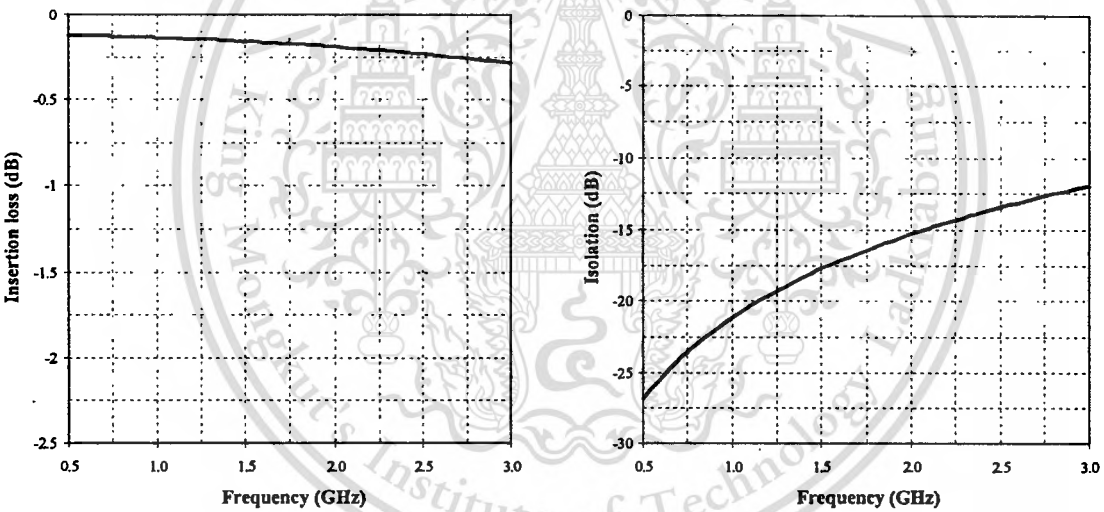

(a) (b)

Fig. 2.8 The simulated results of the PIN diode models: (a) insertion loss of 10 mA forward biased diode, (b) isolation of zero biased diode.

The Philips BAP51-02 surface mounted PIN diodes are used in this thesis. The diode is specified to operate from 0.5 GHz to 3.0 GHz. The characteristics of the BAP51-02 PIN diode are shown in Fig. 2.7(a) and 2.7(b) [15]. The insertion loss is better than 0.25 dB in the case of 10 mA biased diode, and the isolation is better than 12.5 dB in the case of zero biased diode. The PIN diode models for ON-state and OFF-state diode are required for antenna design and simulation. The PIN diode models can be derived from

the equivalent circuits of the PIN diode presented above. The ON-state and OFF-state PIN diode models are established by referring to the characteristics of the BAP51-02 PIN diode for the case of 10 mA biased diode and zero biased diode, respectively. The *RLC* circuits are built and simulated using IE3D simulator [16] to obtain the resistance, inductance and capacitance, which satisfy the specification of BAP51-02 PIN diode. The characteristics of the ON-state PIN diode model and the OFF-state PIN diode model are simulated. Fig. 2.8(a) shows the insertion loss of 10 mA forward biased diode and Fig. 2.8(b) shows the isolation of zero biased diode. The simulated results of PIN diode models agree well with the characteristics of the BAP51-02 PIN diode. This agreement is obtained as the resistance R_f, inductance L_p and capacitance C_p in Fig. 2.6(b) are 1.4 Ω, 1 nH and 0.1 pF, respectively, and the resistance R_s, inductance L_p, capacitance C_p and C_j in Fig. 2.6(c) are 10 kΩ, 1 nH, 0.14 pF and 0.5 pF, respectively. Using these diode models, the switched-beam single patch antenna is simulated using IE3D simulator.

2.2.3. Results

The switched-beam single patch antenna is designed based on the antenna operation presented in the section 2.2.1. By using the antenna configuration shown in Fig. 2.5, the antenna was simulated using the IE3D simulator at the frequency of 1.95 GHz. In simulations, for the antenna an FR-4 substrate with a dielectric constant of 4.3 and a thickness of 1.5 mm, having the width and length of 7.6 cm was assumed. The PIN diode is Philips BAP51-02 surface mounted PIN diode and the PIN diode models presented in the section 2.2.2 were included in the simulation. The antenna was fabricated and tested to verify the simulated results. The prototype of the switched-beam single patch antenna is shown in Fig. 2.9. It was made of a 7.6 × 7.6 cm^2 FR-4 PCB, with a dielectric constant of 4.3 and a thickness of 1.5 mm. The coaxial-probe feeding was accomplished by employing an SMA connector at the center of the antenna. Two Philips BAP51-02 PIN diodes were soldered on each edge of the antenna.

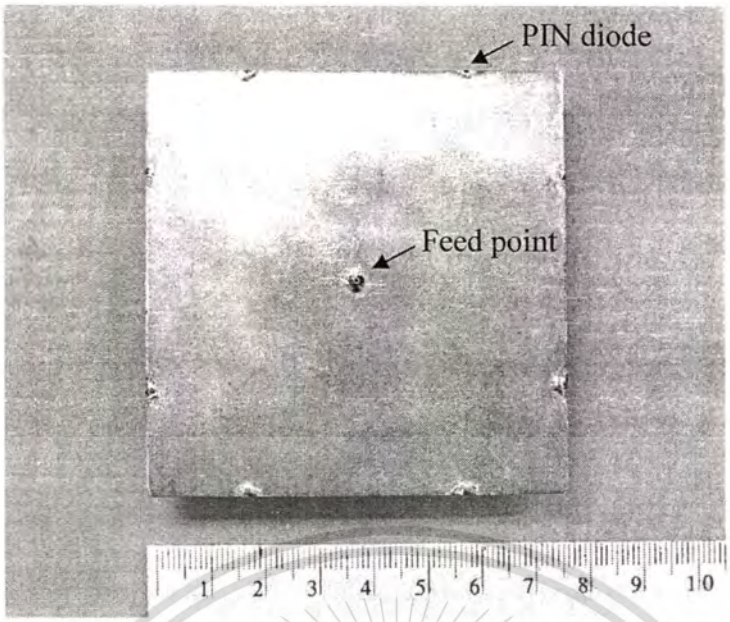

Fig. 2.9 Prototype of the switched-beam single patch antenna.

The bias voltages of +5V and -5V were applied as the forward and reverse bias, respectively. The PIN diodes were biased through the coaxial-probe feed with +5V dc and 10 mA current so that the PIN diodes on the front and rear edges were shorted while the others were opened, yielding the radiation pattern in x direction. Similarly, the radiation pattern in y direction was obtained when -5V dc bias was applied that the PIN diodes on the left and right edges were shorted. The radiation patterns of the switched-beam single patch antenna were measured at the frequency of 1.95 GHz with the HP8510C network analyzer and using a linearly polarized patch antenna as a transmitting antenna. The radiation patterns were measured and compared with the simulated results. The H-plane patterns in x and y directions are shown in Fig. 2.10(a). The E-plane pattern is shown in Fig. 2.10(b). The simulated and measured results show good agreement.

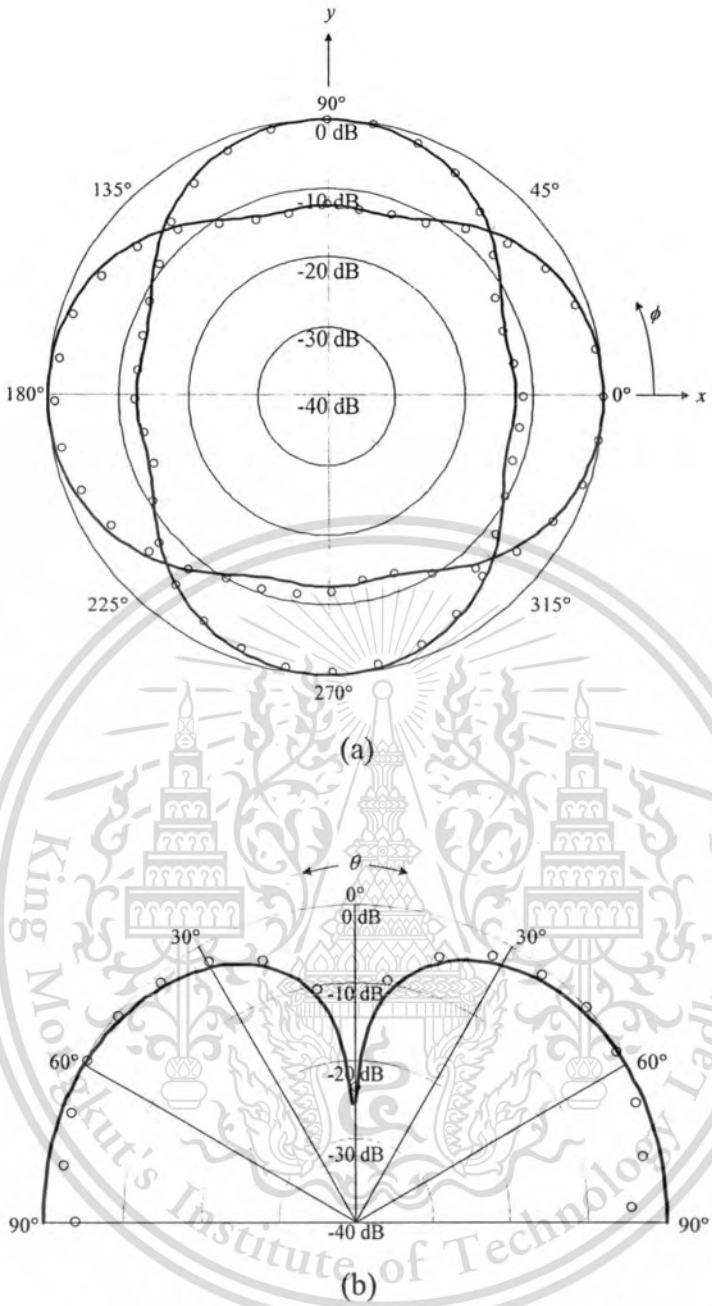

Fig. 2.10 Radiation patterns of the switched-beam element: (a) *H*-plane, (b) *E*-plane.
—— simulation, ○ measurement

2.3 A Flat Four-Beam Compact Phased Array Antenna

A flat four-beam compact phased array antenna described in [10] was designed to switch beam in azimuth direction. A four-element circular array antenna and four 1-bit phase shifters were designed to provide four beam directions. The circular patch elements having omnidirectional pattern were used to form the flat and compact structure. The antenna characteristics as a function of array radius are shown in Table 2.1. The array

radius was chosen as 0.375λ by which the satisfactory characteristics were obtained. Beamwidth is larger than 90°, so all directions in azimuth can be covered by employing four beams. Higher front-to-back ratio (F/B) is obtained as well. The branch-line hybrid coupler reflection type phase shifters were used to switch beam of the array.

Following the preceding work, the flat four-beam compact phased array antenna is modified to operate at the frequency of 1.95 GHz. An aperture-coupled circular patch antenna is used as the array element. This antenna element is etched on a substrate, and uses dielectric foam to enhance the operational bandwidth. The switched delay line phase shifter is used to reduce the size of the phase shifter. In addition, the branch-line coupler is added to couple the received signal to the signal processing unit. The configuration of a flat four-beam compact phased array antenna is shown in Fig. 2.11. The design and results of the flat four-beam compact phased array antenna are presented in this section.

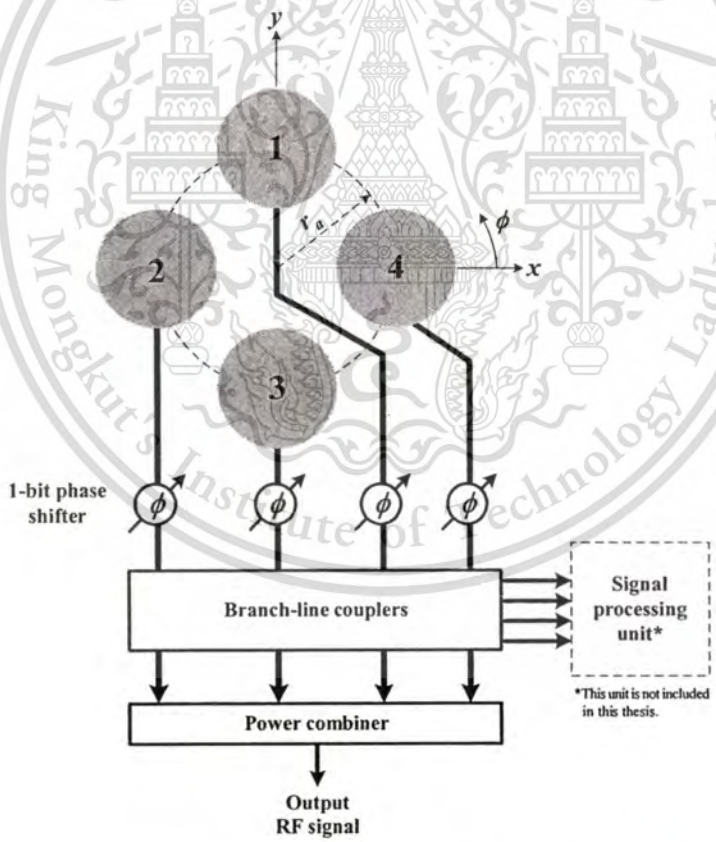

Fig. 2.11 The configuration of a flat four-beam compact phased array antenna.

Table 2.1 Antenna characteristics as a function of array radius [10]

r_a/λ	Antenna characteristics				
	HPBW	**F/B (dB)**	**Directivity (dBi)**	**Correlation coefficient ρ**	**Beam shape**
0.25	186°	7.05	5.63	0.87	
0.375	116°	20.45	7.65	0.44	
0.5	86°	4.36	8.13	0.26	
0.75	54°	0.16	8.09	0.02	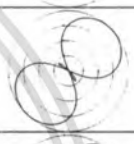
1.0	42°	11.48	7.88	0.47	

2.3.1. Aperture-coupled circular patch antenna

The configuration of aperture-coupled circular patch antenna is shown in Fig. 2.12. The circular patch of diameter $2a$ is etched on the patch substrate with height h_1 and dielectric constant ε_{r1}. The foam layer with thickness h_2 and dielectric constant ε_{r2}, which is very close to the dielectric constant of air, is inserted between the patch substrate and the feed substrate to enhance the antenna bandwidth as well as to provide structural support. The feed substrate is copper clad on both sides with height h_3 and dielectric constant ε_{r3}. The upper side (ground plane) of the feed substrate is etched to create coupling aperture of width w_a and length l_a. The feed line of length l_f and width w_f is etched on the bottom side of the feed substrate. l_s is the length of the open circuited stub of the feed line.

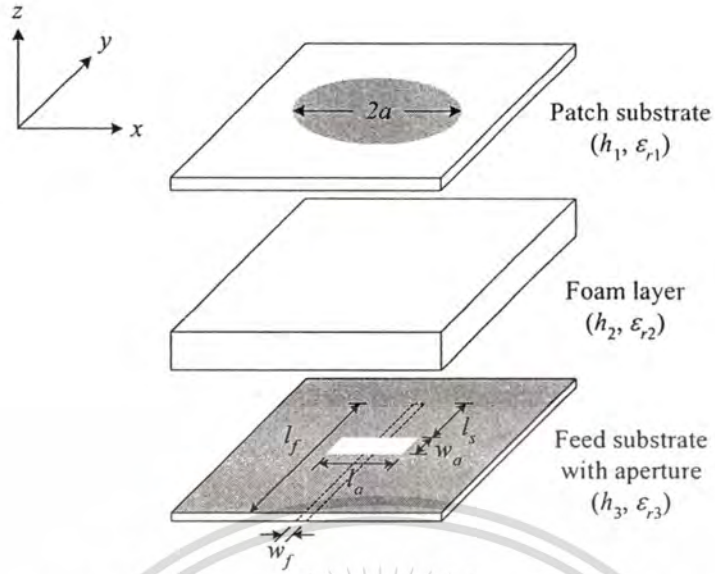

Fig. 2.12 The configuration of aperture-coupled circular patch antenna.

Initially, the size of a circular patch is calculated. For the patch excited at TM_{mn0} mode, the effective radius a_e of the patch is determined from

$$a_e = \frac{\chi'_{mn} c}{2\pi f_r \sqrt{\varepsilon_r}} \tag{2.32}$$

where χ'_{mn} represents the zero of the first derivative of the mn-th order Bessel function, c is the velocity of light in free space, f_r is the design frequency and ε_r is the dielectric constant of the substrate. In this thesis, the patch is designed on an FR-4 substrate, with a dielectric constant ε_{r1} of 4.3 and a thickness h_1 of 1.5 mm, and the design frequency is 1.95 GHz. The TM_{210} mode is chosen to provide omnidirectional pattern in xy-plane; therefore, $m = 2$, $n = 1$ and $\chi'_{21} = 3.0542$. Consequently, the effective radius of the patch of 36 mm is obtained.

For the feed substrate, the RO3003 material, with a dielectric constant ε_{r3} of 3.0 and a thickness h_3 of 0.75 mm is used. The dimension of the aperture (w_a, l_a) and the length of the open circuited stub of the feed line l_s are defined as the variable parameters. By varying the parameters w_a, l_a and l_s, the characteristic of the antenna, the return loss, is calculated at the design frequency of 1.95 GHz using IE3D simulator. Then, the values of w_a, l_a and l_s are chosen for the better result of return loss. Firstly, the aperture width w_a is

varied with the fixed values of a = 36 mm, h_2 = 15 mm, w_f = 2 mm, $l_a = 0.5\lambda_d$ and $l_s = 0.05\lambda_d$. Varying w_a from $0.02\lambda_d$ to $0.08\lambda_d$, the calculated result of the return loss at 1.95 GHz is shown in Fig. 2.13. The return loss is better when w_a is increased to $0.06\lambda_d$, for which the return loss of -6.49 dB is obtained, and it trends to be worse when w_a is larger than $0.06\lambda_d$. Therefore, the aperture width w_a of $0.06\lambda_d$ is chosen.

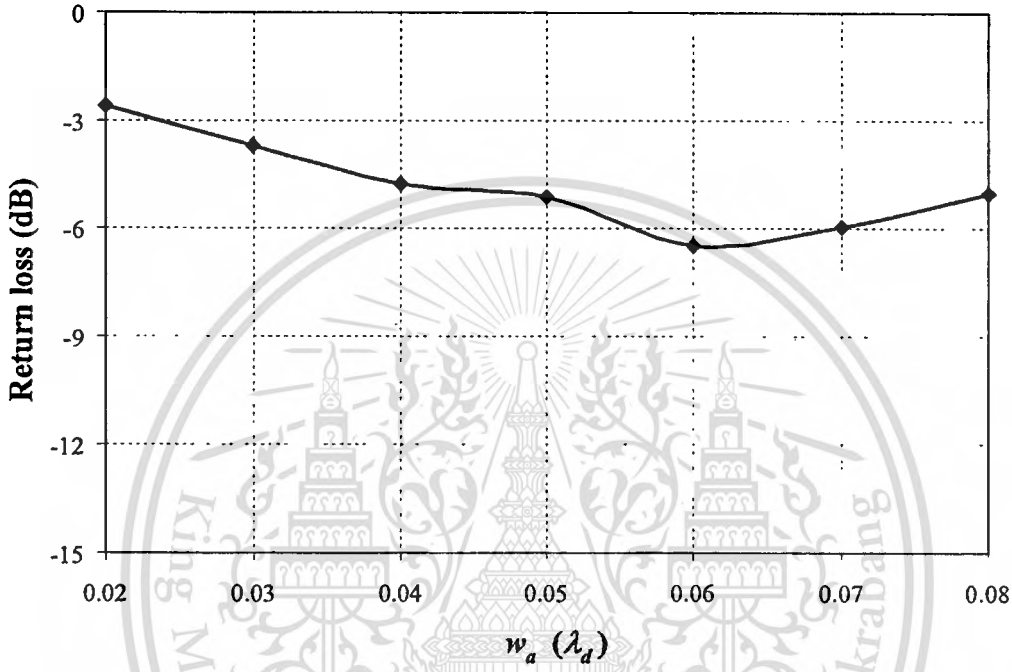

Fig. 2.13 The return loss of the antenna when the aperture width w_a is varied with the fixed values of a = 36 mm, h_2 = 15 mm, w_f = 2 mm, $l_a = 0.5\lambda_d$ and $l_s = 0.05\lambda_d$.

To find out the aperture length l_a, it is varied from $0.2\lambda_d$ to $0.8\lambda_d$ with the fixed values of a = 36 mm, h_2 = 15 mm, w_f = 2 mm, $w_a = 0.06\lambda_d$ and $l_s = 0.05\lambda_d$. The calculated result of the return loss for various aperture lengths is shown in Fig. 2.14. It shows that the return loss is better for the aperture length of $0.6\lambda_d$. The return loss of -8.46 dB is obtained. Choosing the aperture width w_a of $0.06\lambda_d$ and the aperture length l_a of $0.6\lambda_d$, the length of the open circuited stub l_s is varied to obtain better characteristic of antenna with the fixed values of a = 36 mm, h_2 = 15 mm and w_f = 2 mm. As shown in Fig. 2.15, l_s is varied from $0.02\lambda_d$ to $0.08\lambda_d$, and the better characteristic of antenna at the design frequency of 1.95 GHz is obtained by the return loss of -13.58 dB when l_s is equal to $0.04\lambda_d$. As a result, the aperture width w_a of $0.06\lambda_d$, the aperture length l_a of $0.6\lambda_d$ and the length of the open circuited stub l_s of $0.04\lambda_d$ are chosen.

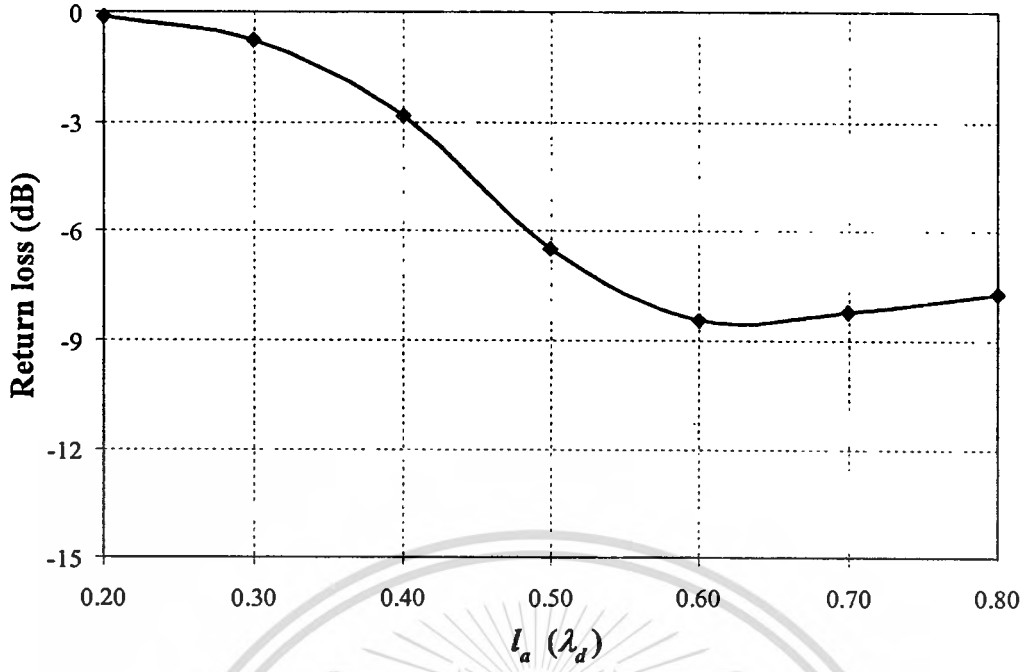

Fig. 2.14 The return loss of the antenna when the aperture length l_a is varied with the fixed values of a = 36 mm, h_2 = 15 mm, w_f = 2 mm, $w_a = 0.06\lambda_d$ and $l_s = 0.05\lambda_d$.

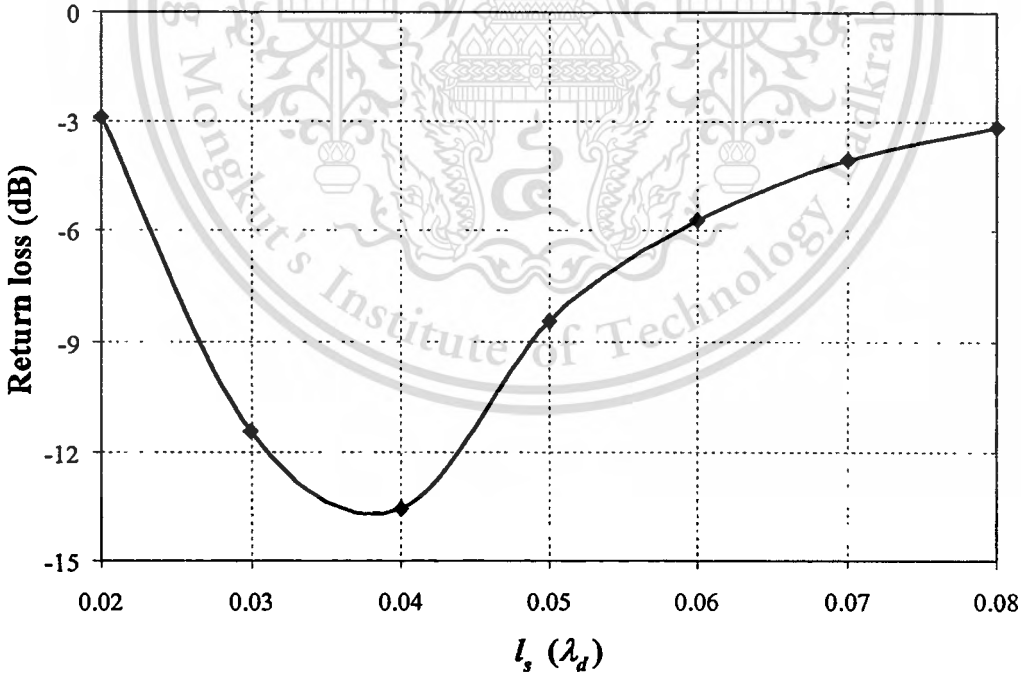

Fig. 2.15 The return loss of the antenna when the length of the open circuited stub l_s is varied with the fixed values of a = 36 mm, h_2 = 15 mm, w_f = 2 mm, $w_a = 0.06\lambda_d$ and $l_a = 0.6\lambda_d$.

Since the patch radius of 36 mm used in previous calculation is the effective radius of the patch, which is normally larger than the actual radius of the patch due to the fringe field radiation, the patch radius is adjusted to obtain the actual radius of the patch that gives the better antenna characteristic. The radius of the patch a is varied from 32.5 mm to 36 mm. The return loss of the antenna is calculated using IE3D simulator and the result is presented in Fig. 2.16. The better return loss of -20.43 dB at the design frequency of 1.95 GHz is obtained from the radius of the patch of 34 mm. In addition, the effect of the thickness of foam layer h_2 on the characteristic of the antenna is disclosed. With the antenna parameters of a = 34 mm, w_f = 2 mm, $w_a = 0.06\lambda_d$ and $l_a = 0.6\lambda_d$ and $l_s = 0.04\lambda_d$, the return loss of the antenna for h_2 = 10 mm, 15 mm and 20 mm are calculated. The calculated result of the return loss as a function of frequency is shown in Fig. 2.17. It is found that the resonant frequency at 1.95 GHz is given by h_2 = 15 mm, and the thicker foam layer gives the lower resonant frequency.

Therefore, the antenna parameters of the designed aperture-coupled circular patch antenna in physical dimensions are summarized in Table 2.2.

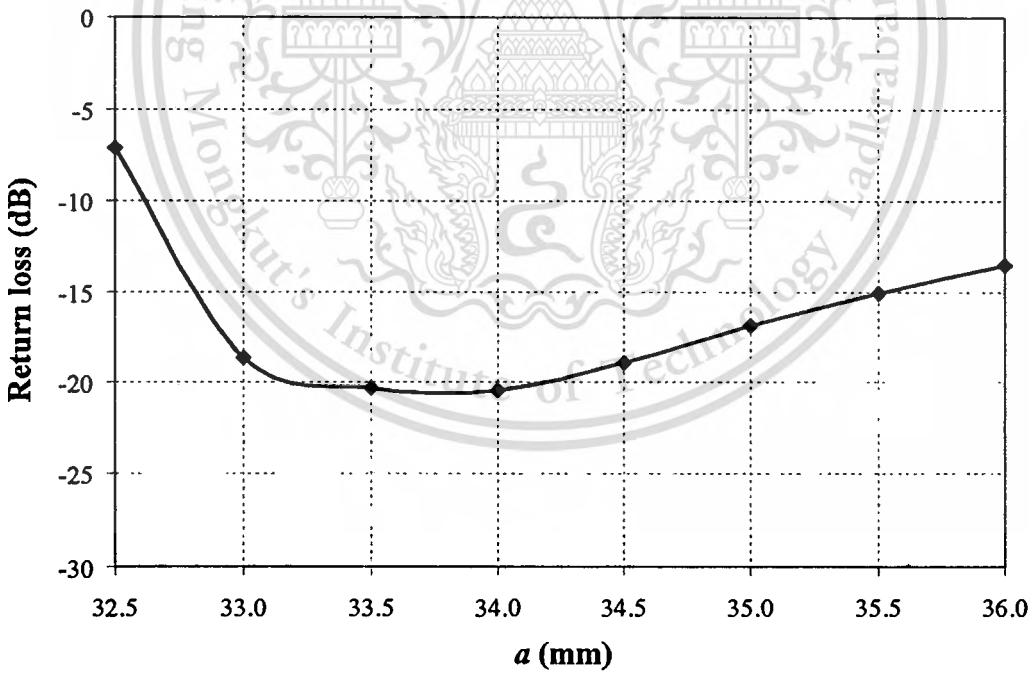

Fig. 2.16 The return loss of the antenna when the radius of patch a is varied with the fixed values of h_2 = 15 mm, w_f = 2 mm, $w_a = 0.06\lambda_d$ and $l_a = 0.6\lambda_d$ and $l_s = 0.04\lambda_d$.

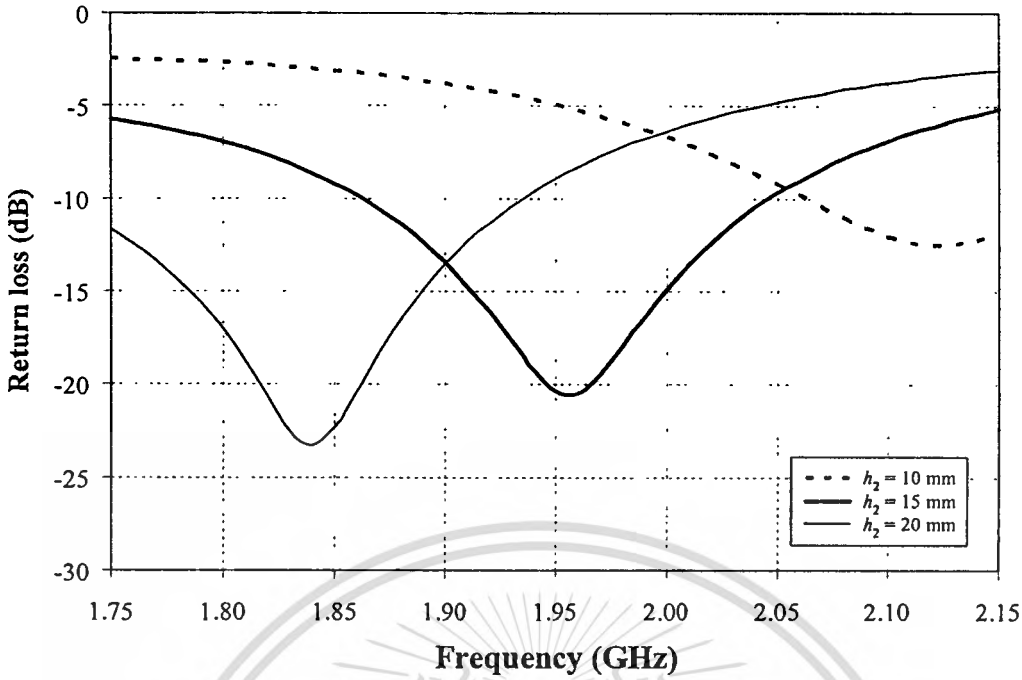

Fig. 2.17 The return loss of the antenna for h_2 = 10 mm, 15 mm and 20 mm with the antenna parameters of a = 34 mm, w_f = 2 mm, $w_a = 0.06\lambda_d$ and $l_a = 0.6\lambda_d$ and $l_s = 0.04\lambda_d$.

Table 2.2 List of the antenna parameters of the designed aperture-coupled circular patch antenna

Antenna parameters	Dimensions
Radius of patch a	34.00 mm
Thickness of foam layer h_2	15.00 mm
Aperture width w_a	5.33 mm
Aperture length l_a	53.30 mm
Feed line width w_f	2.00 mm
Length of open circuited stub l_s	3.55 mm

2.3.2. Phase shifter

The configuration of the flat four-beam compact phased array antenna is shown in Fig. 2.11. A four-element circular array is formed with the array radius r_a of 0.375λ by arranging the element 1, 2, 3 and 4 on the xy plane at the positions of ϕ = 90°, 180°, 270° and 0°, respectively. The phase shifter is used to shift the phase excitation of each element to switch the beam toward the defined direction. According to the circular array

theory, the main beam in (θ_0,ϕ_0) direction can be obtained by choosing the phase excitation of the n^{th} element (α_n) to be

$$\alpha_n = -kr_a \sin\theta_0 \cos(\phi_0 - \phi_n) \tag{2.33}$$

where $k = 2\pi/\lambda$, r_a is the array radius, ϕ_n is the position of the n^{th} element. The phase excitation of the array elements are listed in Table 2.3. The peak beam direction θ_0 of 30° is defined to tilt the beam of antenna for the specific coverage area. The phase excitation of 0°, 67.5° and -67.5° are required for switching the beam in azimuth directions ϕ_0 of 0°, 90°, 180° and 270°, while the phase excitations of 47.7° and -47.7° are required for switching the beam in azimuth directions ϕ_0 of 45°, 135°, 225° and 315°. By simply redefining the switched beam directions, it becomes apparent that the number of differential phases is reduced and, in this case, the 1-bit phase shifter with the differential phase of 95.4° can be applied for the four-beam phased array antenna.

Table 2.3 Phase excitation of the flat four-beam compact phased array antenna for the four beam directions

Phase excitation / Beam direction ϕ_0	Element 1	Element 2	Element 3	Element 4
0°	0°	67.5°	0°	-67.5°
90°	-67.5°	0°	67.5°	0°
180°	0°	-67.5°	0°	67.5°
270°	67.5°	0°	-67.5°	0°
45°	-47.7°	47.7°	47.7°	-47.7°
135°	-47.7°	-47.7°	47.7°	47.7°
225°	47.7°	-47.7°	-47.7°	47.7°
315°	47.7°	47.7°	-47.7°	-47.7°

In the phased array antenna system, the phase shifter is the main component of the beam forming network. The ferrite phase shifter and the semiconductor diode phase shifter are generally used. The ferrite phase shifter is not planar and the phase shifting mechanism is of analog type. The semiconductor diode phase shifter is planar in configuration and the phase shifting operation is of digital nature; therefore it is called

digital phase shifter. Usually, the semiconductor diode phase shifter or the digital phase shifter is classified into two types: transmission type and reflection type. The transmission type phase shifter is two-port circuit whereas the reflection type phase shifter is one-port circuit. Therefore, the phase of transmission coefficient of the circuit is shifted in the transmission type phase shifter by switching operation, but in the reflection type phase shifter the phase of reflection coefficient of the circuit is shifted by creating an open or short circuit at a certain reference plane. The transmission type phase shifter can be categorized as switched delay line, loaded line and high-pass/low-pass phase shifters.

The basic configuration of a switched delay line phase shifter is shown in Fig. 2.18. The switched delay line phase shifter uses different length of transmission lines to produce a differential phase shift. Two transmission lines of length l_1 and $l_1 + \Delta l$ with the characteristic impedance z_0 are reference path and delayed path, respectively. Four identical switches s_1, s_1', s_2 and s_2' are used to switch the signal path. When switches s_1 and s_1' are connected to the transmission line of length l_1 and switches s_2 and s_2' are disconnected to the transmission line of length $l_1 + \Delta l$, the signal passes through the reference path of length l_1. When switches s_1 and s_1' are disconnected to the transmission line of length l_1 and switches s_2 and s_2' are connected to the transmission line of length $l_1 + \Delta l$, the signal passes through the delayed path of length $l_1 + \Delta l$. The delay of the signal is the difference of line length Δl; therefore, the phase shift of $\beta \Delta l$ is produced.

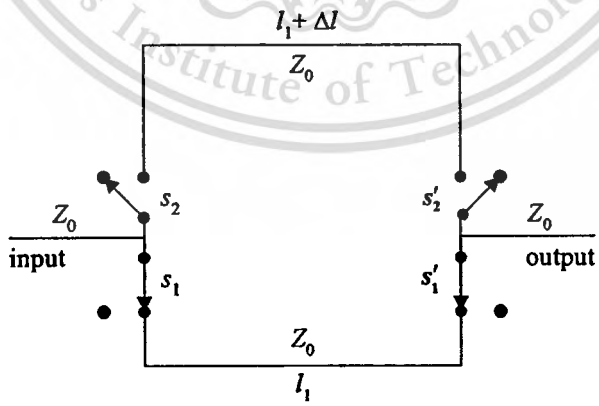

Fig. 2.18 Switched delay line phase shifter.

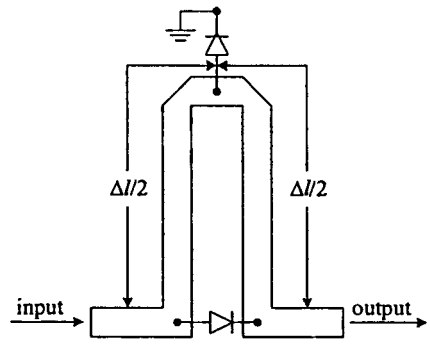

Fig. 2.19 A series- and shunt-mounted 2-diode switched delay line phase shifter.

In accordance with the principle of switched delay line phase shifter, the compact phase shifter with the least number of diodes is designed. A series- and shunt-mounted 2-diode switched delay line phase shifter is shown in Fig. 2.19. The series diode is directly connected to input and output ports, and the shunt diode is connected at the middle of the delay line. When the diodes are forward biased, the signal passes through the series diode, while the shunt diode is shorted to ground. Since the series diode is directly connected to input and output ports, the reference path is equivalent to zero in length. When the diodes are zero biased, the series diode is open circuited and the signal cannot pass through the diode. Also, the shunt diode is open circuited, so the signal can flow through the delay path of length Δl producing the phase shift of $\beta\Delta l$ in degree. In this case, the phase shift of 95.4° is required at the design frequency of 1.95 GHz. Therefore, the length of delay line Δl is approximately 27.0 mm.

2.3.3. Power combiner and branch-line coupler

The T-junction power divider is a simple three-port network that can be used for power division or power combining. The lossless T-junction can be modeled as a junction of three transmission lines, shown in Fig. 2.20. In general, there are fringing fields and higher order modes associated with the discontinuity at such a junction, leading to stored energy that can be accounted for by a lumped susceptance, B. In order for the divider to be matched to the input line of characteristic impedance Z_0, we must have

$$Y_{in} = jB + \frac{1}{Z_1} + \frac{1}{Z_2} = \frac{1}{Z_0} \tag{2.34}$$

If the transmission lines are assumed to be lossless, then the characteristic impedances are real. If we also assume $B = 0$, then (2.34) reduces to

$$\frac{1}{Z_1}+\frac{1}{Z_2}=\frac{1}{Z_0} \tag{2.35}$$

The output line impedances Z_1 and Z_2 can then be selected to be two 100-Ω output lines for the input line impedance $Z_0 = 50$ Ω. If necessary, quarter-wave transformers can be used to bring the output line impedances back to the desired impedances.

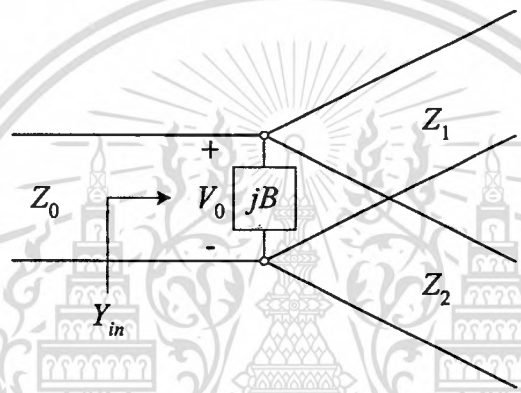

Fig. 2.20 Transmission line model of a lossless T-junction.

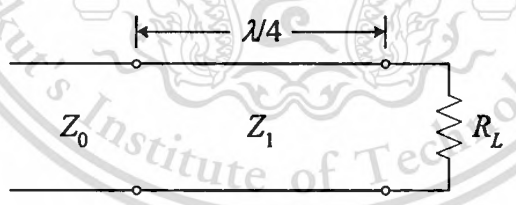

Fig. 2.21 The quarter-wave transformer.

The quarter-wave transformer is a useful and practical circuit for impedance matching. Fig. 2.21 shows a circuit employing a quarter-wave transformer. The load resistance R_L, and the feedline characteristic impedance Z_0, are both real and assumed to be given. These two components are connected with a lossless transmission line of characteristic impedance of Z_1 and length of $\lambda/4$. It is desired to match the load to the Z_0 line, by using the $\lambda/4$ line, and so make no reflection looking into the $\lambda/4$ matching section. The input impedance Z_{in} can be found as

$$Z_{in} = Z_1 \frac{R_L + jZ_1 \tan \beta l}{Z_1 + jR_L \tan \beta l} \tag{2.36}$$

To evaluate this for $\beta l = (2\pi/\lambda)(\lambda/4) = \pi/2$, we can divide the numerator and denominator by $\tan \beta l$ and take the limit as $\beta l \to \pi/2$ to get

$$Z_{in} = \frac{Z_1^2}{R_L} \tag{2.37}$$

In order for no reflection, we must have $Z_{in} = Z_0$, which yields the characteristic impedance Z_1 as

$$Z_1 = \sqrt{Z_0 R_L} \tag{2.38}$$

Therefore, a T-junction power divider/combiner with a 50-Ω input line needs two 100-Ω output lines. In addition, the quarter-wave transformer is used to bring the output line impedances back to the impedances of 50 Ω by using a transmission line of characteristic impedance of 70.7 Ω and length of $\lambda/4$. The layout of microstrip T-junction power divider/combiner with a quarter-wave transformer is shown in Fig. 2.22.

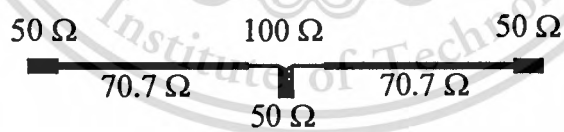

Fig. 2.22 T-junction power divider/combiner with a quarter-wave transformer.

To couple the received signal of each element to the signal processing unit, the branch-line coupler is added. The branch-line coupler is 3 dB directional couplers with 90° phase difference in the outputs of the through and coupled arms. This type of coupler is shown in Fig. 2.23. The basic operation of the branch-line coupler is as follows. With all ports matched, power entering port 1 is evenly divided between ports 2 and 3, with a 90° phase shift between these outputs. No power is coupled to port 4. Observe that the

branch-line coupler has a high degree of symmetry, as any port can be used as the input port. The output ports will always be on the opposite side of the junction from the input port, and the isolated port will be the remaining port on the same side as the input port.

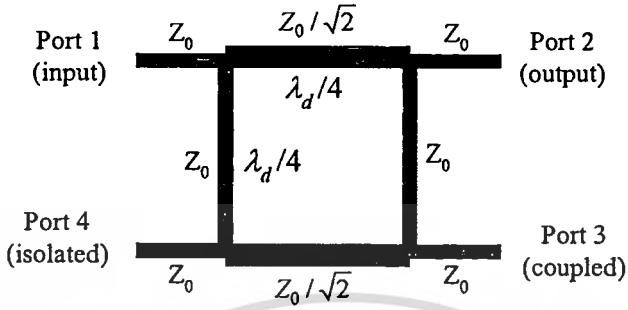

Fig. 2.23 Branch-line coupler.

Applied to the array antenna, Port 1 (input) is connected to the output of each element. The signal will be passed through Port 2 (output) and be summed at the power combiner; simultaneously, the signal is coupled through Port 3 (coupled), which is connected to the signal processing unit. Port 4 (isolated) is terminated by a 50-Ω resistor.

2.3.4. Results

A flat four-beam compact phased array antenna is developed by integrating antenna elements and a beam forming network. The aperture-coupled circular patch antennas are used as antenna elements. Four circular patches with a diameter of 68 mm are etched on an FR-4 substrate to form a circular array with an array radius of 57.7 mm. The feed substrate, which is RO3003 copper clad on both sides, comprises the coupling apertures of width 5.33 mm and length 53.3 mm etched on the upper side and 1-bit phase shifters, branch-line couplers and 2-stage T-junction power combiner etched on the lower side. The foam layer with a thickness of 15 mm is inserted between the patch substrate and the feed substrate. Fig. 2.24 shows the layout of the flat four-beam compact phased array antenna, which is employed in the IE3D simulator. Port 1, 2, 3 and 4 are coupled ports at which the received signal of each antenna element is coupled to a signal processing unit. Port 5 is the array output port where the received signals of four elements are combined. The prototype of a flat four-beam compact phased array antenna was fabricated, as shown in Fig. 2.25.

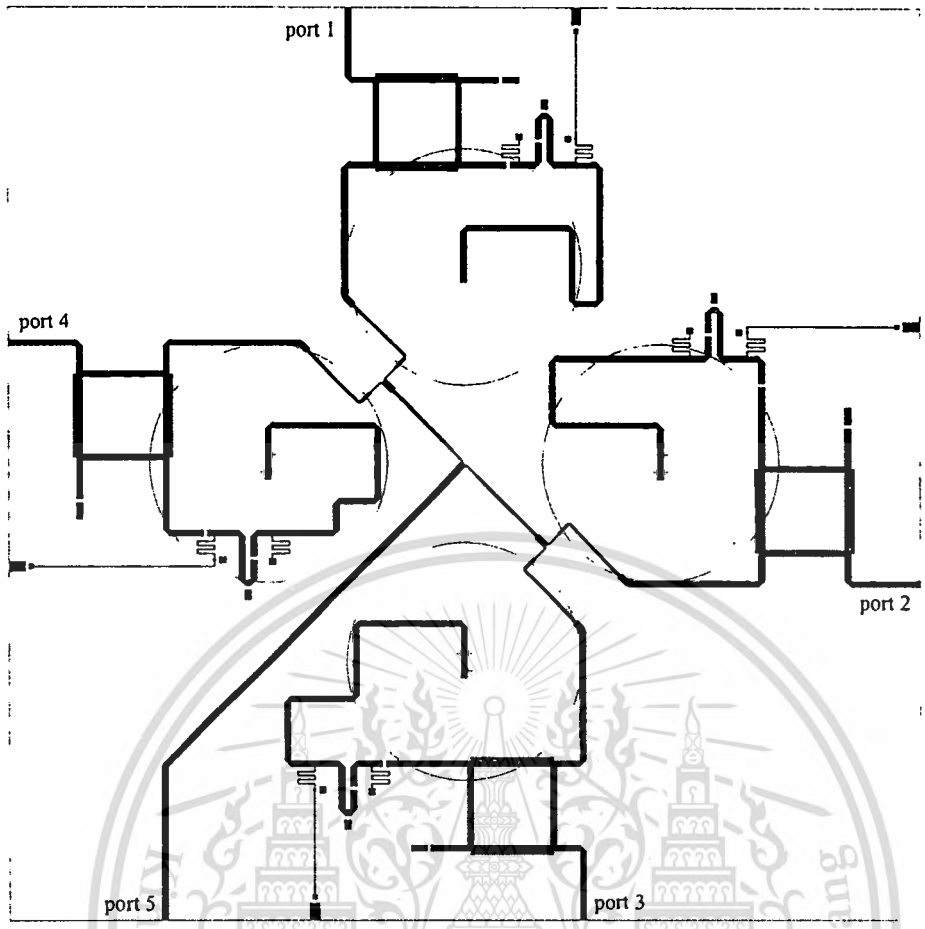

Fig. 2.24 Layout of the flat four-beam compact phased array antenna.

Table 2.4 States of phase shifters of the flat four-beam compact phased array antenna for the four-beam switching

Beam direction	Status of phase shifter			
	Element 1	Element 2	Element 3	Element 4
45°	OFF	ON	ON	OFF
135°	OFF	OFF	ON	ON
225°	ON	OFF	OFF	ON
315°	ON	ON	OFF	OFF

The radiation patterns of the array are measured in an in-house anechoic chamber using an HP8510C network analyzer. The test frequency is 1.95 GHz. The azimuth pattern of array is measured at $\theta = 30°$. The measured results are compared with the calculation as depicted in Fig. 2.26. The solid line represents the simulation and the circle represents the measured result. The results show that the beam of array can be switched to the four directions of 45°, 135°, 225° and 315° in azimuth plane. The four-beam

switching is achieved by controlling states of the phase shifters as shown in Table 2.4. ON and OFF status are given by forward and zero biasing the PIN diodes, respectively.

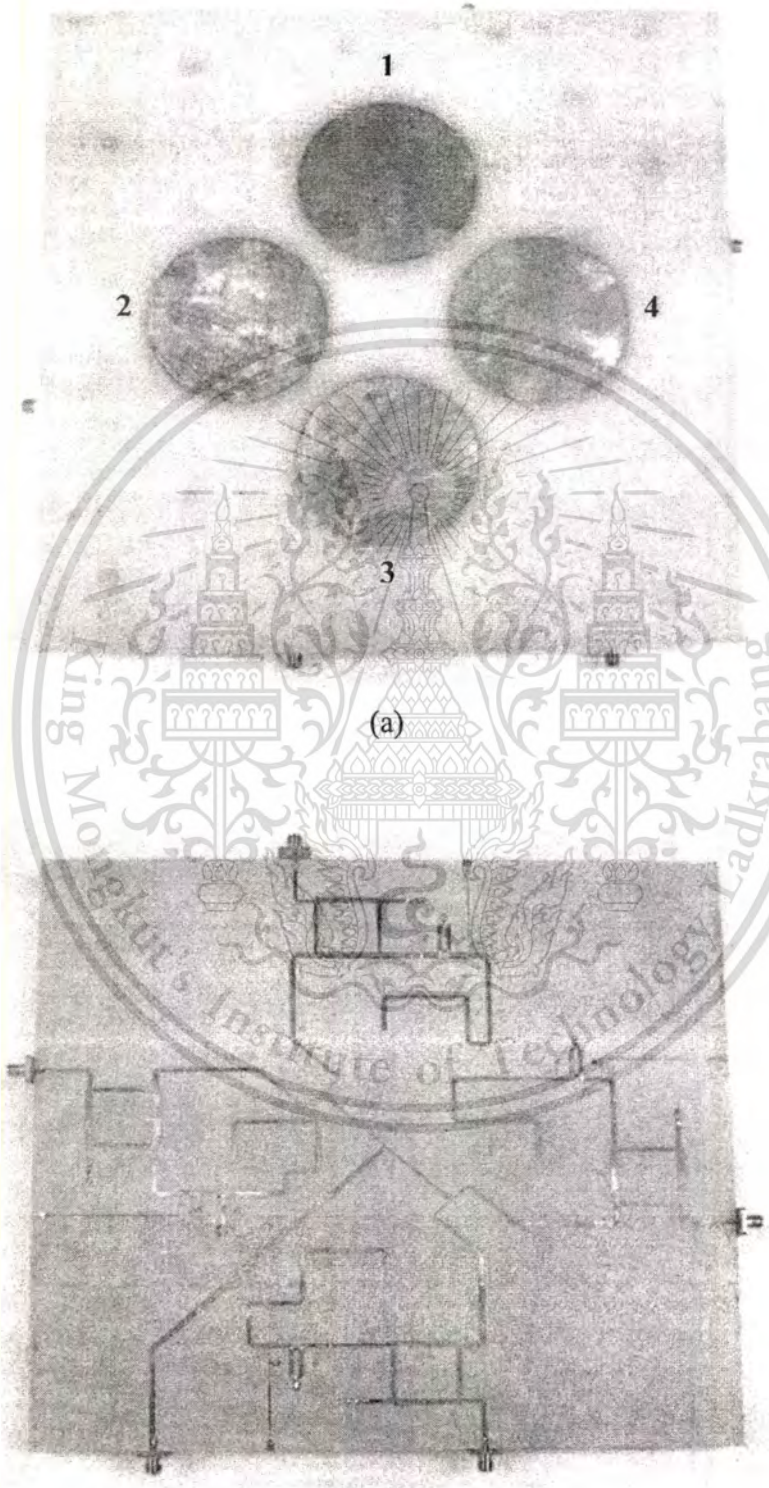

Fig. 2.25 Prototype of a flat four-beam compact phased array antenna: (a) four-element circular patch array, (b) feeding network.

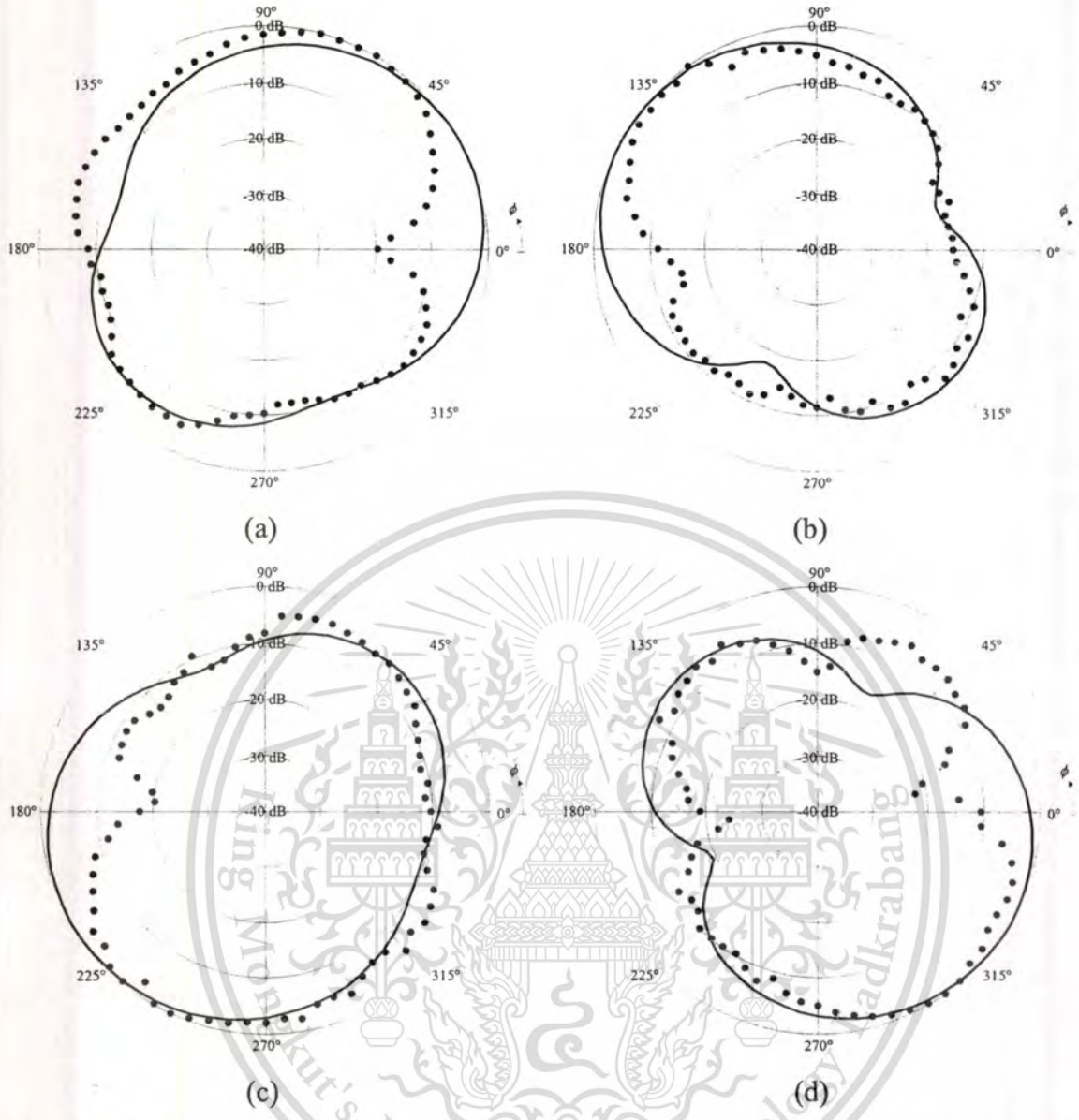

Fig. 2.26 Radiation patterns of a flat four-beam compact phased array antenna in azimuth plane at $\theta = 30°$: (a) 45° beam direction, (b) 135° beam direction, (c) 225° beam direction, and (d) 315° beam direction.

—— simulation, ● measurement

2.4 Conclusion

In this chapter, two switched-beam antennas, a switched-beam single patch antenna and a flat four-beam compact phased array antenna have been presented. The principles, design and test results of these switched-beam antennas have been described. For a switched-beam single patch antenna, the patch antenna has been proposed to switch the beam in azimuth direction by changing the operation modes of antenna with the use of RF switches. The two-beam switching in x and y direction is accomplished. For a flat

four-beam compact phased array antenna, 1-bit phase shifters are employed to achieve the beam switching. The work presented in this thesis has resulted from modifying the designs reported in [10]. An aperture-coupled circular patch antenna is used as the array element. This antenna uses dielectric foam to enhance the operational bandwidth. The switched line phase shifter is used to reduce the phase shifter size. In addition, the branch-line coupler is added to tap the received signal to the signal processing unit. The accomplished tests show that by using 1-bit phase shifters the array is capable of switching its radiation patterns in azimuth directions of 45°, 135°, 225° and 315°. The materials presented in this chapter forms the foundation for designing and developing a phased array antenna of switched-beam elements.

CHAPTER 3
IMPLEMENTATION OF A PHASED ARRAY ANTENNA OF SWITCHED-BEAM ELEMENTS

3.1 Introduction

In chapter 2, the designs of the switched-beam single patch antenna and the flat four-beam compact phased array antenna was presented. These two antennas form a foundation for the design of a phased array antenna of switched-beam elements. The main difference between the flat four-beam compact phased array antenna, presented in chapter 2 and a new phased array antenna of switched-beam elements, presented in this chapter, is due to the use of a new array element. The new array antenna uses the switched-beam single patch antenna instead of the omnidirectional element. The use of such a new element antenna enhances the capabilities of the switched-beam array antenna. By using switched-beam elements, the null pattern can be changed and the degree of freedom can be increased without increasing the number of array elements. The design and characteristics of the phased array antenna of switched-beam elements are presented in this chapter.

3.2 Antenna design

The configuration of a phased array antenna of switched-beam elements is shown in Fig. 3.1. It is composed of switched-beam elements, 1-bit phase shifters and a power combiner. The switched-beam single patch antenna is applied as the switched-beam element, the 1-bit phase shifters are utilized to switch main beam of the array in azimuth directions of ϕ_0 of 45°, 135°, 225° and 315°, and the Wilkinson power divider/combiner is used to combine the received signals of the array antenna.

A phased array antenna of switched-beam elements is a four-element circular array antenna. This array antenna is designed at the frequency of 1.95 GHz. A four-element circular array is formed with the array radius (r_a) of 0.5λ by locating the switched-beam element No. 1, No. 2, No. 3 and No. 4 on the *xy*-plane at the positions of ϕ = 90°, 180°, 270° and 0°, respectively. The array radius of 0.5λ is chosen for the minimum array radius. To switch main beam of the array, the phase excitation of the n^{th}

element (α_n) is calculated for the main beam in directions of ϕ_0 = 45°, 135°, 225° and 315°, and θ_0 = 90°, by using (2.33). The phase excitations are shown in Table 3.1.

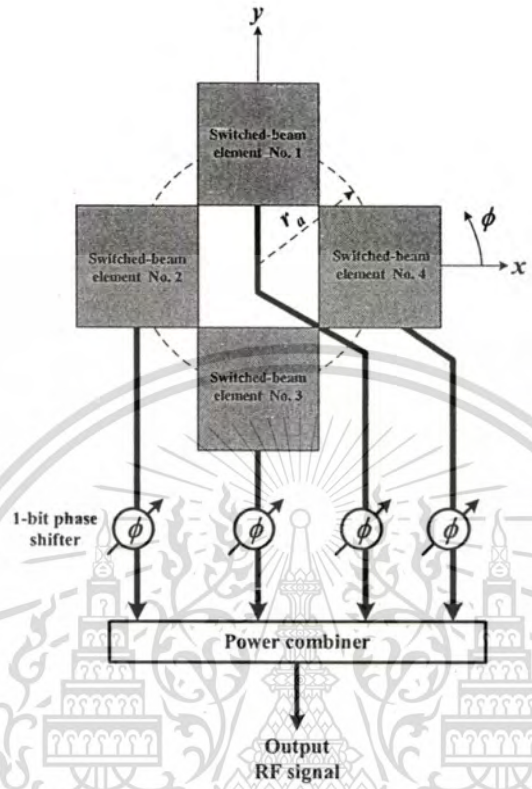

Fig. 3.1 Configuration of the phased array antenna of switched-beam elements.

Table 3.1 Phase excitations of the phased array antenna of switched-beam elements for the four beam directions.

Beam direction ϕ_0 \ Phases	Element No. 1	Element No. 2	Element No. 3	Element No. 4
45°	127.3°	-127.3°	-127.3°	127.3°
135°	127.3°	127.3°	-127.3°	-127.3°
225°	-127.3°	127.3°	127.3°	-127.3°
315°	-127.3°	-127.3°	127.3°	127.3°

3.2.1. Phase shifter

The 1-bit phase shifter having differential phase of 105.4° (phases of ±127.3°) is designed and implemented to switch the beam of the phased array antenna. A switched

delay line phase shifter with two PIN diodes, as described in section 2.3.2, is applied as a 1-bit phase shifter. It is designed on the Rogers RO3003 PCB, with a dielectric constant of 3.0 and a thickness of 0.75 mm, to provide 105.4° phase shift at the designed frequency of 1.95 GHz. The phase shifter is designed and simulated using the IE3D. The PIN diodes, blocking capacitors, dc bias line and dc ground path are included in the simulation. The layout of the designed 1-bit phase shifter is shown in Fig. 3.2. The RF choke is accomplished in the form of a thin zig-zag line, and the lumped chip capacitors are used as blocking capacitors. Two Philips BAP51-02 PIN diodes are used for switching the delay line and matching circuit. There are two dc bias lines in the phase shifter circuit. The one dc bias line is for the phase shifter, and the added one is for the array element that the dc current is driven through the coaxial line connected to the array element to control the PIN diodes for element-pattern switching. The prototype of 1-bit phase shifter is fabricated and tested. The prototype of the designed phase shifter is shown in Fig. 3.3. The characteristics of the designed phase shifter are tested over the operating band of 1.92 – 1.98 GHz using an HP8510C network analyzer. The PIN diodes were biased with +5V dc and 10 mA current. The tested results are shown in Table 3.2. The return loss is better than 16 dB, insertion loss is 1.2 dB and phase error is less than 2° throughout the operating band.

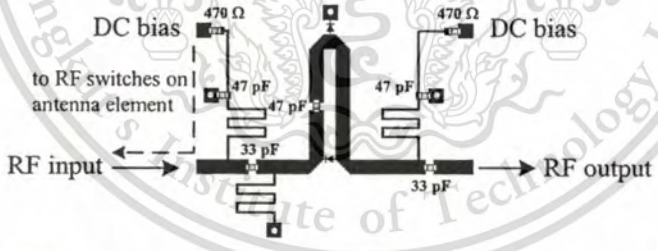

Fig. 3.2 Layout of the designed 1-bit phase shifter.

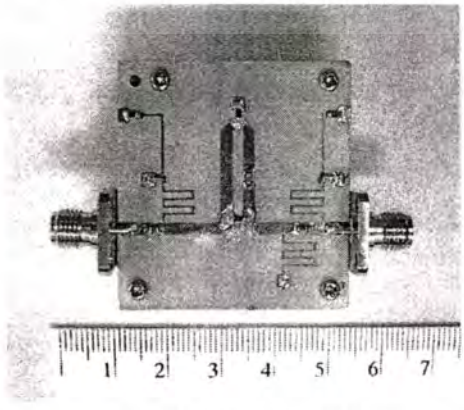

Fig. 3.3 Prototype of the designed 1-bit phase shifter.

Table 3.2 Characteristics of the designed phase shifter.

frequency (GHz)	Return Loss (dB)	Insertion Loss (dB)	Phase Errors
1.92	16.28	1.20	-1.9°
1.95	17.41	1.20	-1.3°
1.98	18.71	1.21	-0.5°

3.2.2. Wilkinson power combiner

The Wilkinson power divider/combiner is a lossy three-port network that can be made having all ports matched with isolation between the output ports. The transmission line model of an equal-split Wilkinson power divider/combiner can be shown in Fig. 3.4. For a 50-Ω system impedance (Z_0 = 50 Ω), the quarter-wave lines have characteristic impedance of 70.7 Ω and shunt resistance is 100 Ω. In this work, a four-way Wilkinson power combiner is employed to combine the received signals of four array elements. It is also designed and fabricated on the Rogers RO3003 PCB. The prototype of a four-way power combiner is shown in Fig. 3.5. The characteristics of the power combiner are tested using an HP8510C network analyzer. The return loss is 20 dB, insertion loss is 6.6 dB and isolation is 17 dB.

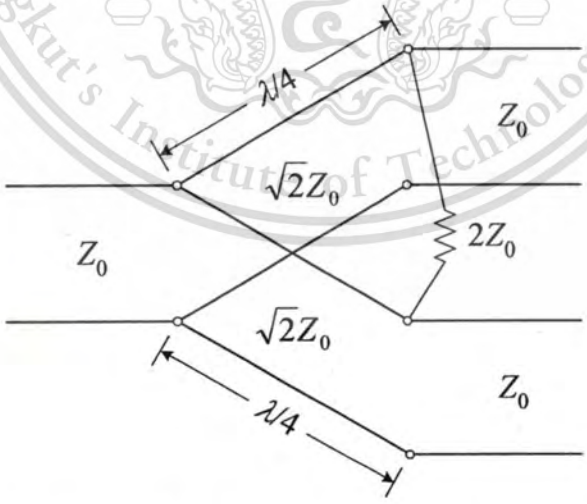

Fig. 3.4 The transmission line model of an equal-split Wilkinson power divider/combiner.

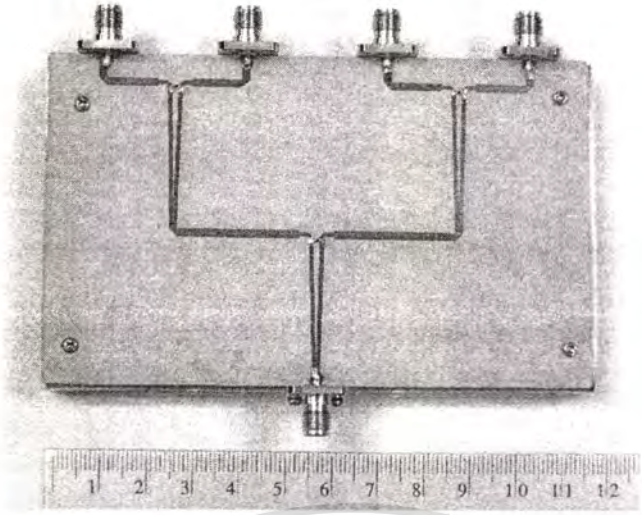

Fig. 3.5 Prototype of the four-way power combiner.

3.3 Antenna characteristics

Having obtained satisfactory characteristics of individual components including switched-beam elements, 1-bit phase shifters and power combiner, the entire phased array antenna of switched-beam elements is developed. The prototype of the phased array antenna of switched-beam elements is shown in Fig. 3.6. Four switched-beam elements are arranged as a circular array with the radius of 7.6 cm. Each switched-beam element, with the dimension of 7.6×7.6 cm^2, is connected to the phase shifter via coaxial line, and the received signals of four elements are combined by the four-way power combiner. Since the switched-beam element, which can provide the two-beam switching in x and y directions, was applied as the array element, the degree of freedom of the phase array antenna of switched-beam elements can be increased by various combinations of the element patterns. Four switched-beam elements provide $2^4 = 16$ combinations of the element patterns as the four-beam switching of the phased array antenna of switched-beam elements is also realized by using the phase shifters. Accordingly, one main beam direction possesses 16 null patterns with respect to 16 combinations. Therefore, the phased array antenna of switched-beam elements gives 64 radiation patterns, which are four main beam patterns with 16 changeable null patterns. The array characteristics were evaluated by simulations and measurements. The VSWR and radiation patterns of the phased array antenna of switched-beam elements are presented.

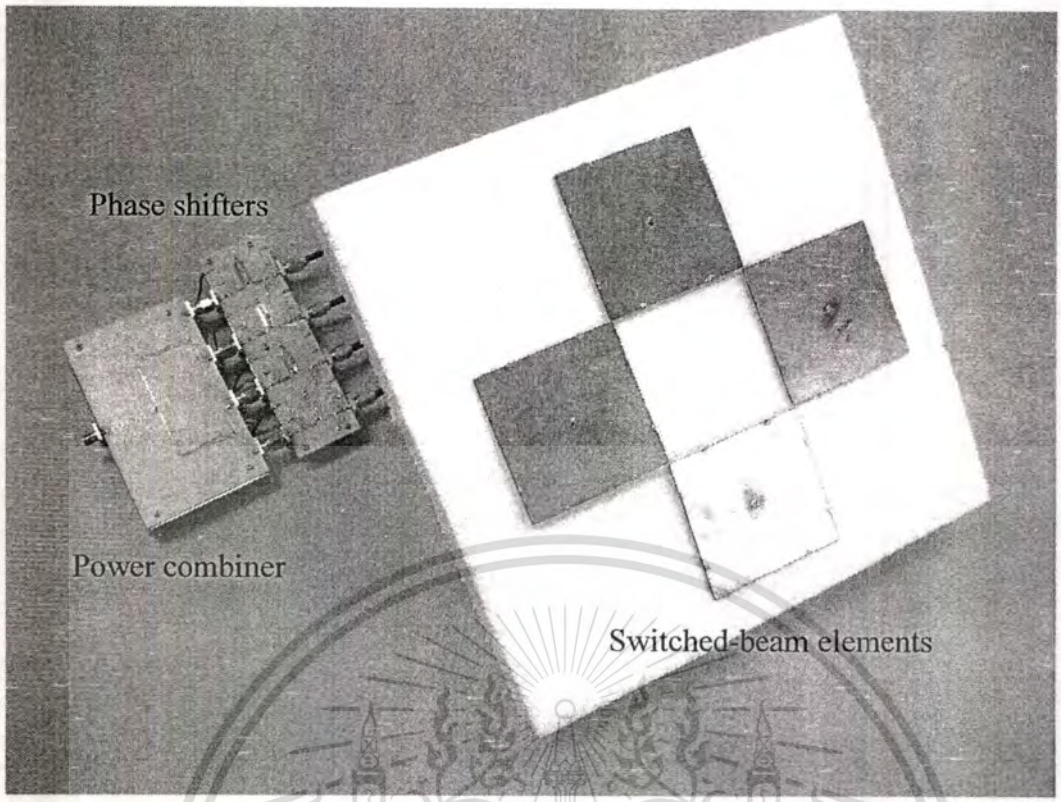

Fig. 3.6 Prototype of the phased array antenna of switched-beam elements.

3.3.1 VSWR

VSWR of the phased array antenna of switched-beam elements is investigated experimentally. The VSWR is measured using an HP8510C network analyzer. The measurement is done over the frequency of 1.8 – 2.1 GHz. In case that the main beam is switched, the result of VSWR as a function of frequency for the four-beam switching with the *x x x x* combination, for which the beam direction of four switched-beam elements are switched in *x* direction, is shown in Fig. 3.7. It can be seen that the VSWR is less than 2:1. At the design frequency of 1.95 GHz, the VSWR of 1.48, 1.59, 1.69 and 1.53 are obtained for the main beam switched to 45°, 135°, 225° and 315°, respectively. Furthermore, VSWR of the phased array antenna of switched-beam elements is measured when the combination of element patterns is changed. The measured results of VSWR with the *x x x y*, *y x x y*, *x y y y* and *y y y y* combinations are presented in Fig. 3.8. The main beam direction is 45°. The VSWR < 2:1 is also observed in this case. At the design frequency of 1.95 GHz, the VSWR of 1.44, 1.45, 1.40 and 1.42 are obtained. The results show that the VSWR of the phased array antenna of switched-beam elements is slightly affected by switching the main beam and changing of the combinations of element patterns.

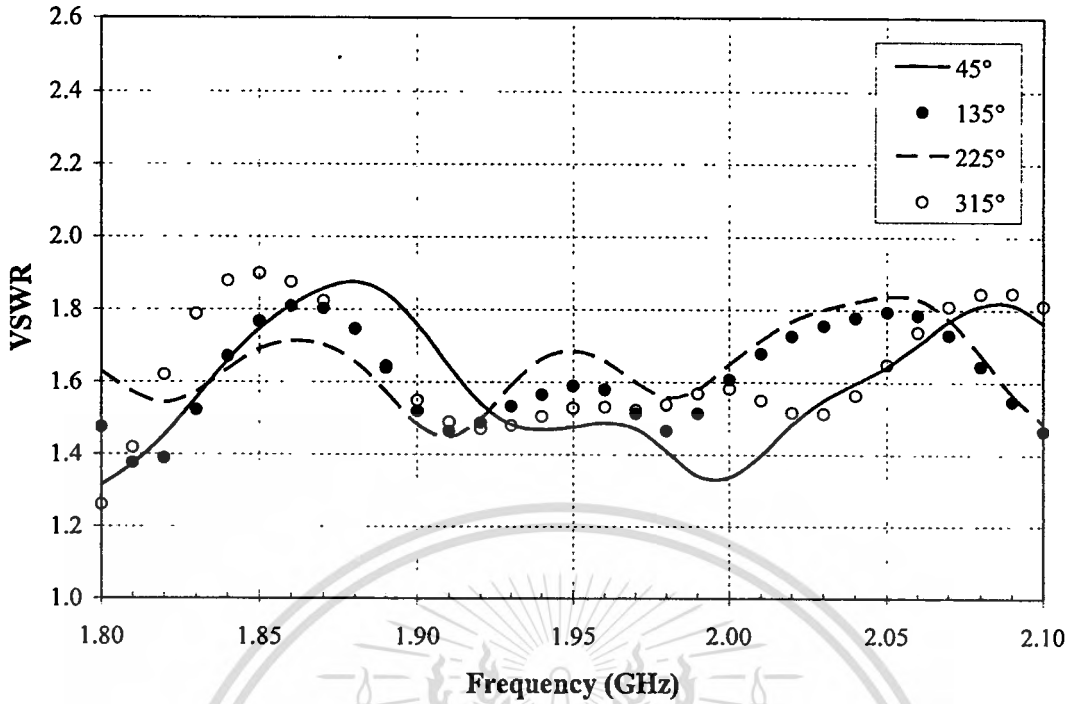

Fig. 3.7 VSWR of the phased array antenna of switched-beam elements for four-beam direction with the *x x x x* combination.

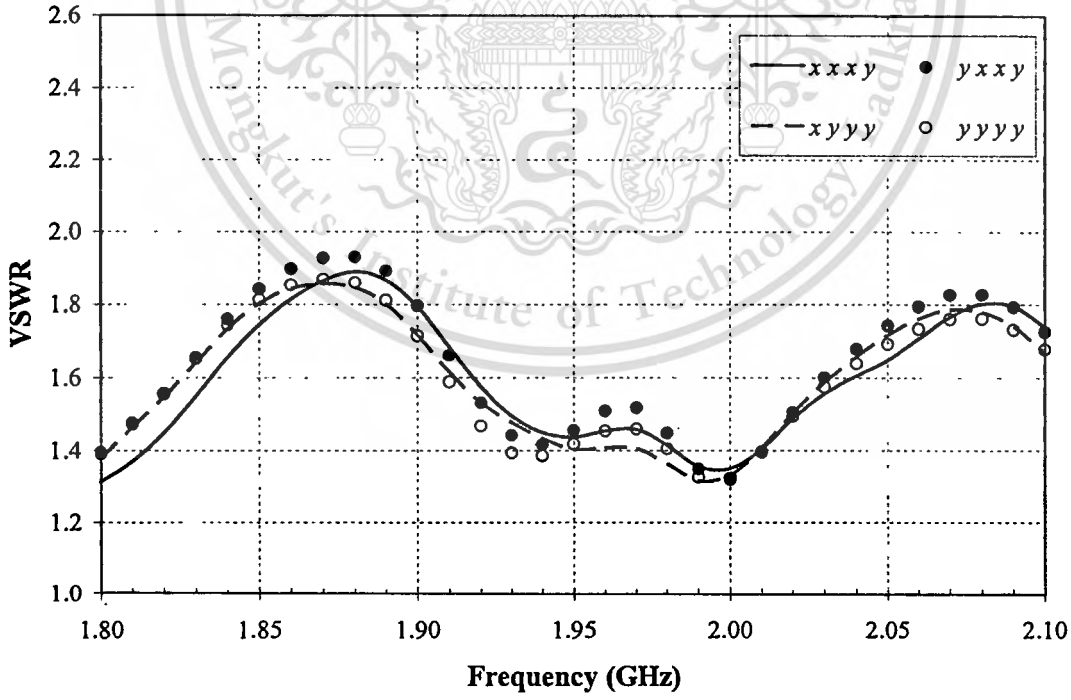

Fig. 3.8 VSWR of the phased array antenna of switched-beam elements for 45° beam direction with various combinations of element patterns.

3.3.2 Radiation patterns

The radiation pattern of the phased array antenna of switched-beam elements is investigated at the frequency of 1.95 GHz. First, the radiation patterns for the four-beam switching with 16 combinations of element patterns are simulated using the IE3D simulator. Four switched-beam elements are arranged as a circular array with the radius of 7.6 cm. The PIN diode models are applied to switch the beam of each element, so that the combination of element patterns can be changed by applying the appropriate PIN diode models to each switched-beam element. The uniform amplitude and different phase of excitation are assigned for each element to obtain the main beam in specified direction. In the next step, the radiation patterns of the phased array antenna of switched-beam elements are measured in an in-house anechoic chamber using an HP8510C network analyzer. The patch antenna with single linear polarization is employed as the transmitting antenna. The antenna under test is mounted on a turntable separated from the transmitting antenna by a distance of 1.5 m. The *H*-plane (*xy*-plane) patterns of the phased array antenna of switched-beam elements are measured. The simulation and measurement are compared and shown in Fig. 3.9 – Fig. 3.24. The radiation patterns of 16 combinations are plotted.

Both the simulated and measured results show that the main beam of the phased array antenna of switched-beam elements can be switched, and the different combination of element patterns given by the beam switching of element can change the null patterns. Since the elements have directional pattern, the increasing number of nulls and narrow beamwidth are observed as well as high side lobe level.

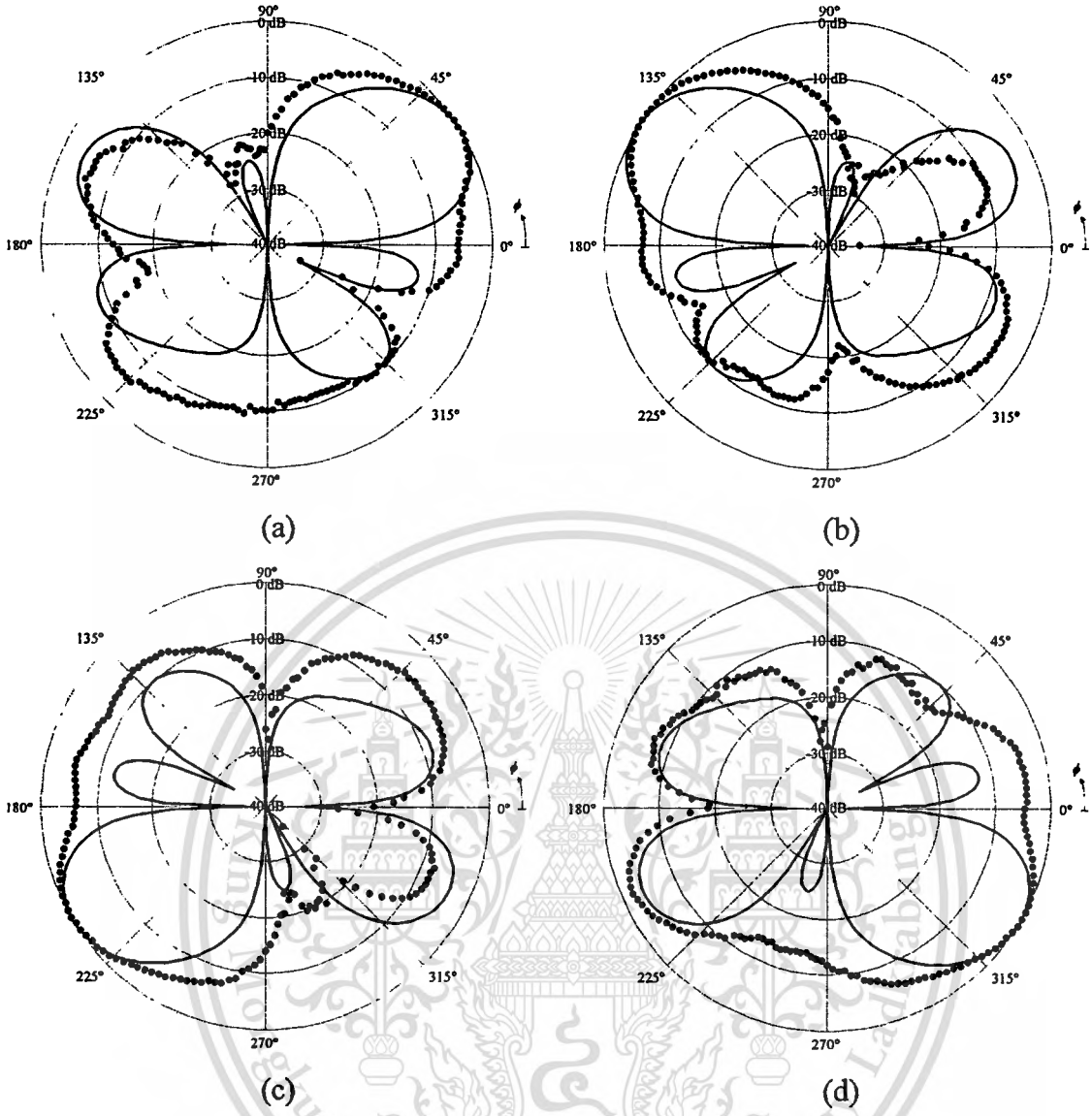

Fig. 3.9 Array patterns with the *x x x x* combination: (a) 45° beam direction, (b) 135° beam direction, (c) 225° beam direction, and (d) 315° beam direction.
——simulation, ● measurement

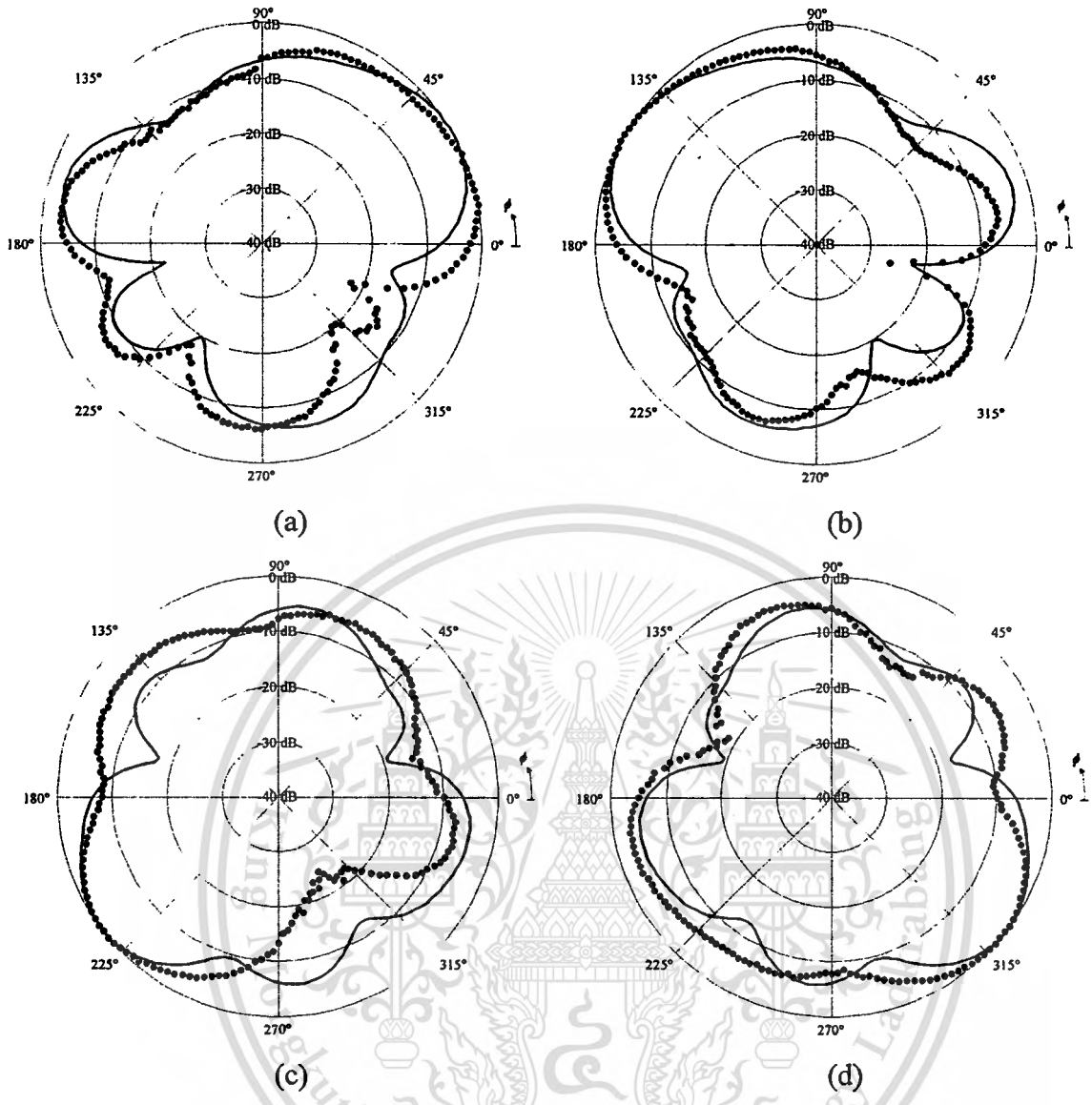

Fig. 3.10 Array patterns with the *y x x x* combination: (a) 45° beam direction, (b) 135° beam direction, (c) 225° beam direction, and (d) 315° beam direction.
—— simulation, ● measurement

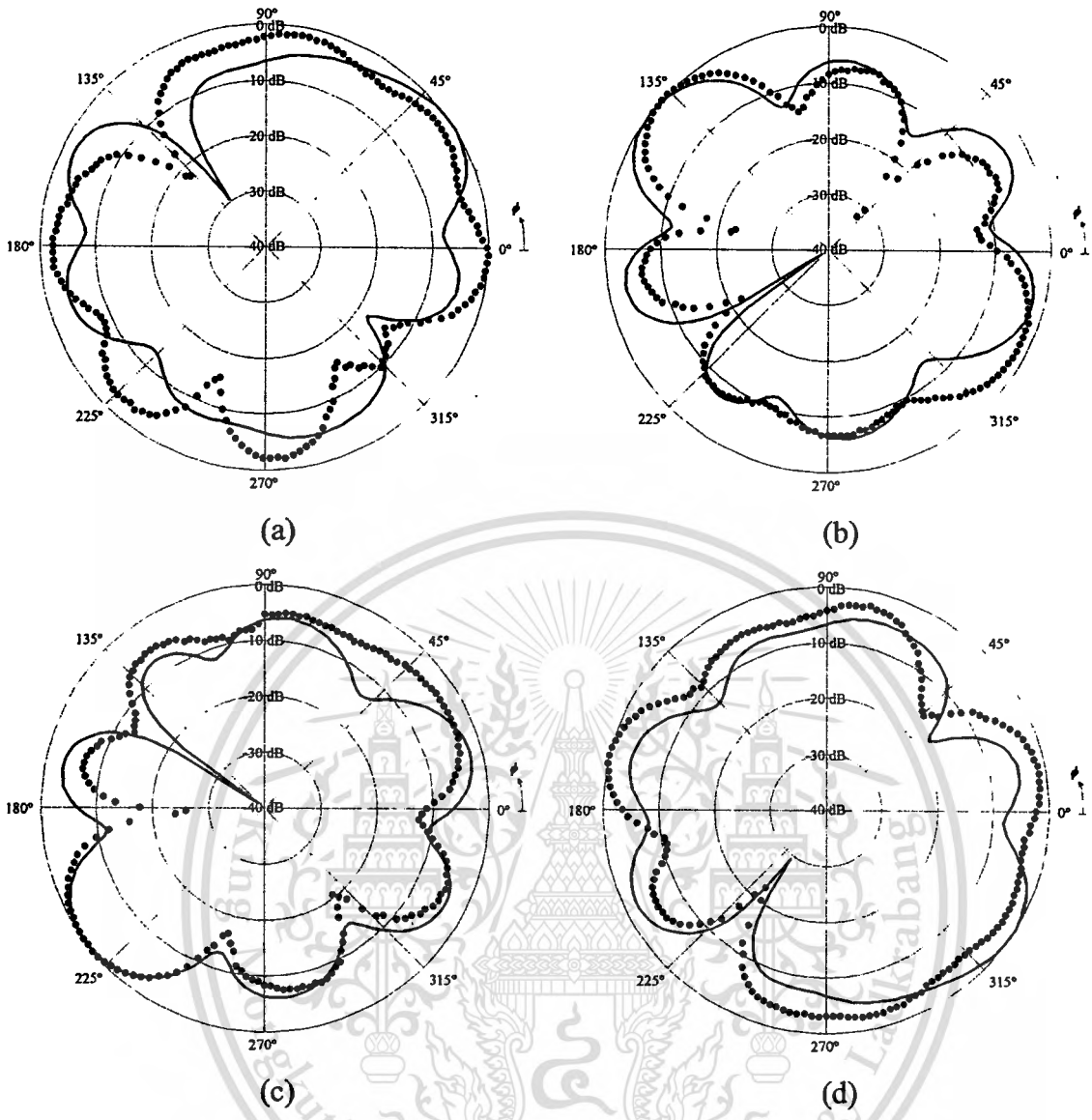

Fig. 3.11 Array patterns with the *x y x x* combination: (a) 45° beam direction, (b) 135° beam direction, (c) 225° beam direction, and (d) 315° beam direction.
—— simulation, ● measurement

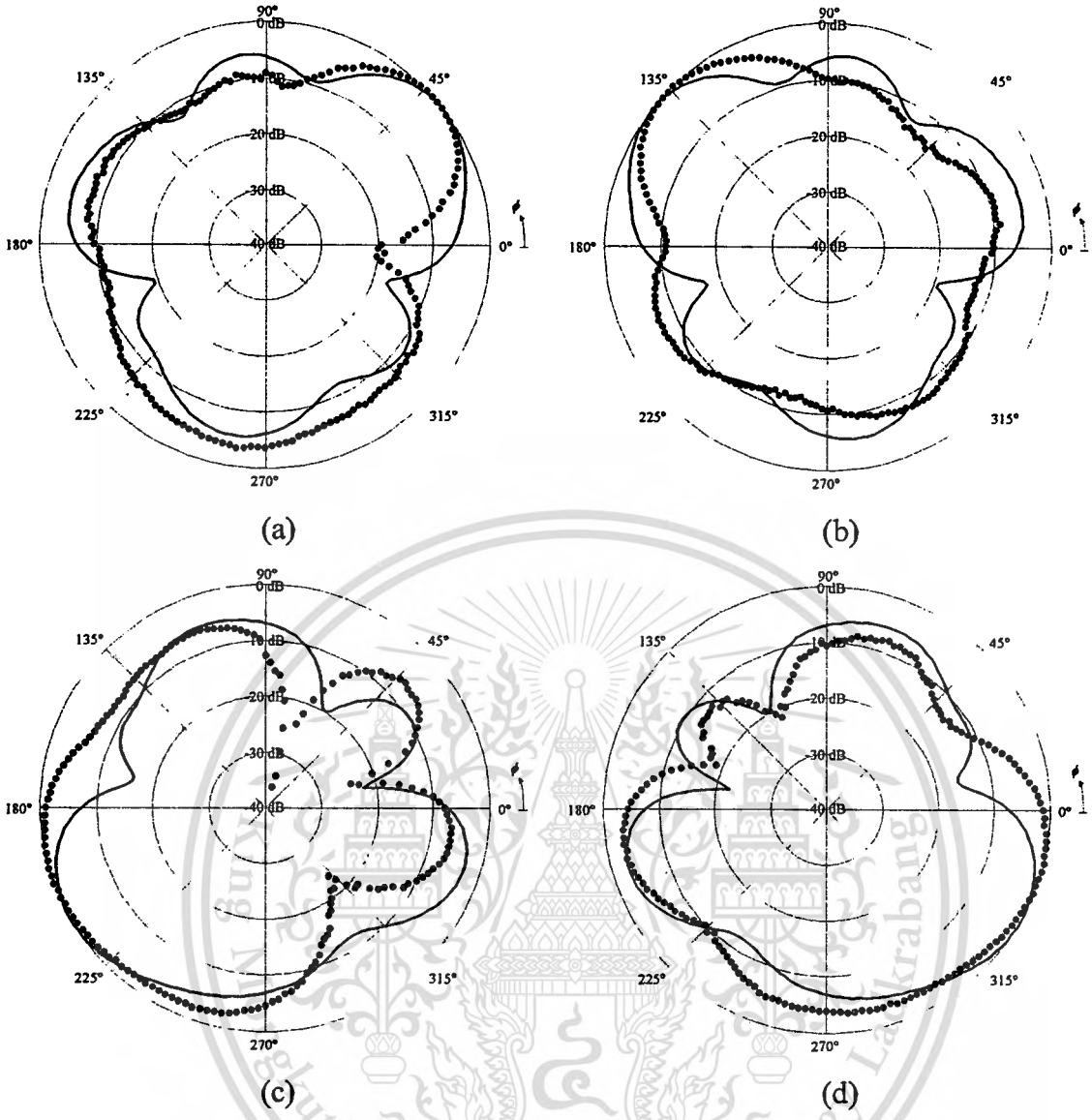

Fig. 3.12 Array patterns with the *x x y x* combination: (a) 45° beam direction, (b) 135° beam direction, (c) 225° beam direction, and (d) 315° beam direction.
—— simulation, ● measurement

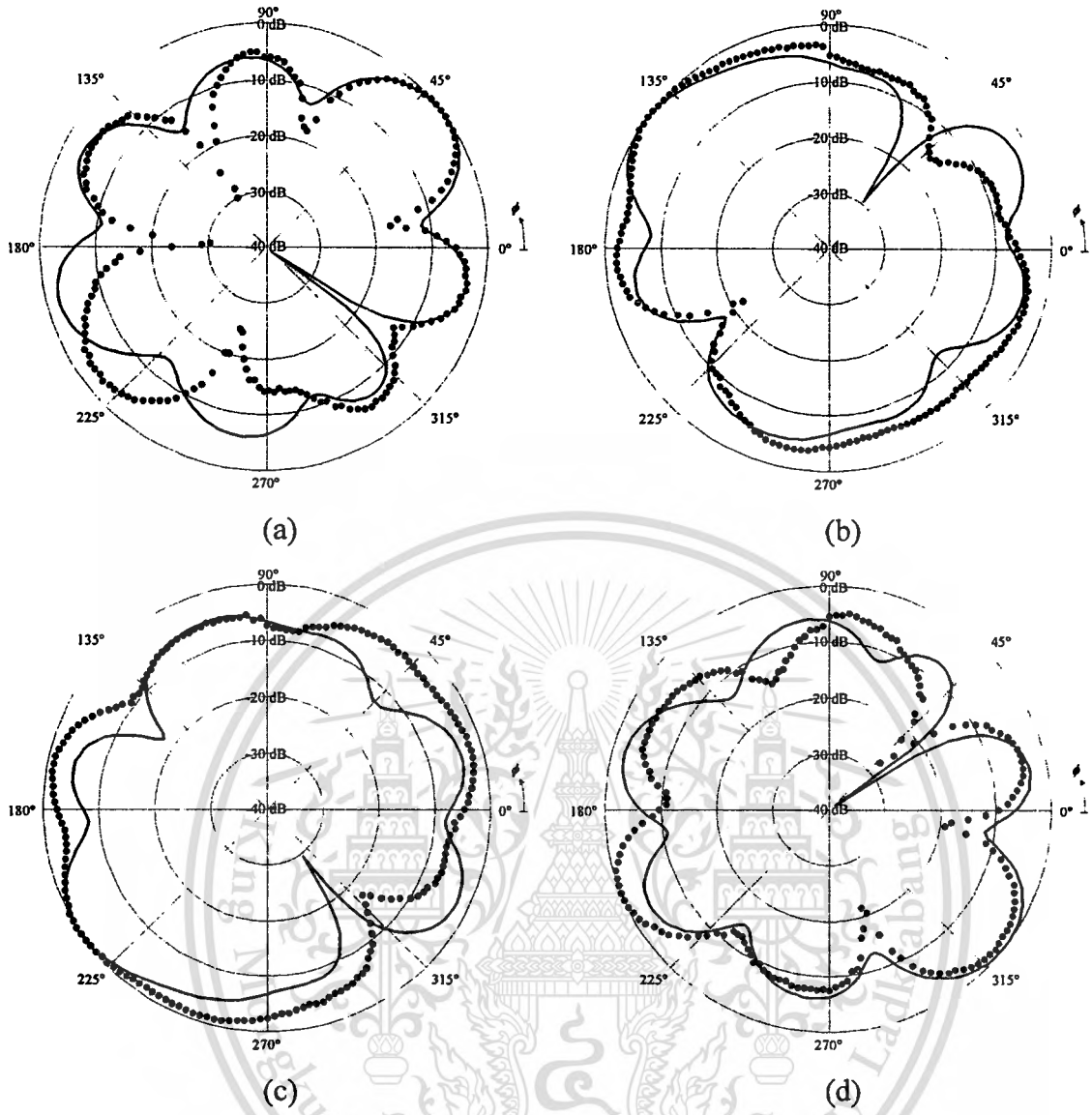

Fig. 3.13 Array patterns with the *x x x y* combination: (a) 45° beam direction, (b) 135° beam direction, (c) 225° beam direction, and (d) 315° beam direction.
—— simulation, ● measurement

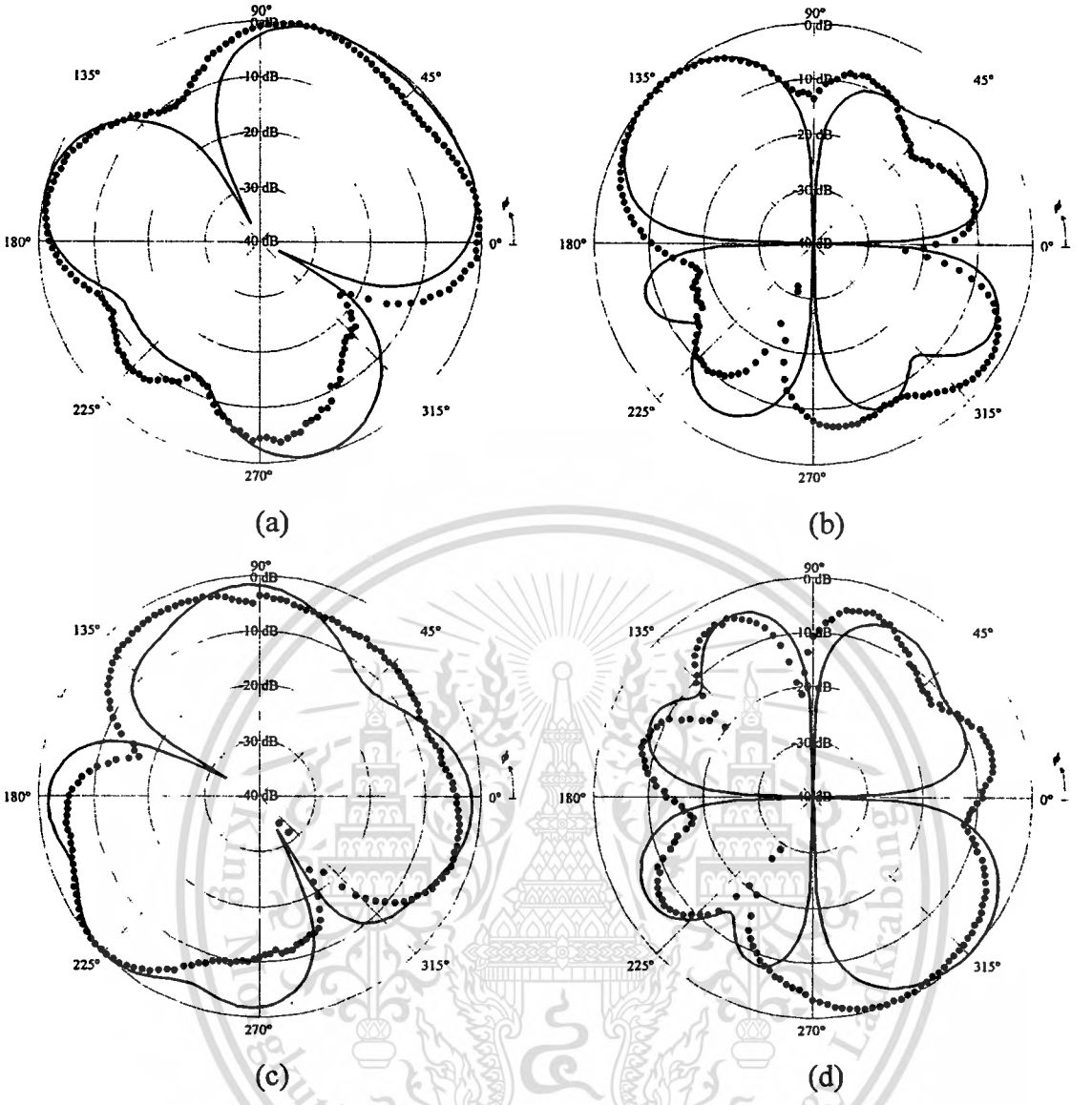

Fig. 3.14 Array patterns with the *y y x x* combination: (a) 45° beam direction, (b) 135° beam direction, (c) 225° beam direction, and (d) 315° beam direction.
—— simulation, ● measurement

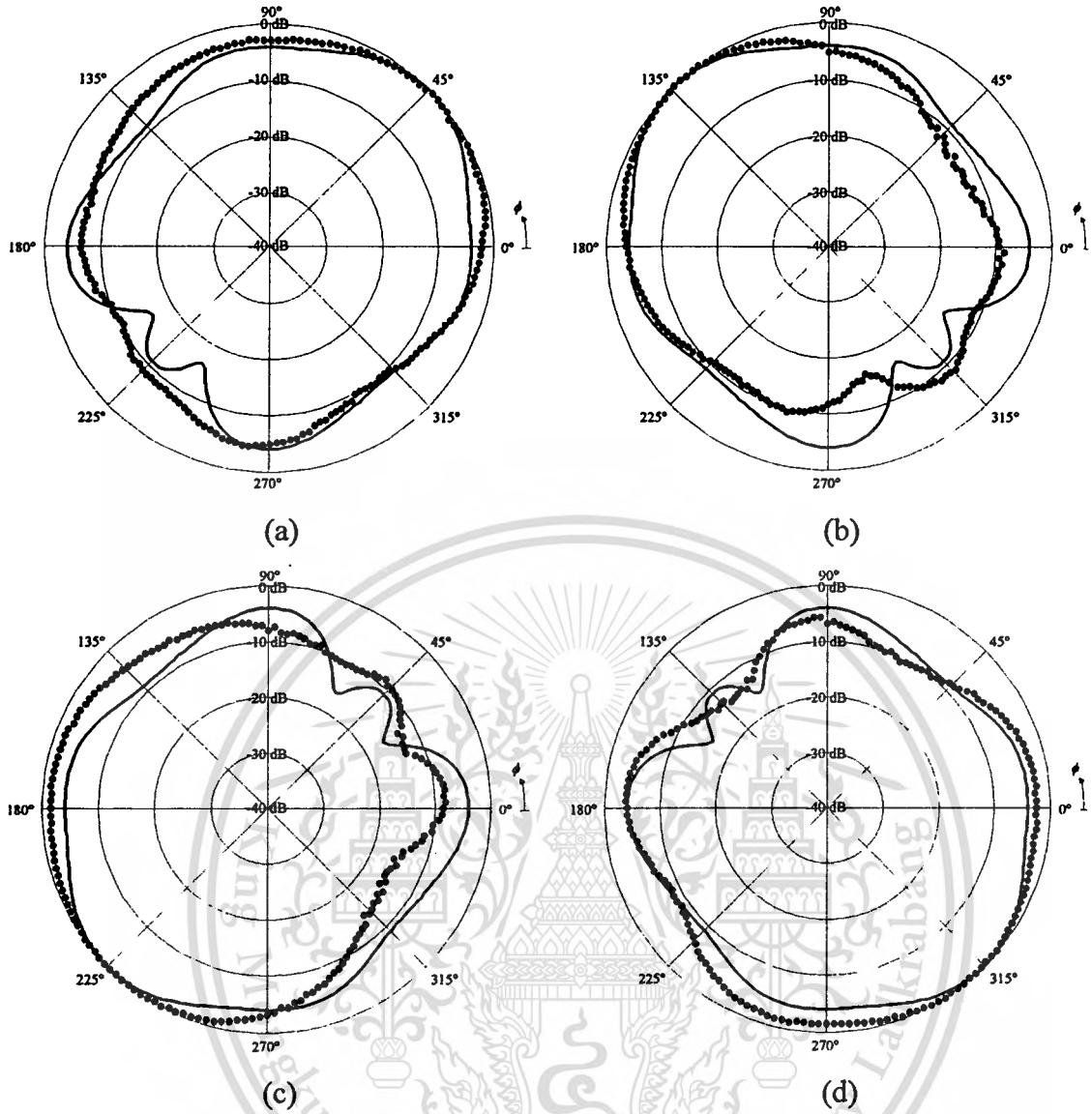

Fig. 3.15 Array patterns with the *y x y x* combination: (a) 45° beam direction, (b) 135° beam direction, (c) 225° beam direction, and (d) 315° beam direction.
—— simulation, ● measurement

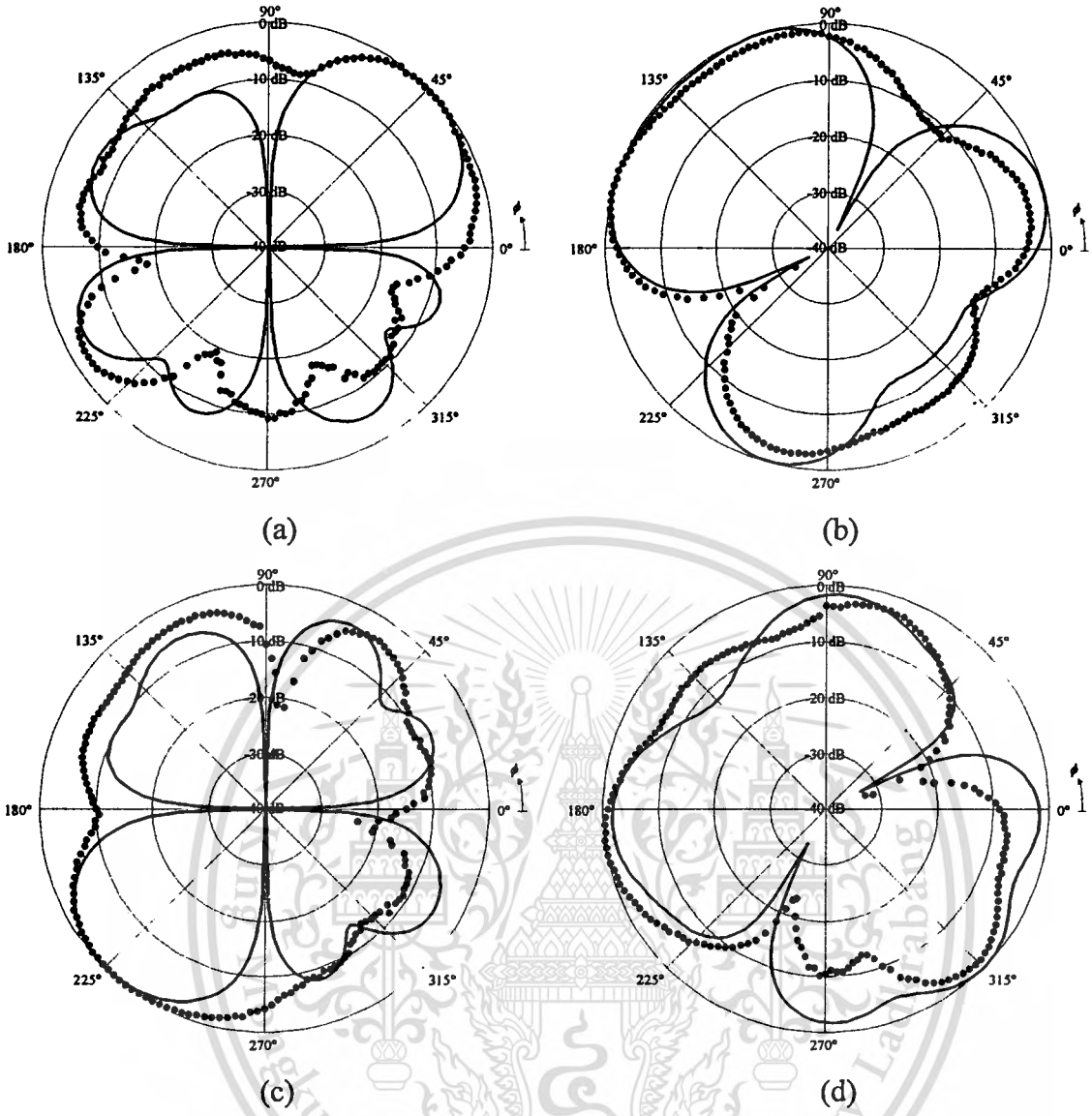

Fig. 3.16 Array patterns with the *y x x y* combination: (a) 45° beam direction, (b) 135° beam direction, (c) 225° beam direction, and (d) 315° beam direction.
—— simulation, ● measurement

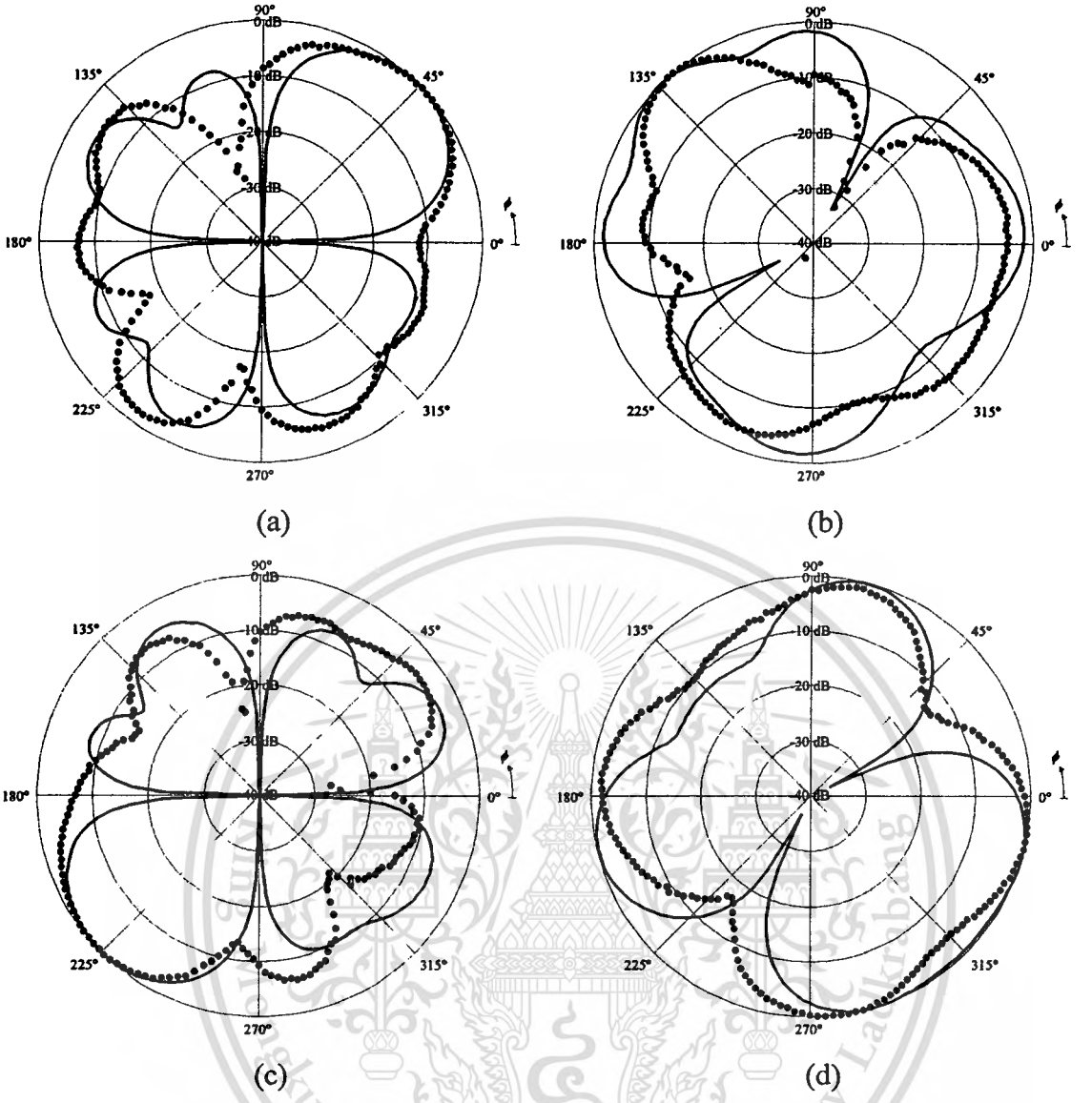

Fig. 3.17 Array patterns with the *x y y x* combination: (a) 45° beam direction, (b) 135° beam direction, (c) 225° beam direction, and (d) 315° beam direction.
—— simulation, ● measurement

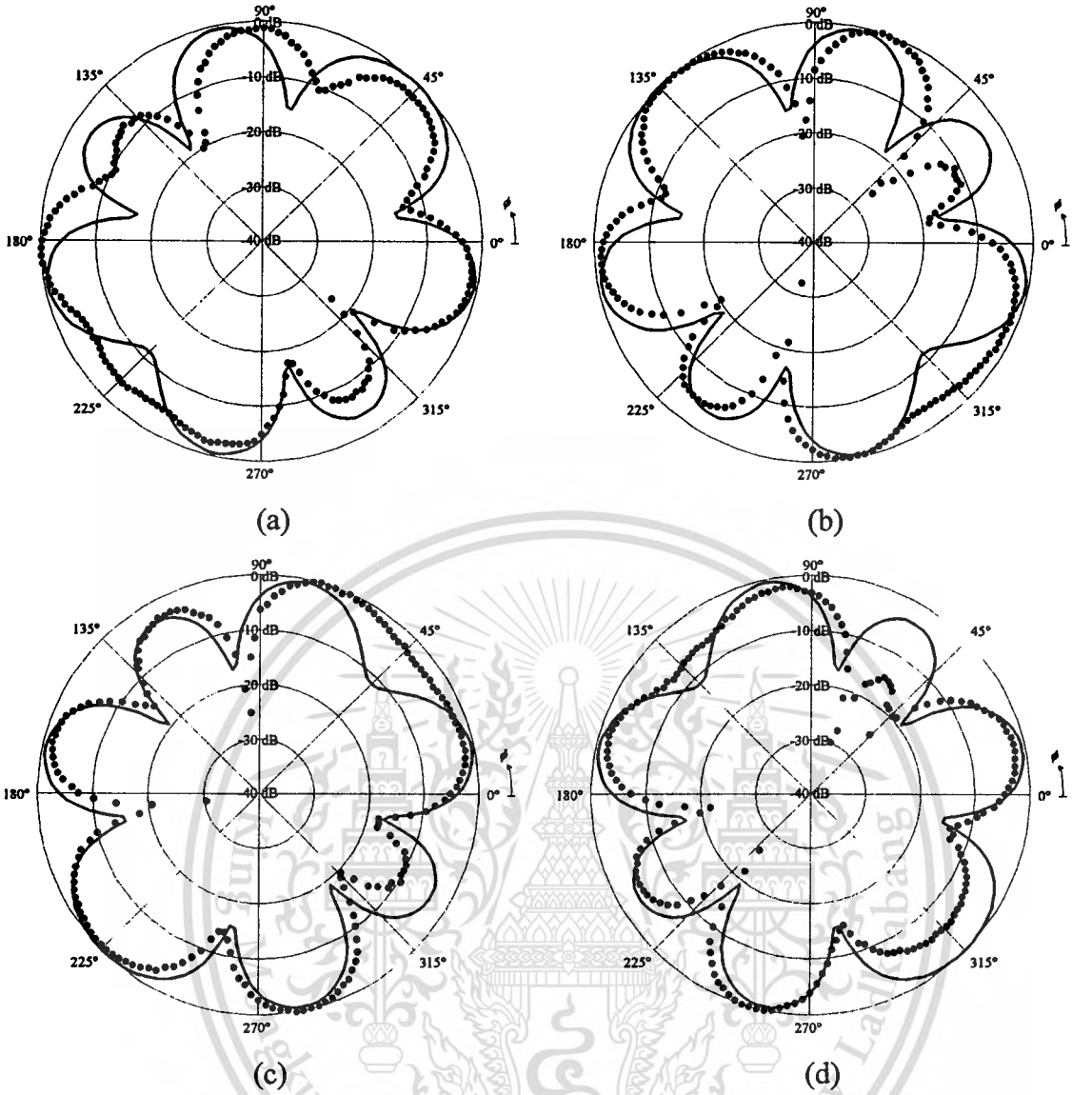

Fig. 3.18 Array patterns with the *x y x y* combination: (a) 45° beam direction, (b) 135° beam direction, (c) 225° beam direction, and (d) 315° beam direction.
—— simulation, ● measurement

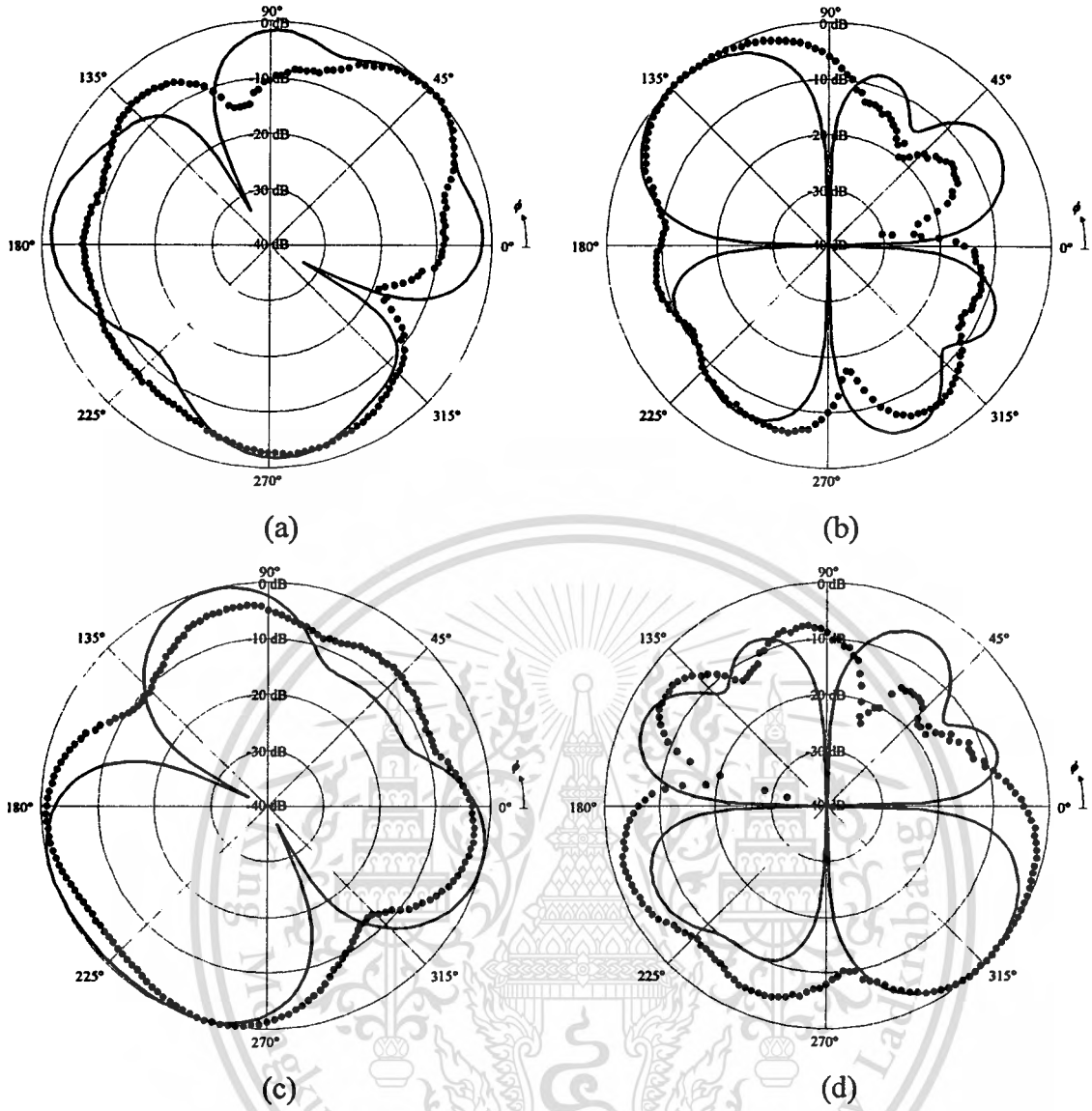

Fig. 3.19 Array patterns with the *x x y y* combination: (a) 45° beam direction, (b) 135° beam direction, (c) 225° beam direction, and (d) 315° beam direction.
—— simulation, ● measurement

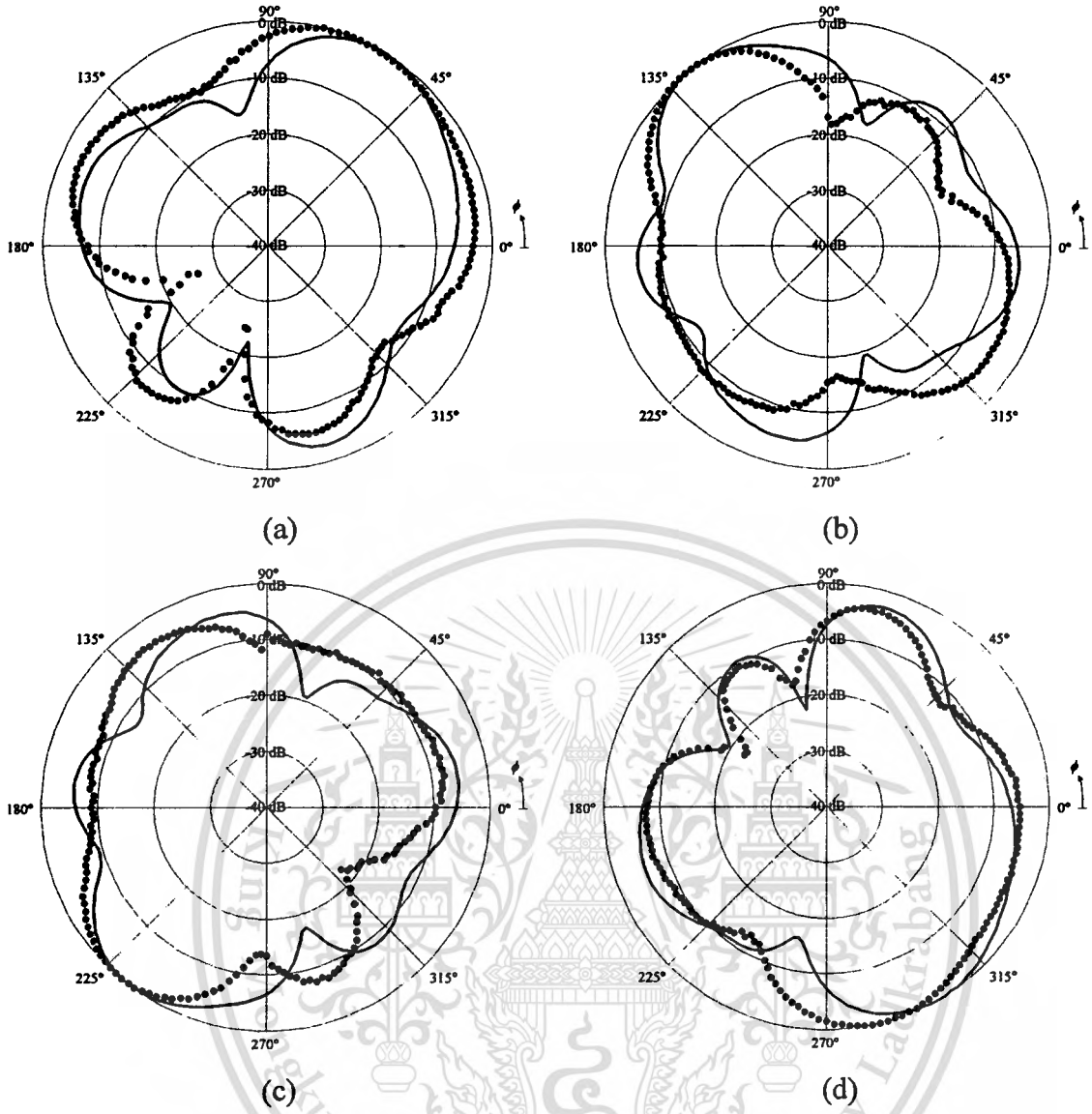

Fig. 3.20 Array patterns with the *y y y x* combination: (a) 45° beam direction, (b) 135° beam direction, (c) 225° beam direction, and (d) 315° beam direction.
—— simulation, ● measurement

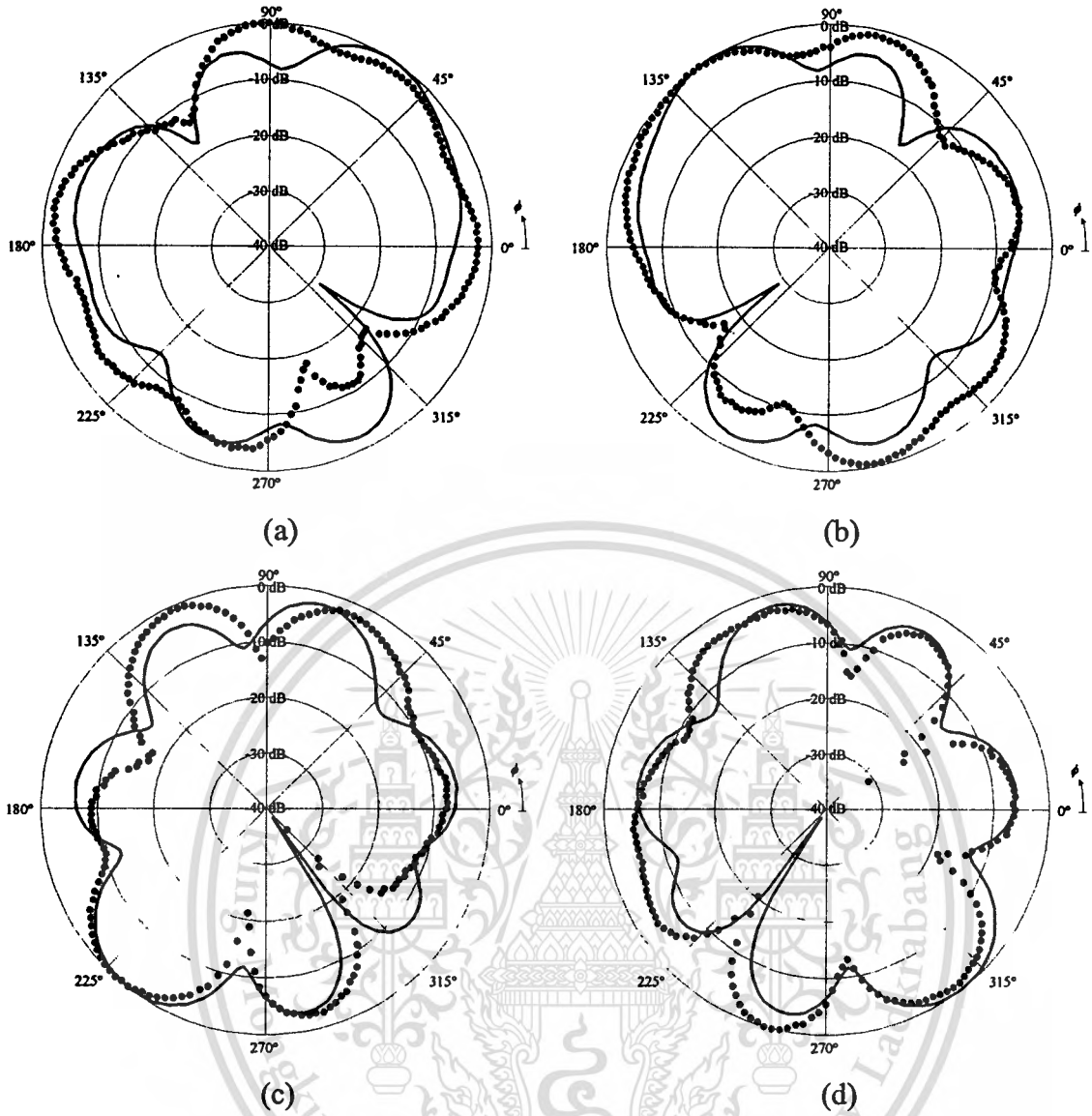

Fig. 3.21 Array patterns with the *y y x y* combination: (a) 45° beam direction, (b) 135° beam direction, (c) 225° beam direction, and (d) 315° beam direction.
—— simulation, ● measurement

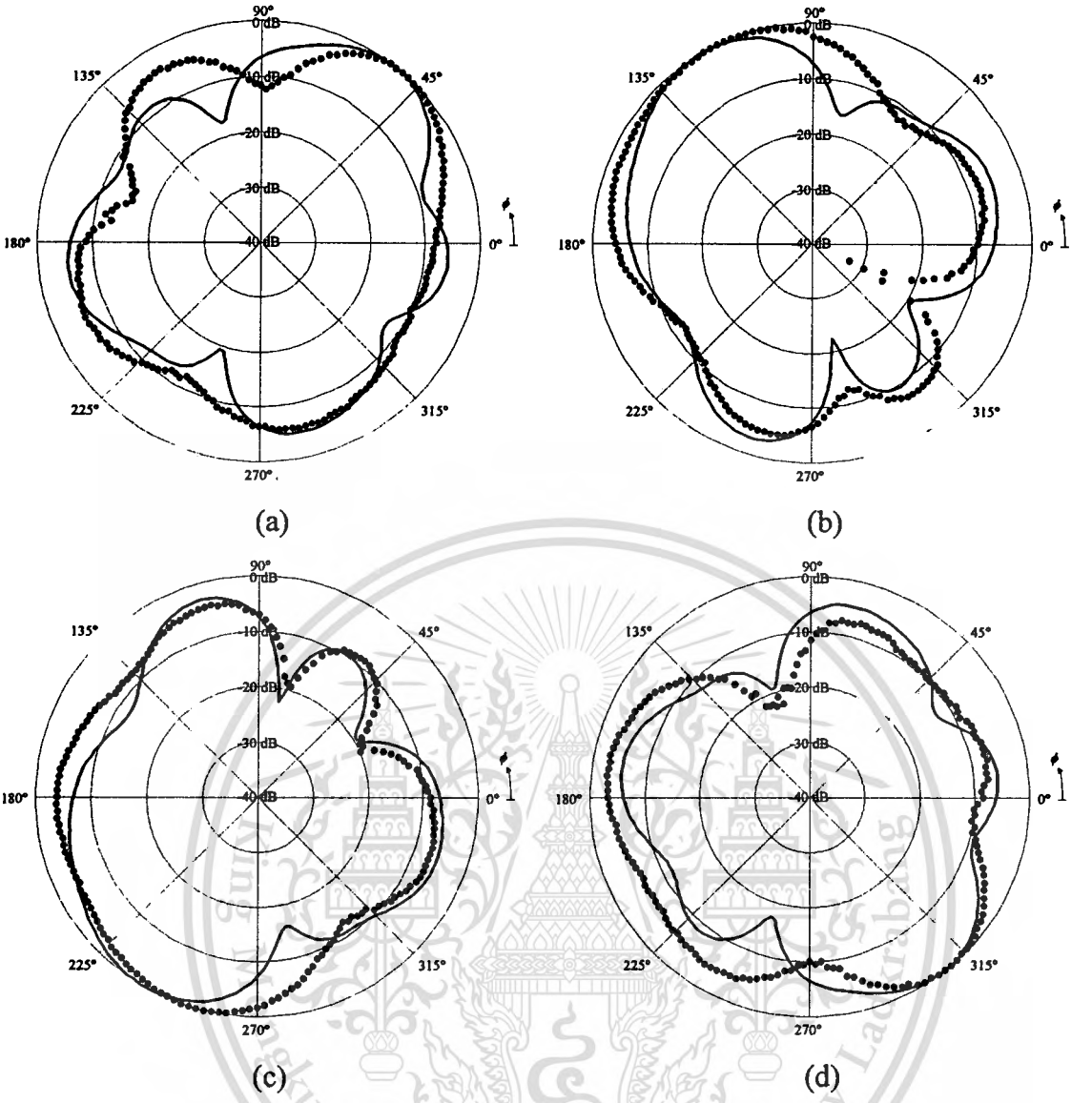

Fig. 3.22 Array patterns with the *y x y y* combination: (a) 45° beam direction, (b) 135° beam direction, (c) 225° beam direction, and (d) 315° beam direction.
—— simulation, ● measurement

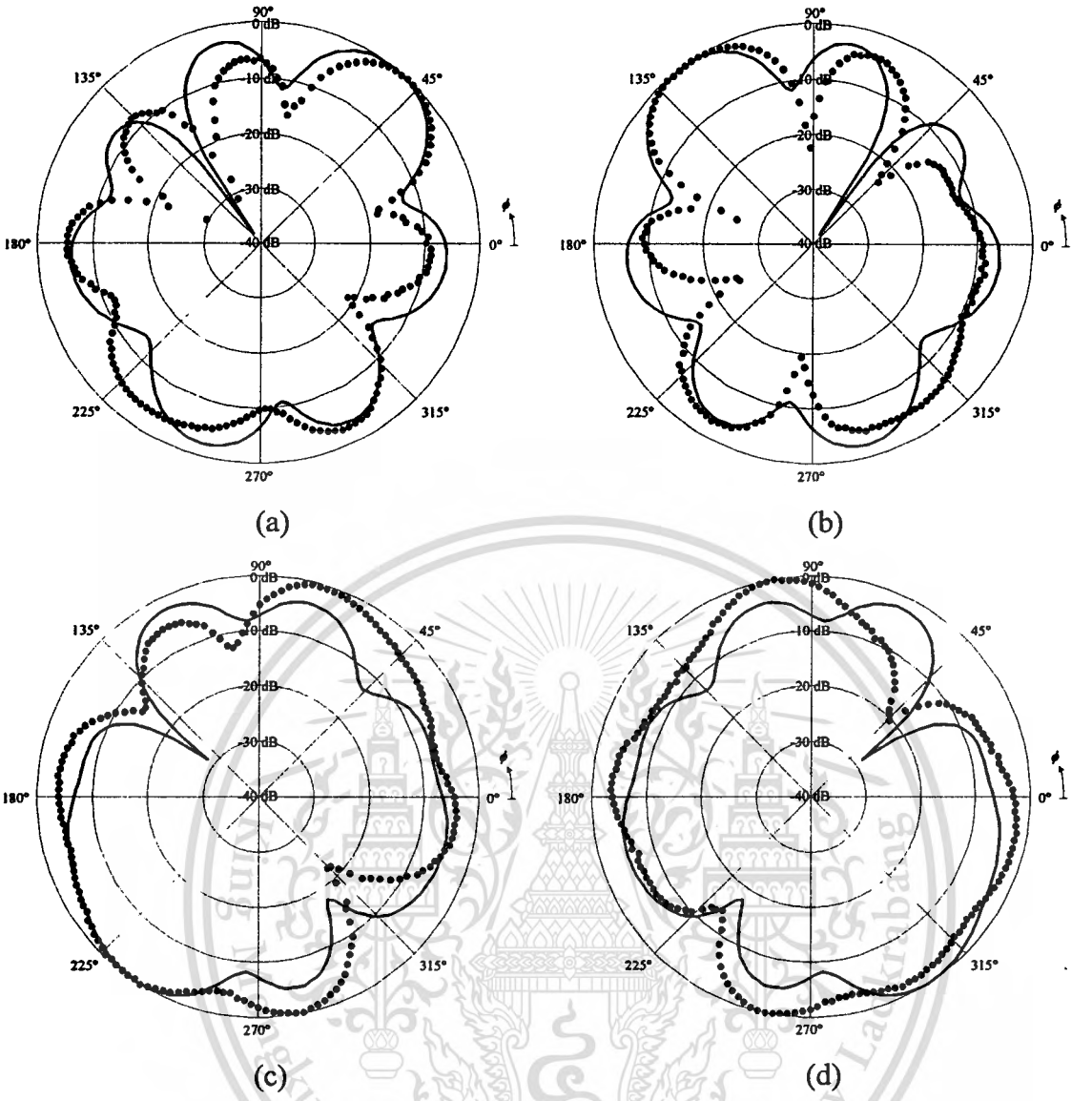

Fig. 3.23 Array patterns with the *x y y y* combination: (a) 45° beam direction, (b) 135° beam direction, (c) 225° beam direction, and (d) 315° beam direction.
—— simulation, ● measurement

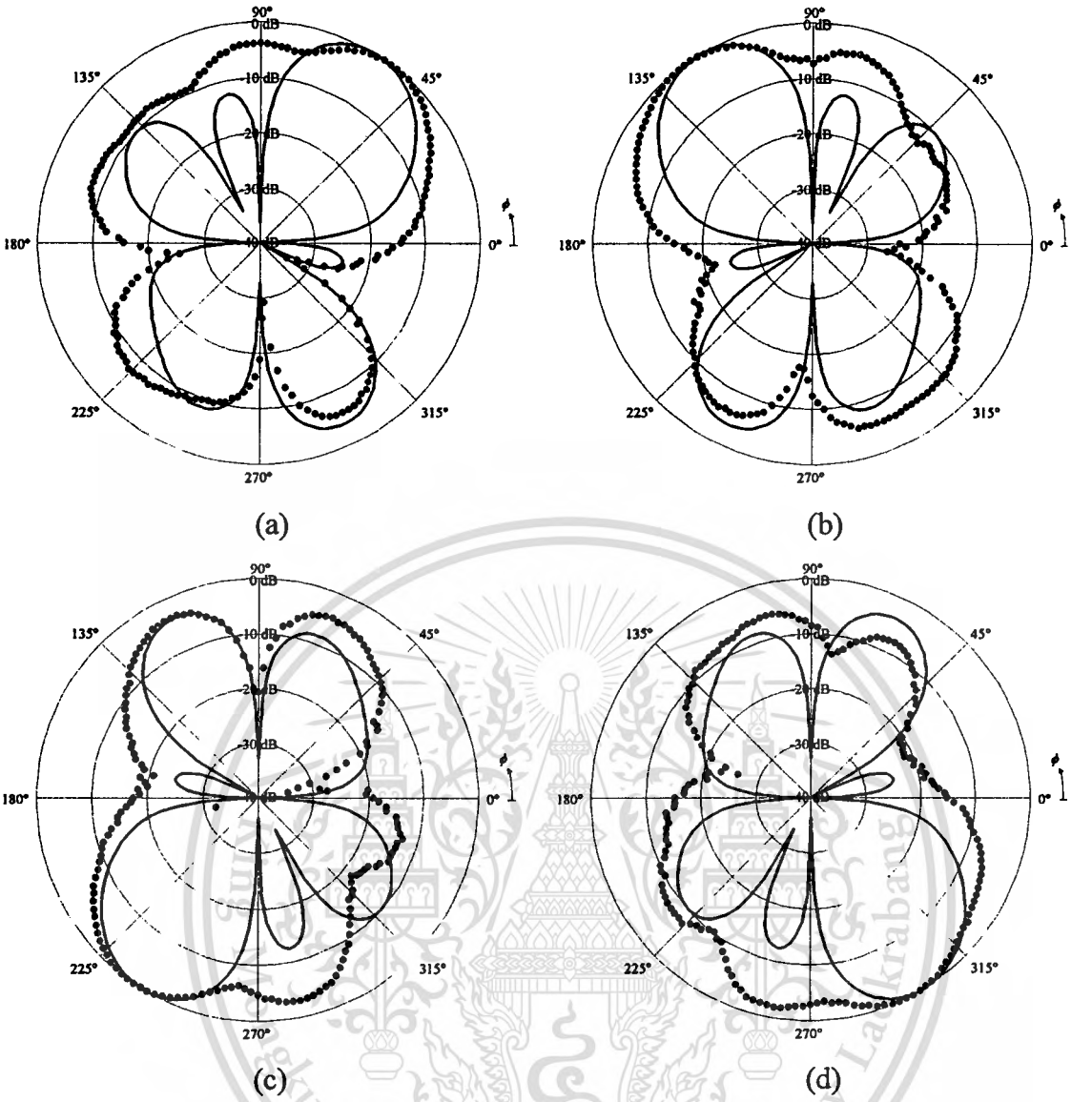

Fig. 3.24 Array patterns with the *y y y y* combination: (a) 45° beam direction, (b) 135° beam direction, (c) 225° beam direction, and (d) 315° beam direction.
——— simulation, ● measurement

3.3.2.1 Distributions of nulls

The distributions of null directions given by the different combinations of element patterns are summarized in Fig. 3.25 – Fig.3.28 for the four main beam directions of 45°, 135°, 225° and 315°. Considering the measured radiation patterns, the levels of null lower than -20 dB are considered and plotted. It can be seen that the null direction can be changed by different combinations of element patterns. Not only the main beam is switched, but also the null directions can be varied. The results show that for each switched beam direction the null directions are distributed diversely due to various combinations of element patterns.

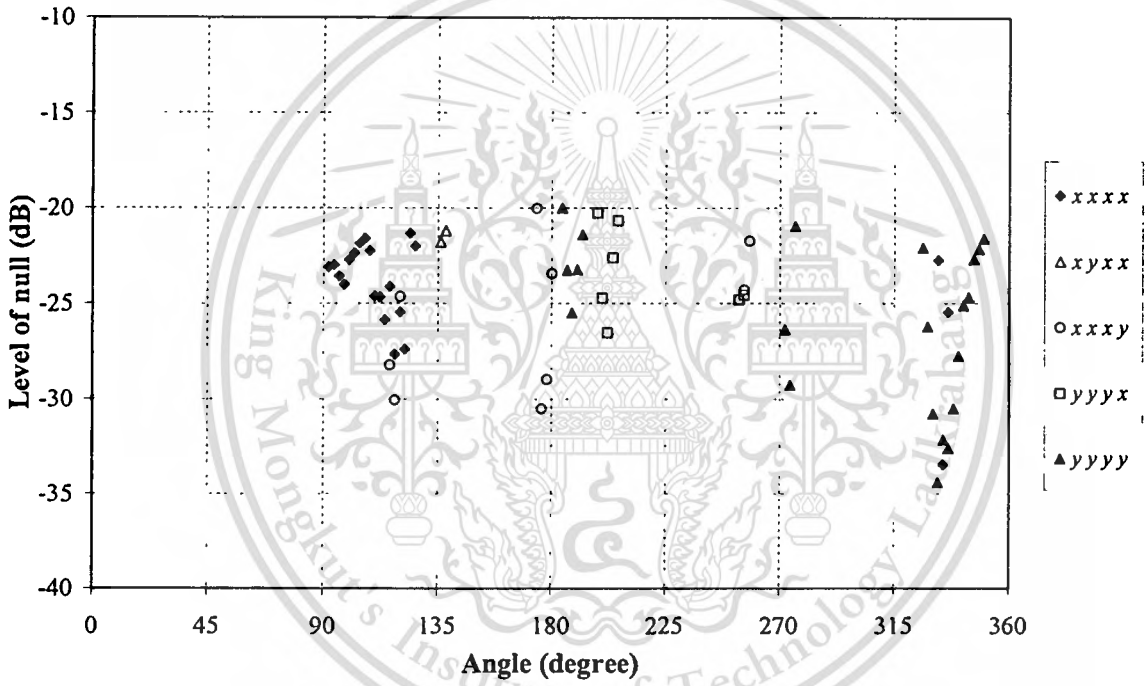

Fig. 3.25 Distribution of null directions obtained for the different combinations of element patterns for the 45° main beam direction.

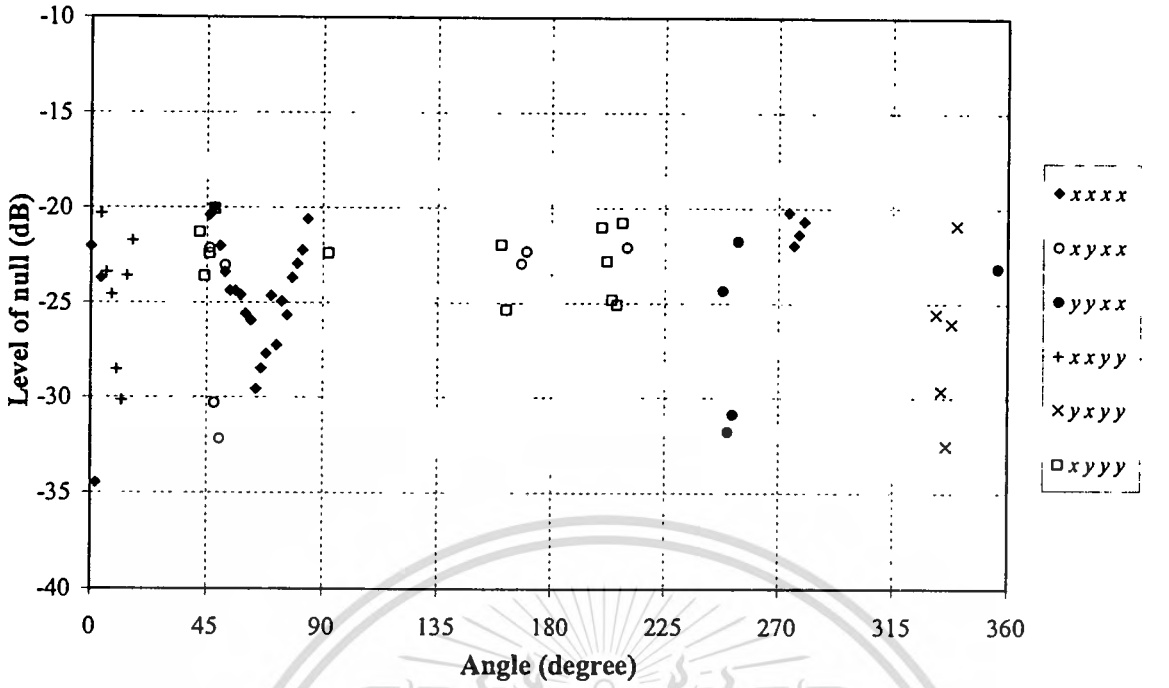

Fig. 3.26 Distribution of null directions obtained for the different combinations of element patterns for the 135° main beam direction.

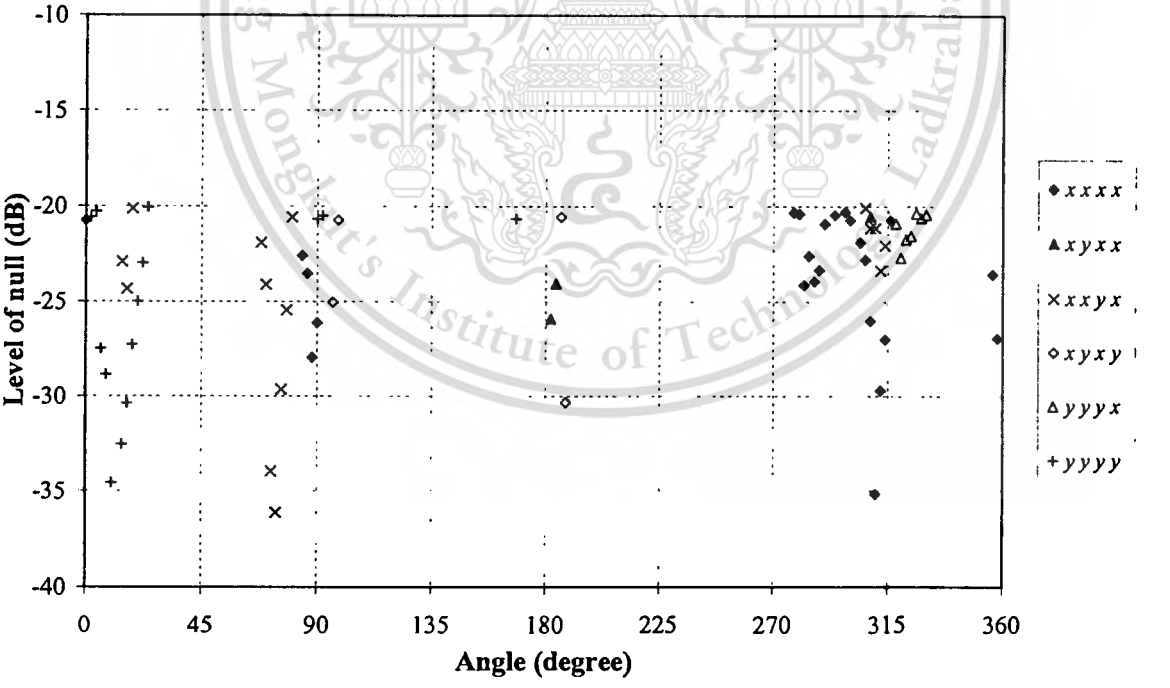

Fig. 3.27 Distribution of null directions obtained for the different combinations of element patterns for the 225° main beam direction.

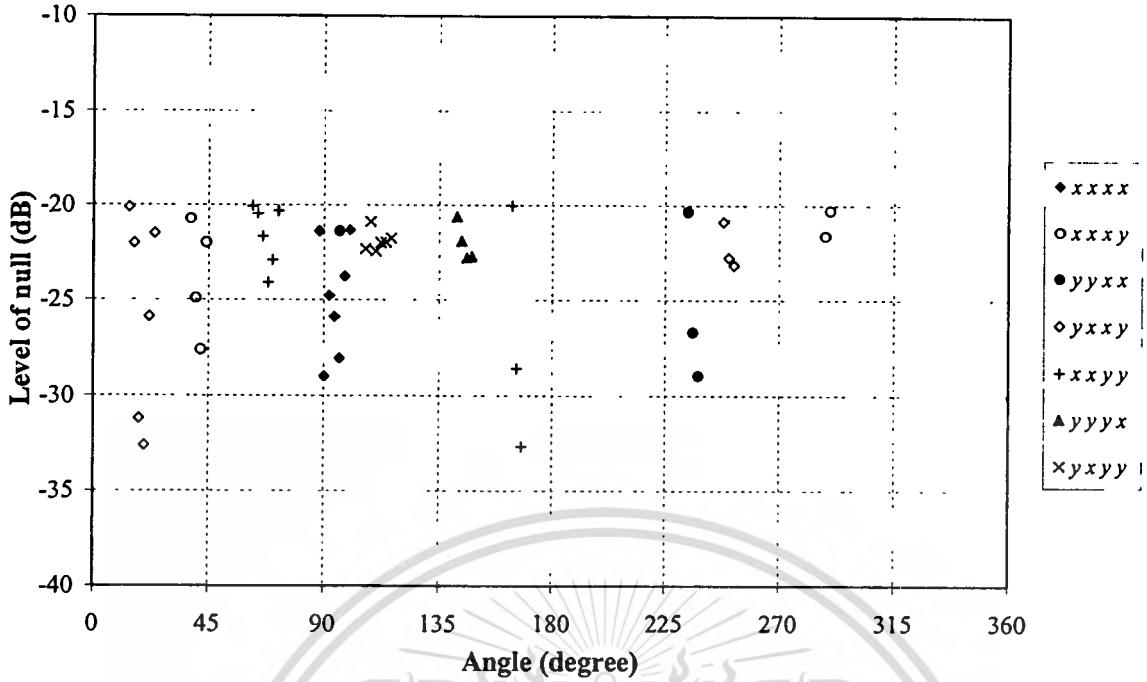

Fig. 3.28 Distribution of null directions obtained for the different combinations of element patterns for the 315° main beam direction.

3.3.2.2 Cross-polarization

Here, the cross-polarization characteristics of the phased array antenna of switched-beam elements are considered. The plots of E_θ and E_ϕ components in H-plane for four beam directions with different combination of element patterns are presented in Fig. 3.29 – Fig. 3.32. It is obvious that E_θ component is dominated, so the phased array antenna of switched-beam elements radiates vertical polarization. E_ϕ component shows the cross-polarization. The measured level of cross-polarization is higher than the simulation due to the non-purity of polarization of the transmitting patch antenna. However, the cross-polarization level is less than -10 dB. In the four main beam directions, the cross-polarization levels of -27, -20, -11.65 and -26.67 dB are found.

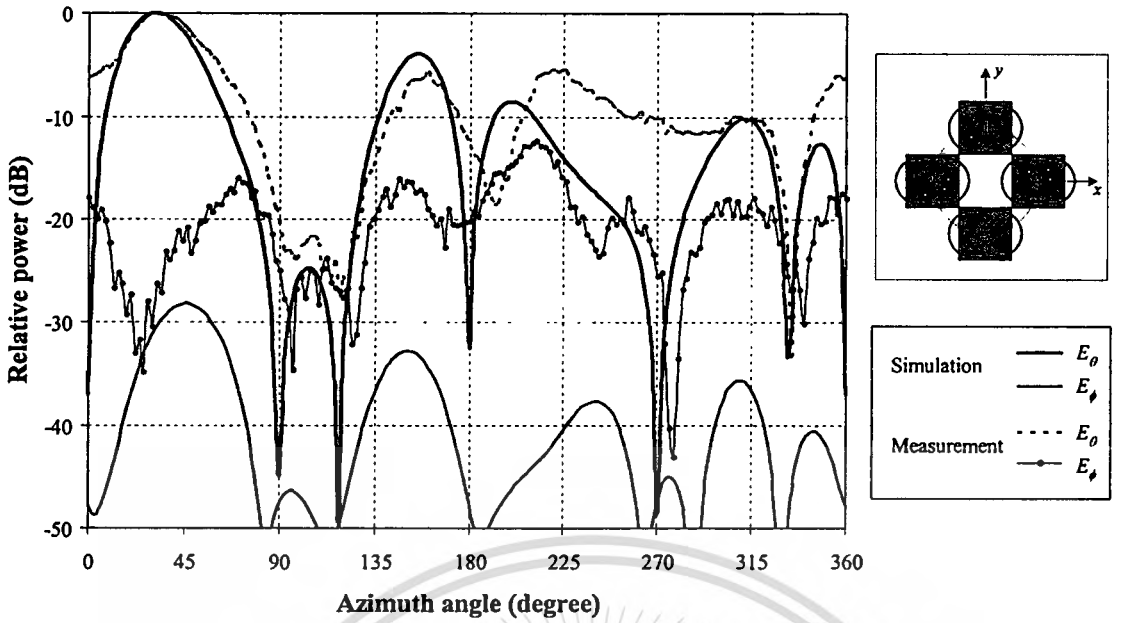

Fig. 3.29 The plots of E_θ and E_ϕ components in H-plane for 45° beam direction with the $x\,x\,x\,x$ combination.

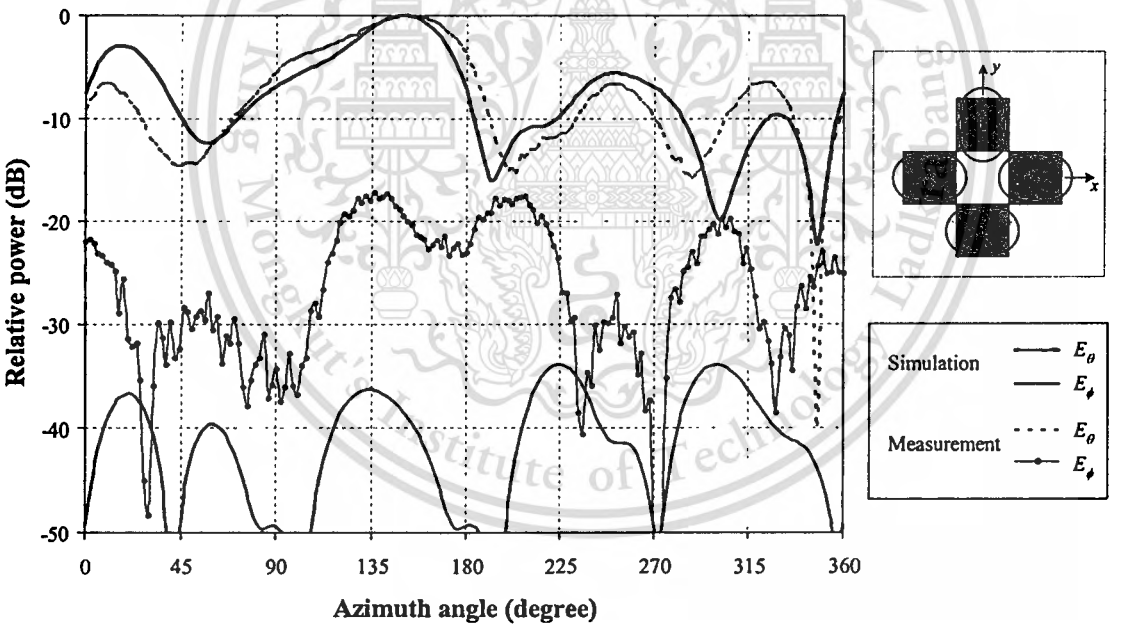

Fig. 3.30 The plots of E_θ and E_ϕ components in H-plane for 135° beam direction with the $y\,x\,x\,x$ combination.

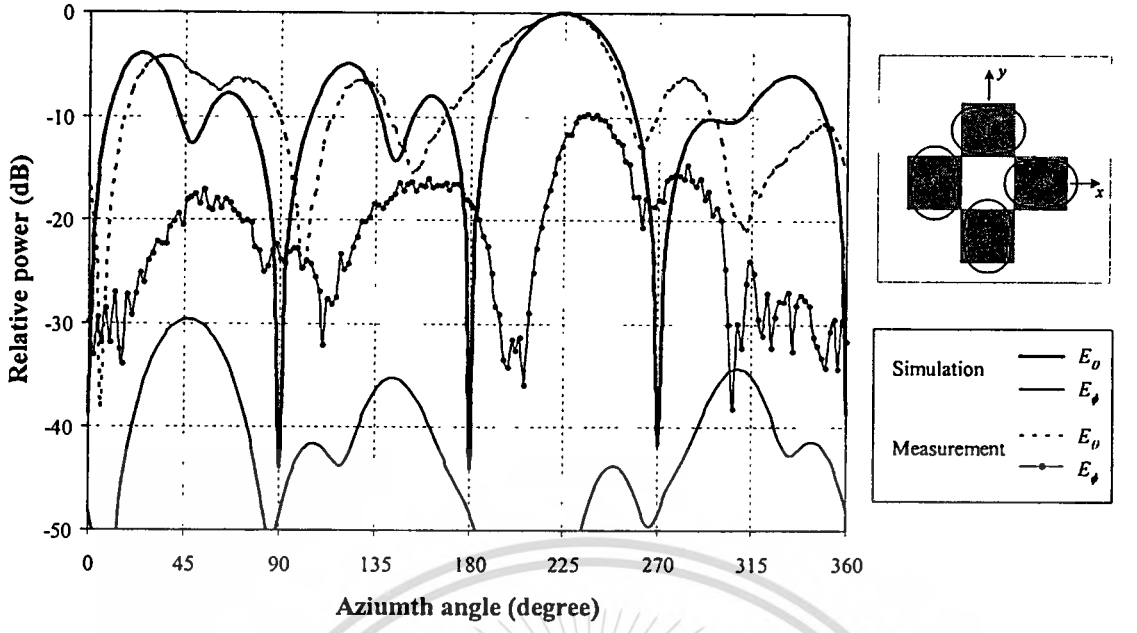

Fig. 3.31 The plots of E_θ and E_ϕ components in H-plane for 225° beam direction with the $x\,y\,y\,x$ combination.

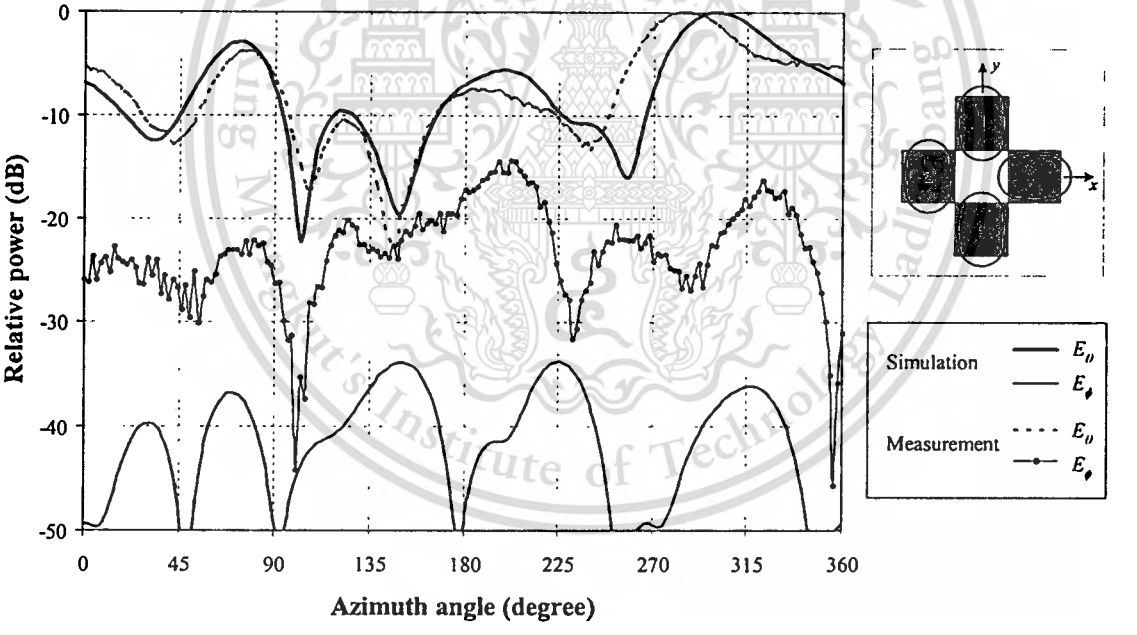

Fig. 3.32 The plots of E_θ and E_ϕ components in H-plane for 315° beam direction with the $y\,y\,y\,x$ combination.

3.4 Conclusion

In this chapter, the development of the phased array antenna of switched-beam elements along with its simulated and measured characteristics has been presented. The design of this array follows the one of the flat four-beam compact phased array antenna,

however, with the difference that the new array uses switched-beam single patch antennas as the array elements. The 1-bit delay lined phase shifter has been designed for switching the main beam of the array antenna. The four-way Wilkinson power combiner has been used to combine the array output. The phased array antenna of switched-beam elements has been fabricated and tested. The VSWR and radiation patterns have been presented. The array features VSWR < 2:1 in the design band. The array offers 64 radiation patterns, since 4 switched-beam elements provide 16 combinations of element patterns. Because of the use of switched-beam elements the array offers radiation patterns with changeable null directions. The tests results have also included cross-polarization characteristics. The cross-polarization level of less than -10 dB has been observed.

CHAPTER 4
PERFORMANCE OF A PHASED ARRAY ANTENNA OF SWITCHED-BEAM ELEMENTS

4.1 Introduction

The design, development and tests results for the phased array antenna of switched-beam elements have been presented in Chapter 3. In this chapter, the antenna performance as a sub-system of a wireless communication system is investigated. A particular interest is in determining the correlation coefficient and diversity gain of the antenna to assess its ability to improve the received signal quality. This is followed by measurements of the signal-to-interference ratio (SIR). Because of changeable null patterns of the phased array antenna of switched-beam elements, the SIR is expected to be improved. A number of experiments are performed to test this hypothesis.

4.2 Correlation coefficient

Usually, the antenna capability to improve quality of received signal is evaluated in terms of correlation coefficient (ρ). This coefficient is calculated from the radiation patterns and the specific angular distribution of received power. In this thesis, the well known Clarke's model [17] is applied to describe an angular distribution of received power. Therefore, the simple expression of correlation coefficient can be written as

$$\rho = \frac{\int_0^{2\pi} E_1(\phi) \cdot E_2^*(\phi) d\phi}{\sqrt{\int_0^{2\pi} E_1(\phi) \cdot E_1^*(\phi) d\phi \cdot \int_0^{2\pi} E_2(\phi) \cdot E_2^*(\phi) d\phi}} \tag{4.1}$$

where E_1 is the complex radiation pattern in one direction and E_2 is the complex radiation pattern switched in other direction. The asterisk (*) denotes the complex conjugate.

The correlation coefficients for four-beam directions of each combination of element patterns are calculated and presented in Table 4.1. Generally, the quality of received signal is expected to be improved when the correlation coefficient is less than 0.7 [18]. The four beams of each combination of element patterns are correlated with the

relatively low correlation coefficient. The four beams of $x\,x\,x\,x$, $y\,x\,x\,x$, $x\,x\,y\,x$, $y\,y\,x\,x$, $y\,x\,x\,y$, $x\,y\,x\,y$, $y\,y\,y\,x$, $y\,x\,y\,y$ and $y\,y\,y\,y$ combinations are correlated with the correlation coefficient of lower than 0.7. The lowest correlation coefficient of 0.37 is found in the beam switching with $x\,x\,x\,x$ combination. For other combinations, the beams in some directions are correlated with the correlation coefficient of larger than 0.7, and the high correlation coefficient of 0.79 is found in $x\,y\,x\,x$ and $x\,y\,y\,y$ combinations.

Table 4.1 Correlation coefficients of the four beams of 16 combinations of element patterns.

Combinations of element patterns	**Main beam directions**					
	45° & 135°	**135° & 225°**	**225° & 315°**	**315° & 45°**	**45° & 225°**	**135° & 315°**
$x\,x\,x\,x$	0.37	0.56	0.58	0.52	0.64	0.56
$y\,x\,x\,x$	0.55	0.62	0.59	0.50	0.56	0.56
$x\,y\,x\,x$	0.58	0.60	0.67	0.79	0.79	0.73
$x\,x\,y\,x$	0.55	0.60	0.57	0.58	0.60	0.47
$x\,x\,x\,y$	0.55	0.72	0.71	0.60	0.70	0.70
$y\,y\,x\,x$	0.50	0.57	0.52	0.55	0.68	0.68
$y\,x\,y\,x$	0.67	0.72	0.62	0.70	0.59	0.50
$y\,x\,x\,y$	0.62	0.64	0.58	0.58	0.66	0.64
$x\,y\,y\,x$	0.57	0.56	0.51	0.60	0.74	0.65
$x\,y\,x\,y$	0.61	0.64	0.59	0.68	0.62	0.51
$x\,x\,y\,y$	0.56	0.60	0.71	0.55	0.73	0.58
$y\,y\,y\,x$	0.52	0.67	0.49	0.62	0.59	0.48
$y\,y\,x\,y$	0.68	0.70	0.67	0.67	0.65	0.73
$y\,x\,y\,y$	0.60	0.70	0.68	0.62	0.59	0.56
$x\,y\,y\,y$	0.56	0.64	0.71	0.61	0.79	0.69
$y\,y\,y\,y$	0.62	0.66	0.68	0.48	0.58	0.62

The phased array antenna of switched-beam elements has 64 radiation patterns. Thus, when the correlation coefficients of one radiation pattern are correlated to the others, 64 × 64 values of the correlation coefficient are obtained. The cumulative

probability function (CPF) of the correlation coefficients is plotted in Fig. 4.1. The CPF of the correlation coefficients shows 62.79% probabilities that the correlation coefficient of less than 0.7 is obtained. It means that the four-beam switching of the phased array antenna of switched-beam elements is mostly switched with the low correlated radiation patterns, leading to the received signal improvement.

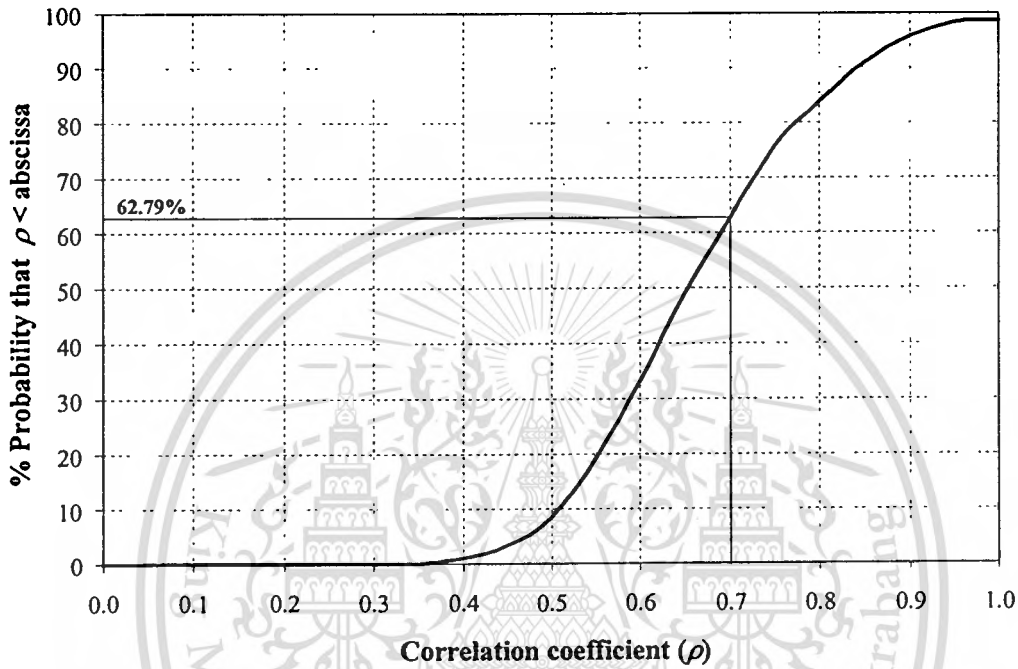

Fig. 4.1 Cumulative probability function of the correlation coefficients of 64 radiation patterns.

4.3 Diversity gain

Having obtained the low correlation coefficient, in the next step, the diversity performance of the phased array antenna of switched-beam elements is evaluated. The phased array antenna of switched-beam elements is considered as the switched diversity antenna. Generally, the diversity performance is measured as diversity gain. It is defined as the ratio of the received signal of the diversity combiner, r_c, relative to its mean value, $\bar{r}_c$, and the received signal of the single branch, r_1, relative to its mean value, $\bar{r}_1$, for a given signal level probability. Thus, the diversity gain describes the improvement in received signal for a given signal level probability. It can be written in decibels as

$$\text{Diversity gain (dB)} = \left[\frac{r_c}{\bar{r}_c}(\text{dB}) - \frac{r_1}{\bar{r}_1}(\text{dB})\right]_{\text{at given probability}} \tag{4.2}$$

where the ratios within this equation are found from the signal cumulative probability functions.

In this work, the diversity gain of switched diversity is evaluated for the case of correlated received signals in Ricean channel. The joint probability density function of two Ricean distributed received signal r_1 and r_2 is given as [19]

$$\begin{aligned} p(r_1,r_2) = {} & \frac{(1+K)^2}{2\pi\cdot\beta^2(1-\rho^2)}\exp\left[\frac{-2K}{1+\rho} - \frac{(1+K)(r_1+r_2)}{(1-\rho^2)\beta}\right] \\ & \times \int_0^{2\pi}\exp\left[\frac{-2\rho(1+K)\sqrt{r_1 r_2}\cos\theta}{(1-\rho^2)\beta}\right] \\ & \times I_0\left(\sqrt{\frac{4K(1+K)(r_1+r_2+2\sqrt{r_1 r_2}\cos\theta}{\beta(1+\rho)^2}}\right)d\theta \end{aligned} \tag{4.3}$$

where K is the Ricean factor and defined as

$$K = \frac{\text{Power of line-of-sight component}}{\text{Power of multipath component}}$$

β is the average power of the signal, $I_0(\cdot)$ is the zero-order modified Bessel function of the first kind. The cumulative probability function of received power after diversity combining for switched combining is written as [20]

$$\text{Prob}(r \le x) = \begin{cases} \int_0^x\int_0^A p(r_1,r_2)dr_1dr_2, & 0 < x < A \\ \int_0^x\int_0^x p(r_1,r_2)dr_1dr_2 + \int_x^\infty\int_A^x p(r_1,r_2)dr_1dr_2, & x \ge A \end{cases} \tag{4.4}$$

where A is the switching threshold. Substituting (4.3) into (4.4), the cumulative probability functions of correlated received signals in Ricean channel with $K = 0$ dB and $K = 10$ dB are plotted in Fig. 4.2. The diversity gain is evaluated for the correlation coefficient of 0.37 and the switching threshold A of -10 dB. It can be seen that the diversity gain is insignificant until the threshold A is reached, at which the diversity gain settles at a constant value of the highest diversity gain obtained with the switched combining. The switched diversity can significantly improve the signal reception when the received power is lower than the switching threshold. For $K = 0$ dB, the diversity gain of 8 dB is obtained at 1% probability. It means that it is 99% reliable that the received power is above -18 dB and -10 dB for reception without and with diversity, respectively. For $K = 10$ dB, the diversity gain is obtained by the same degree of 8 dB but at the smaller probability of 0.001%. The signal reception is more reliable since the line-of-sight component is dominant.

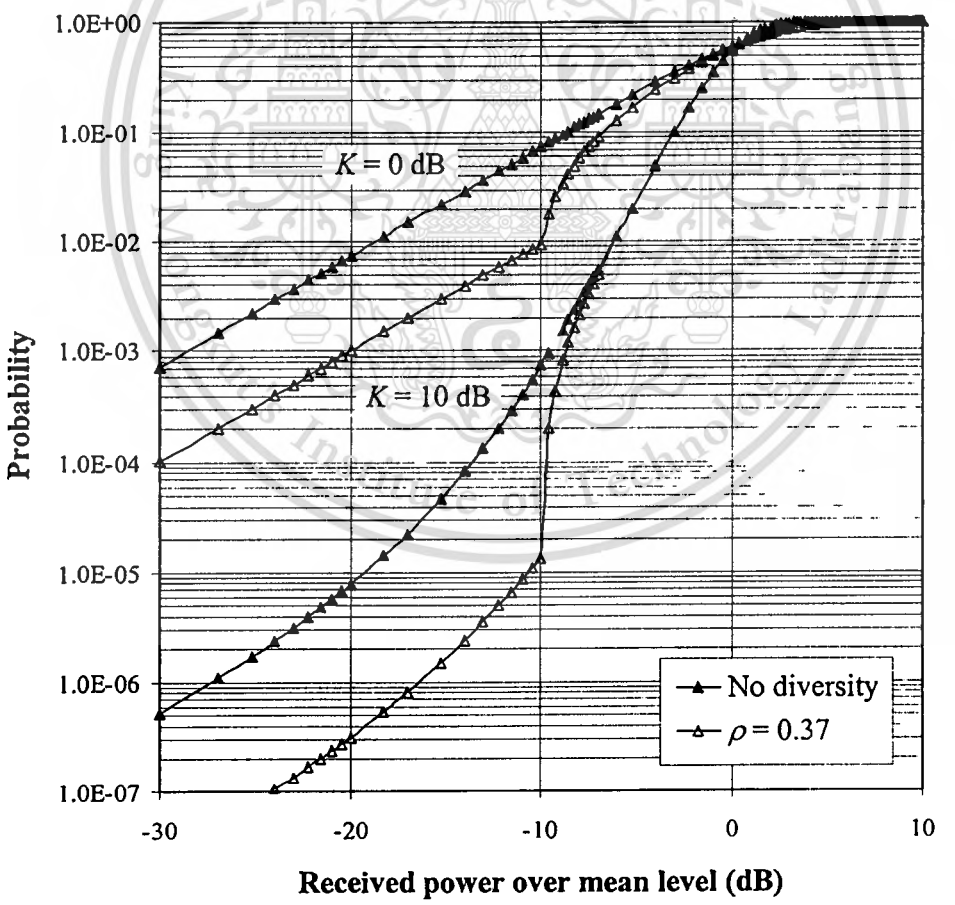

Fig. 4.2 Cumulative probability function of the switched diversity (threshold A = -10 dB).

4.4 Signal-to-interference ratio (SIR) improvement

So far, the received signal improvement due to the use of the phased array antenna of switched-beam elements has been evaluated in terms of correlation coefficient and diversity gain. This improvement can also be assessed in terms of signal-to-interference ratio [21]. While discussing in the previous chapter the radiation patterns of the phased array antenna of switched-beam elements, it has been indicated that the null directions can be changed to achieve received signal diversity. This array capability can be used to advantage to suppress interference. The results of this strategy are presented in this section.

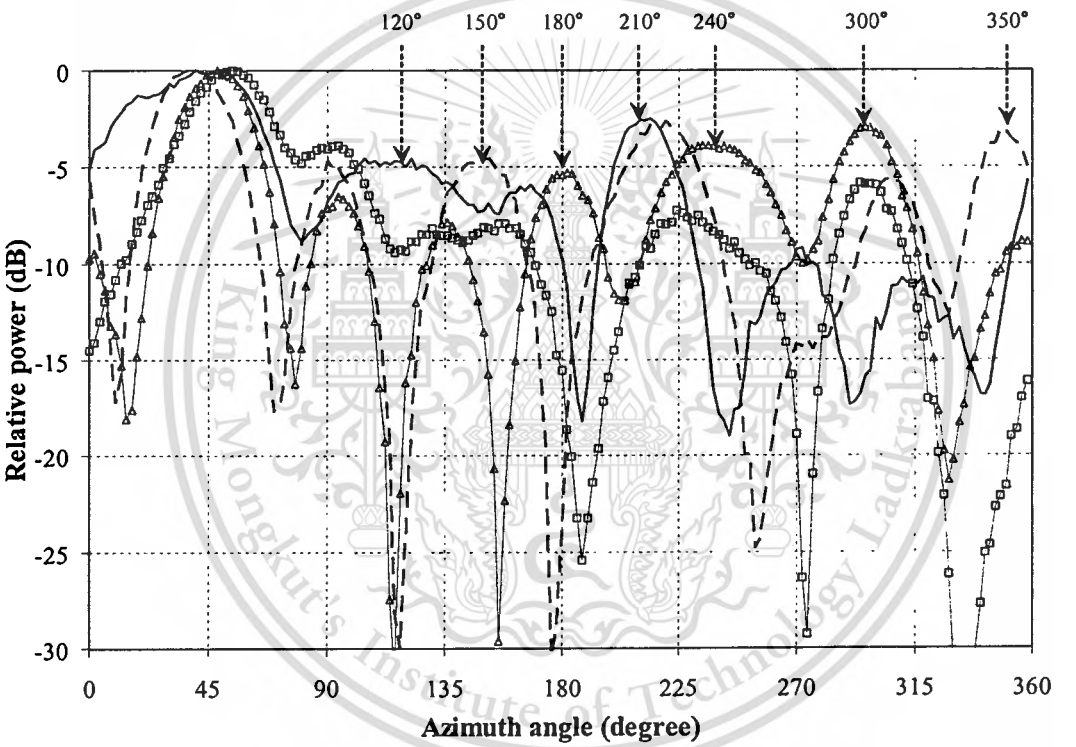

Fig. 4.3 Radiation patterns of various combinations for different interference directions.

--- *x x x y* —— *y x x y* —▲— *x y y y* —□— *y y y y*

The interference suppression performance is investigated assuming the various directions of interference. The radiation patterns with *y x x y*, *x x x y*, *x y y y* and *y y y y* combinations are illustrated in Fig. 4.3. It can be seen that when the interference reaches at 120°, it will be only 4.96 dB suppressed by using *y x x y* combination. However, by switching beam of the first element to *x* direction the *x x x y* combination produces the null direction at 120°, giving the interference at -24.65 dB. Therefore, the interference

suppression will be 19.69 dB improved. When the interference is in direction of 150°, the interference level will be -4.95 dB by using the *x x x y* combination. To suppress the interference, the *x x x y* combination will be changed to be the *x y y y* combination by switching the beams of the second and the third elements to *y* direction. The interference is suppressed down to -13.54 dB, resulting in 8.95 dB suppression more than the *x x x y* combination. When the interference is in direction of 180°, the interference received by the *x y y y* combination will be -5.39 dB. The interference level can be reduced by changing the *x y y y* combination to be the *x x x y* combination. The interference level will be down to -23.45 dB. When the interference is in direction of 210°, the *y y y y* combination will be applied instead of the *x x x y* combination by which the interference can be 10.09 dB suppressed. Considering other directions of 240° 300° and 350°, the *y x x y* combination is chosen to suppress the interference in 240° and 300° with the null level of -17.81 dB and -12.87 dB, while the *y y y y* combination is used so that the interference in 350° can be reduced to -21.60 dB.

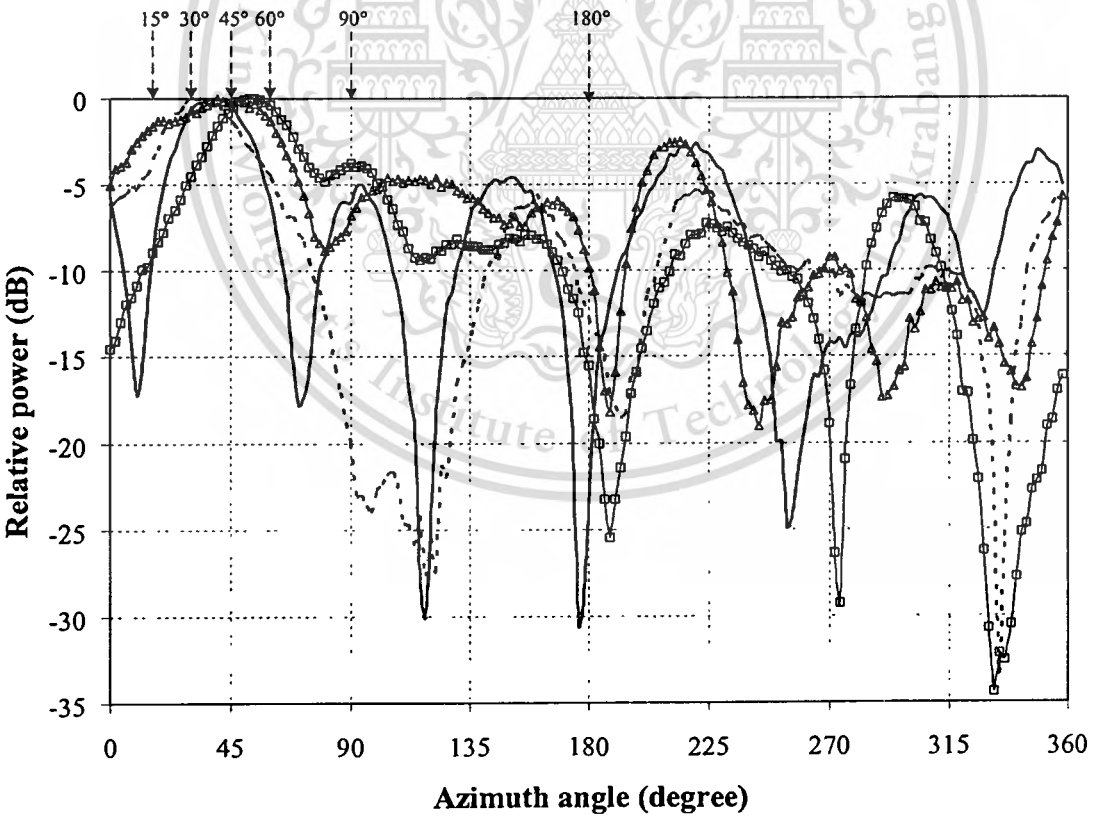

Fig. 4.4 Radiation patterns of various combinations for different desired signal directions.

--- *x x x x* —— *x x x y* —▲— *y x x y* —■— *y y y y*

Furthermore, the performance of the phased array antenna of switched-beam elements is discussed for the case when the desired signal is not exactly at the main beam direction. Let us consider the desired signal directions of 15°, 30°, 45°, 60°and 90°, and assume the interference direction at 180°. First, the arriving signal direction of 45° is considered. The radiation pattern switched to 45° with the *x x x y* combination is chosen to suppress the interference down to -23.45 dB as shown in Fig. 4.4. Next, the desired signal is assumed in direction of 30°. The *x x x x* combination is used since the main beam is in direction of 30° and the interference can be suppressed down to -12.73 dB. For the desired signal direction of 60°, the combination of element patterns is changed to the *y y y y* combination by which the main beam direction is nearly 60° and the interference can be suppressed down to -15.53 dB. The results show that the performance of the phased array antenna of switched-beam elements is acceptable for the desired signal directions of 30° and 60°. However, when the desired signal is assumed in directions of 15° and 90°, the main beam cannot be produced exactly in those directions. With the *y x x y* combination, the levels of the signal in direction of 15° and the interference in direction of 180° are -1.59 dB and -9.86 dB, respectively, relative to the peak main beam. The signal-to-interference ratio is 8.27 dB. For the desired signal in direction of 90°, the signal level is -3.74 dB and the interference level is -15.53 dB for *y y y y* combination. The signal level is -6.07 dB and the interference level is -23.45 dB for *x x x y* combination. Thus, the signal-to-interference ratio is 17.38 dB and 11.79 dB for *x x x y* and *y y y y* combination, respectively. In this case, the *x x x y* combination will be chosen since it provides higher signal-to-interference ratio though the signal level is lower than that of the *y y y y* combination. It should be noted that the performance of the antenna is determined by the signal-to-interference ratio. In a multipath environment, the directional properties of the antenna are not so much important as is its ability to change the pattern. It is clear that the radiation pattern with changeable combination of element patterns provides an advantage in terms of interference suppression.

4.4.1 Measurement setup

Here, details of the measurement set up are given to clearly assess the antenna capability to suppress interference. The signal-to-interference ratio is measured in the practical site. Measurement is set up at the Wireless Communication Laboratory where is full of objects such as desks and equipment, so the multipath environment can be

expected. The layout of the test site is shown in Fig. 4.5. The phased array antenna of switched-beam elements, a receiving antenna, is installed at the center of the test site (point **A**). The RF output of the receiving antenna is connected to the spectrum analyzer for measuring the received power. On the transmitting side, the patch antenna with vertical polarization is used as the transmitting antenna. The desired and interfering signals are transmitted at the frequency of 1.95 GHz with the power of 10 dBm. The desired and interfering signals coming from various directions are assumed by placing the transmitting antenna around the receiving antenna with the distance of 1.5 m (point **B** – point **I**) as illustrated in Fig. 4.5.

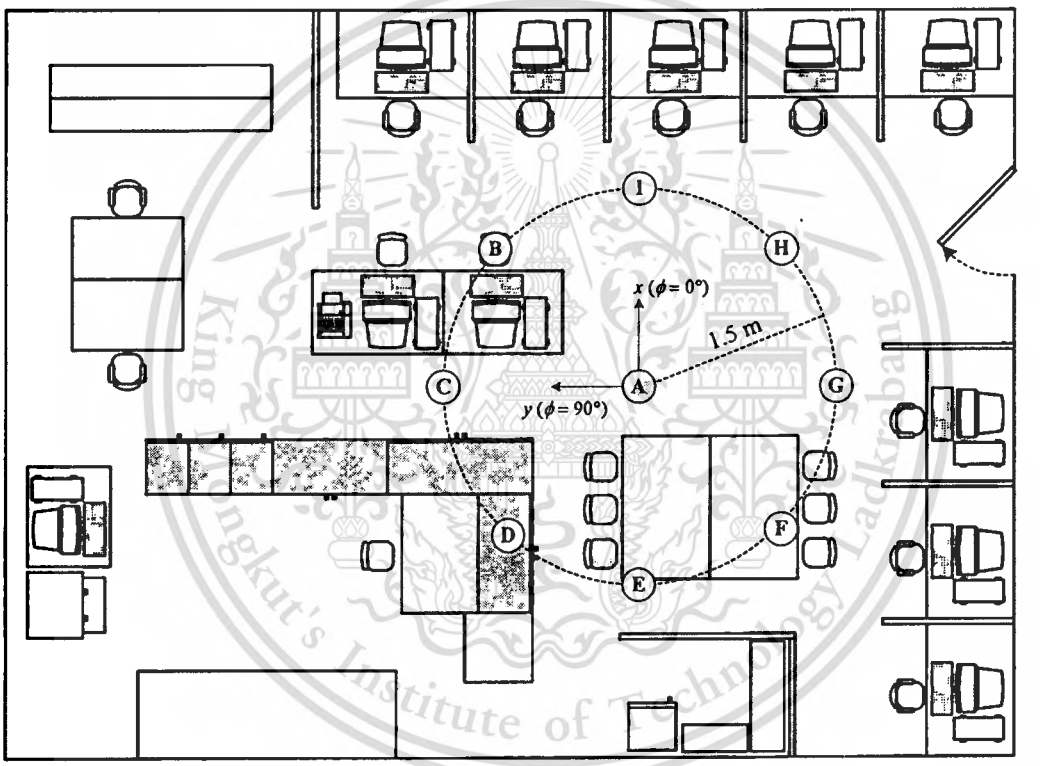

Fig. 4.5 Layout of the test site.

4.4.2 Measured results

The measured results for signal-to-interference ratio are investigated for the cases of changes in desired signal direction and changes in interference direction.

4.4.2.1 Changes in desired signal direction

The directions of the desired signal are given in the directions of 45°, 135°, 225° and 315° (point **B, D, F** and **H**), while the interference is assumed in the direction of 90°

(point **C**). The signal-to-interference ratio is determined from the ratio of the received power of desired signal to the received power of interference. Initially, the RF signal is transmitted from the point **B**, the main beam of the receiving antenna is switched to 45° and the received powers are measured for 16 combinations of element patterns. Then, the RF signal is transmitted from the point **C** and the received powers are measured for 16 combinations of element patterns. Therefore, the signal-to-interference ratios of 16 combinations are obtained. Subsequently, the RF signal is transmitted from the point **D**, **F** and **H** for changes in the desired signal directions of 135°, 225° and 315°, respectively. The main beam is also switched in the desired directions of 135°, 225° and 315°, respectively, and the measurement is repeated.

Table 4.2 Signal-to-interference ratio for changes in desired signal direction with the interference in direction of 90°.

Combination of element patterns	**Signal-to-interference ratio (dB)**			
	Desired Signal Direction			
	45°	**135°**	**225°**	**315°**
xxxx	8.4	-11.1	2.7	3.0
yxxx	7.2	-7.6	0.1	0.6
xyxx	5.2	-10.0	1.3	10.0
xxyx	0.4	-12.5	1.5	1.4
xxxy	4.8	-7.1	5.4	2.0
yyxx	4.8	-6.6	-0.4	5.2
yxyx	1.9	-10.0	-1.2	-1.8
yxxy	9.8	-5.6	1.9	-0.3
xyyx	5.7	-8.7	2.5	3.5
xyxy	6.1	-4.5	*7.3*	7.8
xxyy	0.0	-9.8	2.4	2.2
yyyx	3.3	-9.0	0.0	0.7
yyxy	7.3	***-0.7***	4.1	7.5
yxyy	3.1	-7.6	-0.3	-1.0
xyyy	***10.9***	-5.8	6.5	***12.6***
yyyy	9.2	-4.7	0.0	6.7

The results of signal-to-interference ratio for changes in desired signal direction with the interference in direction of 90° are tabulated in Table 4.2. For the desired signal direction of 45°, the maximum signal-to-interference ratio is 10.9 dB obtained from the *x y y y* combination, whereas the minimum signal-to-interference ratio is 0 dB given by the *x x y y* combination. It is obvious that the signal-to-interference ratio improvement of 10.9 dB is provided. For the desired signal direction of 135°, the signal-to-interference ratio is shown in negative value because the received power of desired signal is less than the interference. Therefore, the minimum signal-to-interference ratio is down to -12.5 dB for the *x x y x* combination; however, the improvement of 11.8 dB can be obtained when the combination of element patterns is changed to the *y y x y* combination by which the signal-to-interference ratio of -0.7 dB is given. Furthermore, it should be noted that the *x y y y* combination, which provides the maximum signal-to-interference ratio of 10.9 dB for the desired signal direction of 45°, gives the signal-to-interference ratio of -5.8 dB when the desired signal direction is 135°. Thus, when the desired signal direction is changed from 45° to 135° the signal-to-interference ratio improvement of 5.1 dB can be obtained by changing the *x y y y* combination to be the *y y x y* combination. When the desired signal direction is 225°, the main beam is switched to 225° with the *y y x y* combination. The signal-to-interference ratio of 4.1 dB is obtained, but the maximum signal-to-interference ratio of 7.3 dB is given by the *x y x y* combination. Therefore, the signal-to-interference ratio can be increased by 3.2 dB by simply switching the beam of the first element. Also, when the desired signal direction is changed to 315°, the main beam is switched to 315° with the *x y x y* combination and the signal-to-interference ratio of 7.8 dB is obtained. The signal-to-interference ratio improvement of 5.1 dB is achieved by switching the beam of the third element to provide the *x y y y* combination that the signal-to-interference ratio of 12.9 dB is obtained.

4.4.2.2 Changes in interference direction

The signal-to-interference ratio improvement is investigated by assuming the interference in 6 directions of 135°, 180°, 225°, 270°, 315° and 0°, and the desired signal is assumed in direction of 45°. Therefore, the interference is transmitted from the point **D**, **E**, **F**, **G**, **H** and **I**, respectively, and the desired signal is transmitted from the point **B**. The main beam of the receiving antenna is switched to 45°. The received powers of desired and interfering signals are measured for each of 16 combinations of element patterns. The signal-to-interference ratios of 16 combinations for different interference directions are

presented in Table 4.3. It is obvious that when the interference direction is changed, the phased array antenna of switched-beam elements can suppress the interference by changing the combination of element patterns. When the interference is in direction of 135°, the maximum signal-to-interference ratio of 12.5 dB is obtained from the *y y x y* combination. Then, the interference direction is changed to 180°, the signal-to-interference ratio of 13.9 dB is provided by the *y y y y* combination, and the signal-to-interference ratio of 9.3 dB is obtained when the interference is in direction of 225°. Since the interference direction is 225°, which is the direction of back lobe, the signal-to-interference ratio is relatively low. For the interference directions of 270°, 315° and 0°, the maximum signal-to-interference ratios of 14.2 dB, 10.1 dB and 18.5 dB are given by the *x y y x*, *x x x y* and *y y y y* combinations, respectively.

Table 4.3 Signal-to-interference ratio for changes in interference direction with the desired signal in direction of 45°.

Combination of element patterns	Signal-to-interference ratio (dB)					
	Interference Direction					
	135°	180°	225°	270°	315°	0°
x x x x	4.7	12.1	2.7	10.0	7.4	12.4
y x x x	6.8	4.5	4.9	11.4	7.0	3.4
x y x x	7.0	3.8	3.2	3.3	6.1	6.2
x x y x	2.1	7.5	2.1	6.2	7.1	3.4
x x x y	7.0	9.2	1.3	1.7	***10.1***	6.3
y y x x	10.5	3.4	6.1	5.5	6.7	3.9
y x y x	5.5	9.8	4.6	6.7	7.8	2.9
y x x y	10.6	5.5	4.4	5.2	7.6	10.6
x y y x	5.6	12.1	3.8	***14.2***	5.7	13.2
x y x y	10.4	3.0	2.8	-0.5	7.6	3.5
x x y y	2.2	4.7	1.7	1.0	10.0	-1.2
y y y x	8.3	7.3	5.2	12.5	6.3	6.7
y y x y	***12.5***	2.3	5.5	1.8	6.4	5.9
y x y y	5.9	13.3	4.6	4.0	9.2	4.0
x y y y	6.3	6.3	2.5	1.4	6.8	1.5
y y y y	12.4	***13.9***	***9.3***	8.7	9.8	***18.5***

4.5 Conclusion

For the developed switched-beam antenna, the correlation coefficient and diversity gain have been evaluated to assess its capability to improve performance of a wireless communication system in the presence of multipath signal propagation. The correlation coefficient of 0.37 has been obtained as the smallest value, and there are 62.79% probabilities that correlation coefficient is less than 0.7 when the 64 radiation patterns are used. With the lowest correlation coefficient of 0.37, the diversity gain has been evaluated for the switched diversity when applied in Ricean channel. The diversity gain has been found out for the Ricean channel with $K = 0$ dB and $K = 10$ dB. By using switched combining, the phased array antenna of switched-beam elements has shown the diversity gain of 8 dB. The performance on interference suppression has also been evaluated. By assuming the interference in various directions, the radiation patterns with different combination of element patterns clearly present the interference suppression improvement. The experimental tests have been performed to verify the interference suppression improvement. The tests have concerned the cases of changes in desired signal direction and changes in interference direction. The interference suppression has been achieved by switching the beam of elements. Using this strategy the signal-to-interference ratio improvement of more than 10 dB has been achieved.

CHAPTER 5

APPLICATIONS OF A PHASED ARRAY ANTENNA OF SWITCHED-BEAM ELEMENTS

5.1 Introduction

This chapter demonstrates the prospective applications of a phased array antenna of switched-beam elements for the future wireless communications system. Multiple-input multiple-output (MIMO) systems and adaptive antenna systems are considered. With respect to the first application, the use of switched-beam array antenna is investigated to reduce the cost and complexity of the MIMO system. With respect to the adaptive antenna system, the switched-beam array antenna is applied to initiate the CMA adaptive algorithm so that the adaptive process can efficiently perform. The preliminary results for these applications are presented.

5.2 Antenna for Multiple-Input Multiple-Output (MIMO) communications system

The outstanding growth of wireless communication during the last years has resulted in an enormous demand for high data rates and increased capacity. Recently, multiple-input multiple-output (MIMO) antenna systems that use diversity at both the transmitter and the receiver have drawn considerable attention. Information theory research has shown that large capacity gains over single antenna systems can be achieved when using MIMO antennas systems by exploiting multipath in the rich scattering wireless environment [22]. Under these conditions capacity grows linearly with the number of antenna elements. Unfortunately, the MIMO system requires high cost of multiple radio transceivers at both transmitting and receiving sides. However, this drawback may be relieved by using switched-beam antenna. The switched-beam antenna having compact size offers multiple beams. In this section, the channel capacity of MIMO system using the phased array antenna of switched-beam elements is analyzed.

5.2.1 Channel capacity

The multiple-input multiple-output (MIMO) system using multiple antennas at both the transmitter and the receiver exploits the multipath environment to increase the

channel in communication link. The channels occurring between transmitting side and receiving side are described by the channel matrix **H.** The channel capacity is a function of the channel matrix. The channel capacity of a MIMO system is written as

$$C = \log_2 \det\left[\mathbf{I} + \frac{\xi}{N}\mathbf{H}\mathbf{H}^H\right] \tag{5.1}$$

where ξ represents the signal-to-noise ratio (SNR). The channel matrix **H** is $M \times N$, where M, N denotes the number of antenna elements at the receiver and transmitter, respectively. $\mathbf{H}^H$ is the complex conjugate transpose of a channel matrix **H**, and **I** is the unit matrix. The element $\mathbf{H}_{ij}$ represents the sub-channel from transmitter j to receiver i, which is given by [23]

$$\mathbf{H}_{ij} = \sum_{l=1}^{L} \alpha_l e^{jk(r_{S_lT_j} + r_{R_iS_l})} g_{T_j}(\phi_l) g_{R_i}(\phi_l) \tag{5.2}$$

where L is the number of scatterers. α_l is a complex Gaussian distributed reflection coefficient with zero mean and unit variance. $g_{T_j}(\phi_l)$ and $g_{R_i}(\phi_l)$ are the radiation pattern of the transmitting and receiving antenna, respectively. $r_{S_lT_j}$ and $r_{R_iS_l}$ are the distance from transmitting antenna j to scatterer l and the distance from scatterer l to receiving antenna i, respectively. Accordingly, the channel capacity of the MIMO system using a phased array antenna of switched-beam elements is investigated theoretically [24]. The results for the MIMO system using four-element transmitting antenna are presented in Fig. 5.1. The channel capacity of the phased array antenna of switched-beam elements is compared with monopole antennas. For illustrative purpose, a 20-dB SNR is used. The channel capacity of four monopoles and of the phased array antenna of switched-beam elements is 17.35 bps/Hz and 34.25 bps/Hz, respectively. With the same number of antenna element, the switched-beam array antenna can substantially increase the channel capacity.

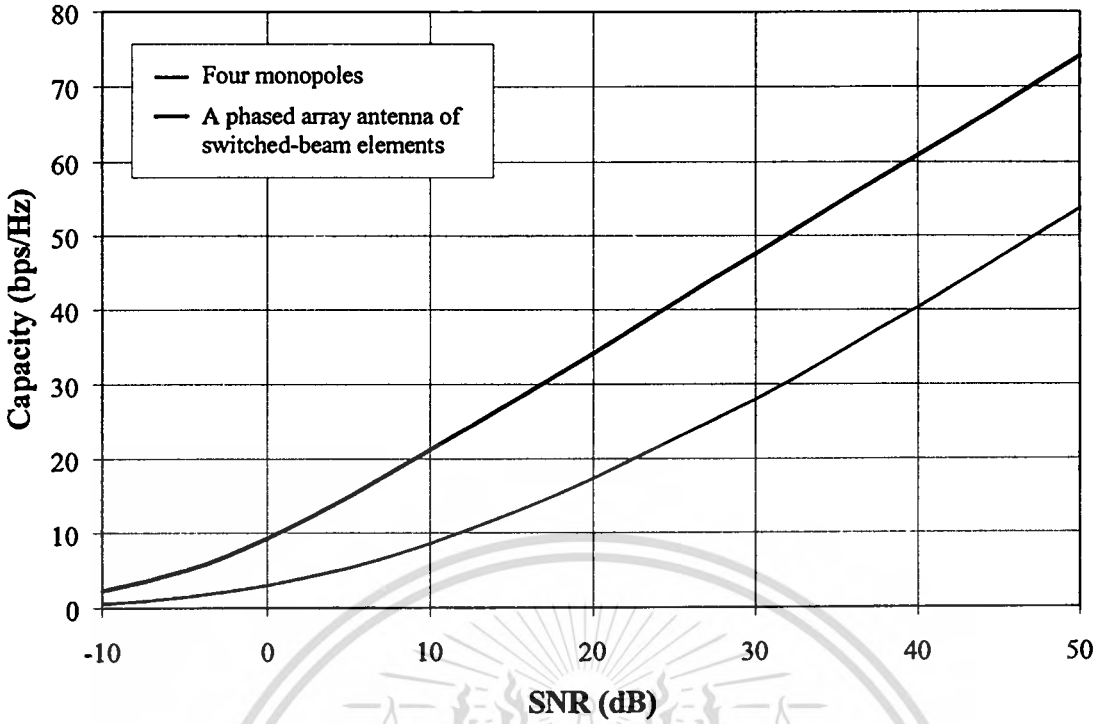

Fig. 5.1 Channel capacity of the MIMO system using four-element transmitting antenna.

5.2.2 Measurement

To experimentally investigate the channel capacity of MIMO system using a phased array antenna of switched-beam elements, the measurement is performed to find out the channel matrix **H**. Therefore, a measurement of 4 × 4 MIMO system is setup. The diagram of measurement setup is shown in Fig. 5.2. The measurement is realized using an HP8510C Network Analyzer. Port 1 and Port 2 of the network analyzer are connected to transmitting and receiving antennas, respectively. The parameter S_{21} is measured. The transmitting signal is amplified using an HP83050A power amplifier. The four elements of transmitting antenna transmit the RF signal almost at the same time by utilizing the 1-to-4 RF switch, whereas the four elements of receiving antenna receive the RF signal using the 4-to-1 RF switch. The synchronizer, which is controlled by the personal computer, is used to synchronize the RF switches at the transmitting and receiving sides and the network analyzer. The personal computer is used to control the measurement system and to record the results obtained from the network analyzer.

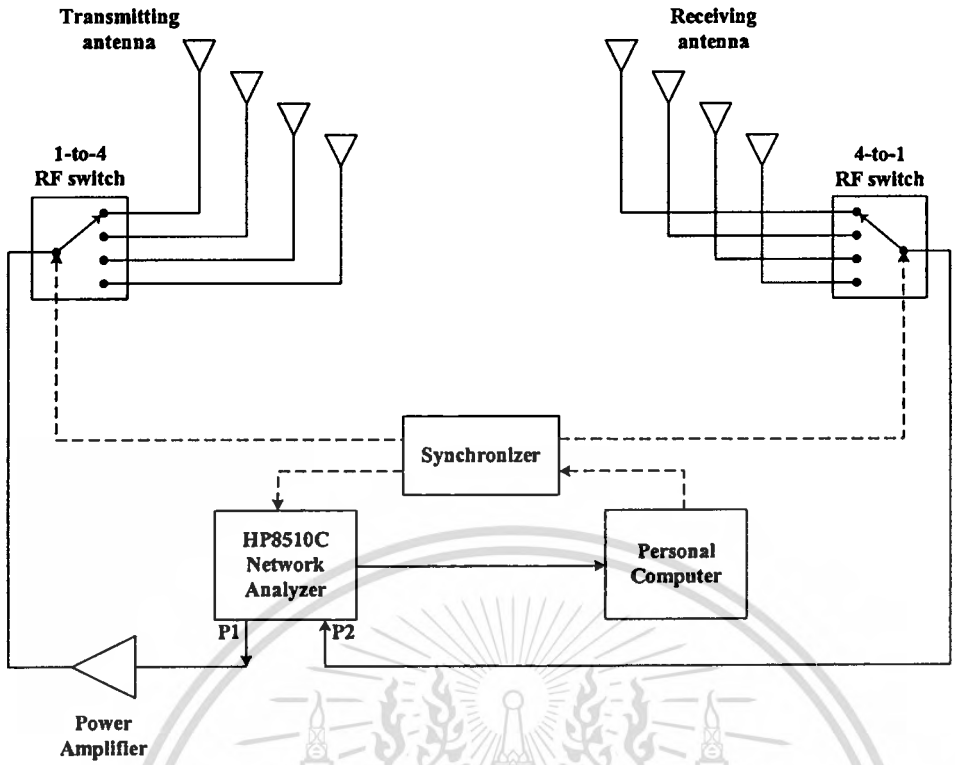

Fig. 5.2 Measurement setup of a 4 × 4 MIMO system

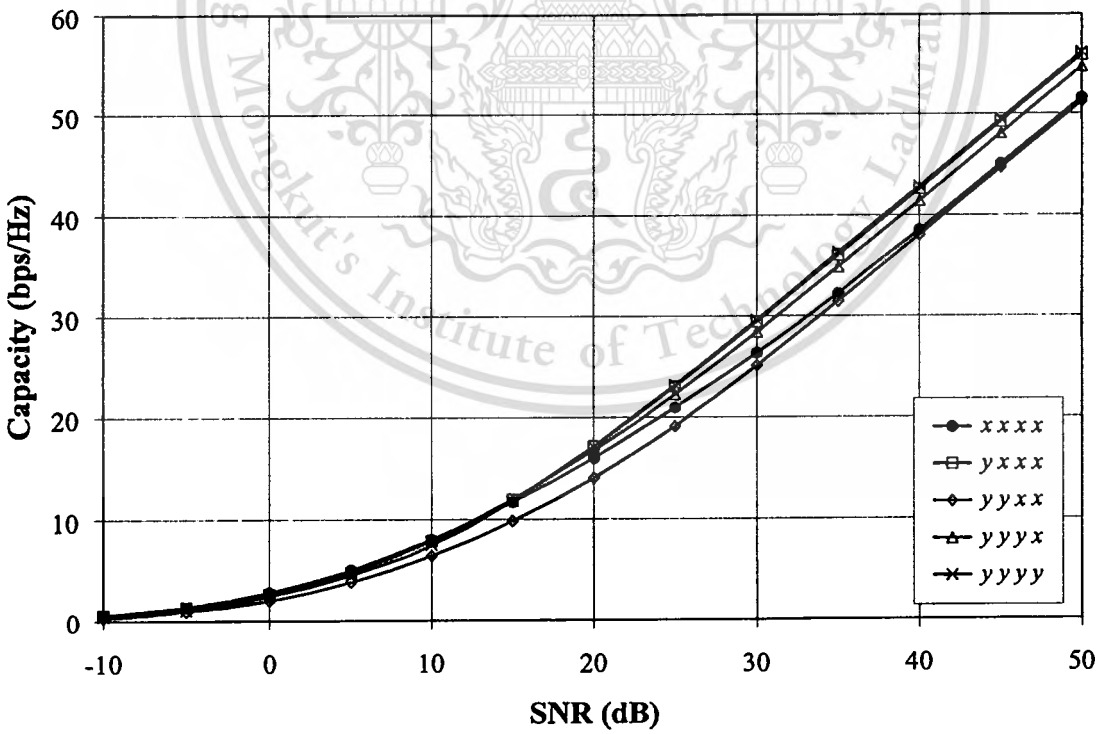

Fig. 5.3 Channel capacity of the MIMO system using a phased array antenna of switched-beam elements.

The measurement is performed at the frequency of 1.95 GHz. Four monopole antennas are used as the transmitting antenna and the phased array antenna of switched-beam elements is used as the receiving antenna. The main beam of the phased array antenna of switched-beam elements is switched to four directions acting as four-element receiving antenna. The channel matrix **H** can be found out experimentally, and then the channel capacity of MIMO system using the phased array antenna of switched-beam elements is evaluated and presented in Fig. 5.3. With various combinations of element patterns, the phased array antenna of switched-beam elements provides the channel capacity ranging from 14.0 to 17.0 bps/Hz at 20-dB SNR.

5.3 Initialization of Constant Modulus Algorithm (CMA) adaptive array antenna

With recent rapid increase in demand for wide-band mobile communication, interference among communications and multipath fading effects clearly becomes a serious problem. It is known that an adaptive antenna system is one solution to mitigate the problem. In the past, coefficient adjustment of an adaptive antenna relied upon a reference signal, which is often referred to as a training sequence. A Least Mean Square (LMS), Recursive Least Square (RLS) algorithm and their derivatives are employed in the systems. During the last decade, *blind* adaptive algorithm has received considerable interest for its application in mobile communication systems [25]. By using blind algorithms, training sequence can be eliminated. One of the most representative methods of blind adaptation is a Constant Modulus Algorithm (CMA) [26]. The algorithm can mitigate interference without a need for training sequence on a condition that the envelope of the transmitted signal is constant. However, the main drawback of applying CMA into adaptive antenna systems is its poor convergence. In addition to the slow convergence, CMA sometimes tends to converge to the wrong solution by capturing interference rather than the desired signal. Therefore, the switched-beam array antenna is introduced in the adaptive antenna system to relieve these problems. Since the switched-beam antenna can provide the beam to desired direction, the received power of the switched-beam antenna can then be exploited as an initial value for CMA algorithm. Thus, the CMA adaptive antenna system using a flat four-beam compact phased array antenna is simulated. The CMA algorithm and preliminary result of simulation are presented in this section.

5.3.1 CMA adaptive array

The CMA algorithm does not require a training sequence and therefore is referred to as a blind adaptive algorithm. To eliminate interference, CMA exploits a known property of transmitted signal, i.e. its constant envelope. Examples of this type of signal include FM, QPSK, etc. Fig. 5.4 depicts a basic architecture of CMA adaptive array. The complex signal received by i^{th} element of the antenna array in the k^{th} symbol interval $\mathbf{X}(k)$ is multiplied by an adjustable complex weight $\mathbf{W}(k)$.

$$\mathbf{X}(k) = [x_0(k)\ x_1(k) \ldots x_{N-1}(k)]^T \tag{5.3}$$

$$\mathbf{W}(k) = [w_0(k)\ w_1(k) \ldots w_{N-1}(k)]^T \tag{5.4}$$

Here, $[\ ]^T$ denotes vector transpose. Then, the output of adaptive array is obtained as

$$\mathbf{Y}(k) = \mathbf{W}(k)^T \mathbf{X}(k) \tag{5.5}$$

The CMA adjusts the weight vector $\mathbf{W}(k)$ in a way that the cost function J_{pq} defined as

$$J_{pq} = E[|| \mathbf{Y}(k) |^p - \sigma^p |^q] \tag{5.6}$$

is minimized. Note that p and q are positive integer and σ is the amplitude of the array output in the absence of interference. For simplicity, p and q are chosen to be 2. The steepest descent algorithm is used as an iterative minimization of the cost function J_{pq}. That is

$$\mathbf{W}(k+1) = \mathbf{W}(k) - \mu \hat{\nabla} J_{pq}(k) \tag{5.7}$$

where μ is a small step size governing convergence rate and $\hat{\nabla} J_{pq}$ is an unbiased estimate of the gradient of the cost function with respect to $\mathbf{W}(k)$,

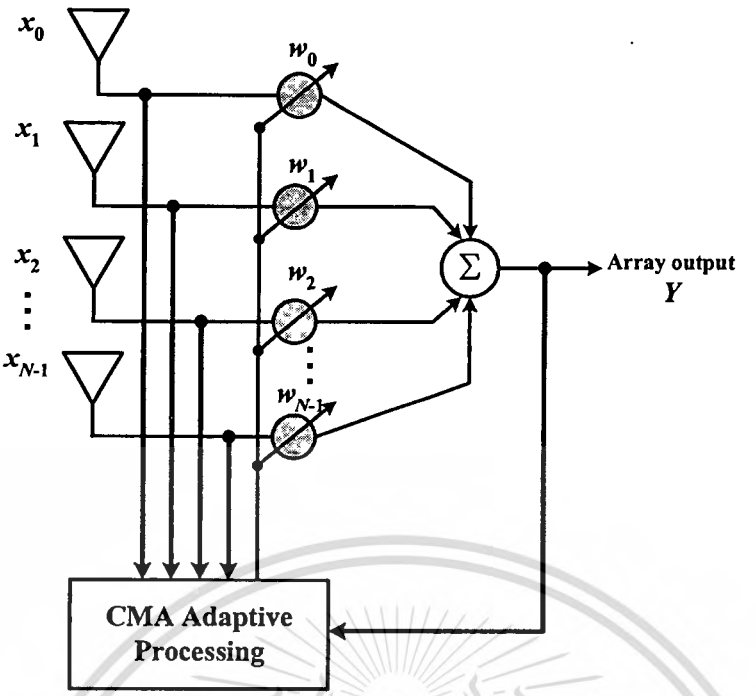

Fig. 5.4 Basic architecture of CMA adaptive array.

$$\nabla J_{pq} = E[qp\mathbf{X}^*(k)\mathbf{Y}(k)|\mathbf{Y}(k)|^{p-2}(|\mathbf{Y}(k)|^p - \sigma^p)^{q-1}(\text{sgn}(|\mathbf{Y}(k)|^p - \sigma^p))^q] \quad (5.8)$$

In practice, instantaneous estimates of the gradient are employed for adaptation. With $p = q = 2$, it is easily verified that

$$\mathbf{W}(k+1) = \mathbf{W}(k) - 4\mu\mathbf{X}^*(k)\mathbf{Y}(k)(|\mathbf{Y}(k)|^2 - \sigma^2) \quad (5.9)$$

5.3.2 Simulation

The simulation has been performed and presented in [27]. The desired and interfering signals are QPSK-modulated and propagated through an Additive White Gaussian Noise (AWGN) channel. The power of the desired signal is 3 dB stronger than that of the interference. The directions of the desired and interfering signals are 30° and 120°, respectively. Since it is assumed that a beam with maximum received power could be perfectly determined it can be used for CMA initialization. The direction of an initial main beam of a flat four-beam compact phased array antenna is 45°. The signal-to-noise ratio (SNR) is 20 dB.

Fig. 5.5 shows the signal constellation at the array output when no beamforming is performed. Scattering plots clearly reveal that eye-pattern is completely closed and indicate that beamforming is necessary. Fig. 5.6(a) illustrates signal constellation of the CMA adaptation after 500 iterations. The eye-pattern still exhibits a closed eye. After 1,000 iterations, the eye-pattern is opened; however, a large phase-offset is found in Fig. 5.6(b). It means that CMA does not converge to a desired solution. For the CMA with the beam-switching initialization, the convergence property is significantly improved. In particular, the convergence rate is faster, i.e. the eye-pattern is opened after 500 iterations, as shown in Fig. 5.7(a). Moreover, after 1,000 iterations no phase-offset presents in Fig. 5.7(b). It can confirm that the desired signal is actually captured. The radiation patterns after adaptation are presented in Fig. 5.9(a) and Fig. 5.9(b), respectively, for 500 iterations and 1,000 iterations. The radiation patterns of the CMA adaptive array antenna with and without beam-switching initialization are compared. The results show that the performance of CMA adaptive array antenna can be improved using the beam-switching initialization.

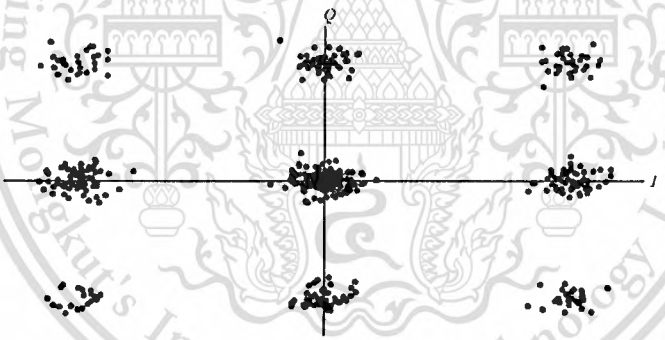

Fig. 5.5 Signal constellation without beamforming.

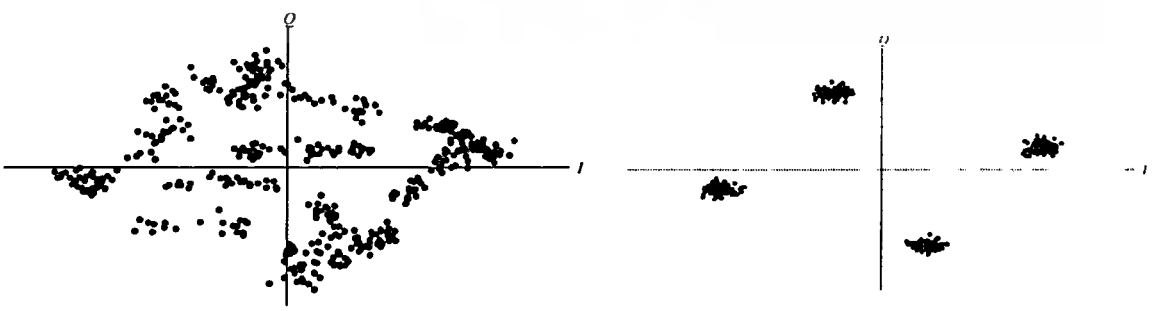

(a) (b)

Fig. 5.6 Signal constellation of CMA beamforming: (a) 500 iterations, (b) 1,000 iterations.

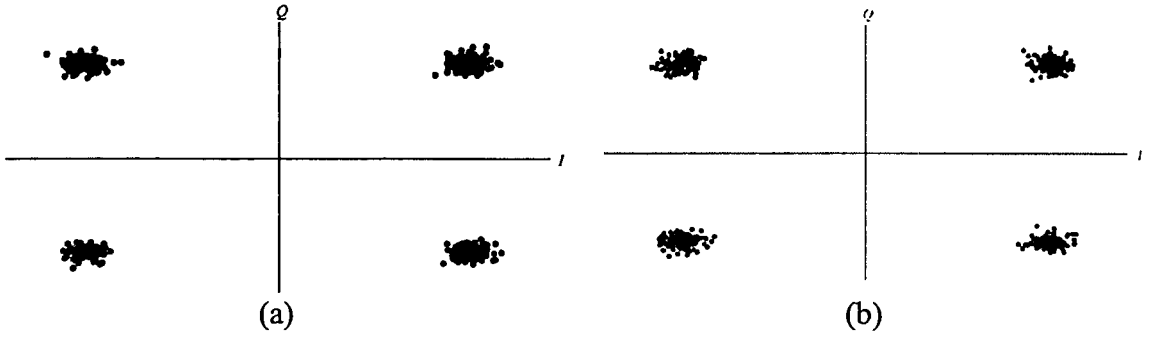

(a) (b)

Fig. 5.7 Signal constellation of CMA beamforming with beam-switching initialization: (a) 500 iterations, (b) 1,000 iterations.

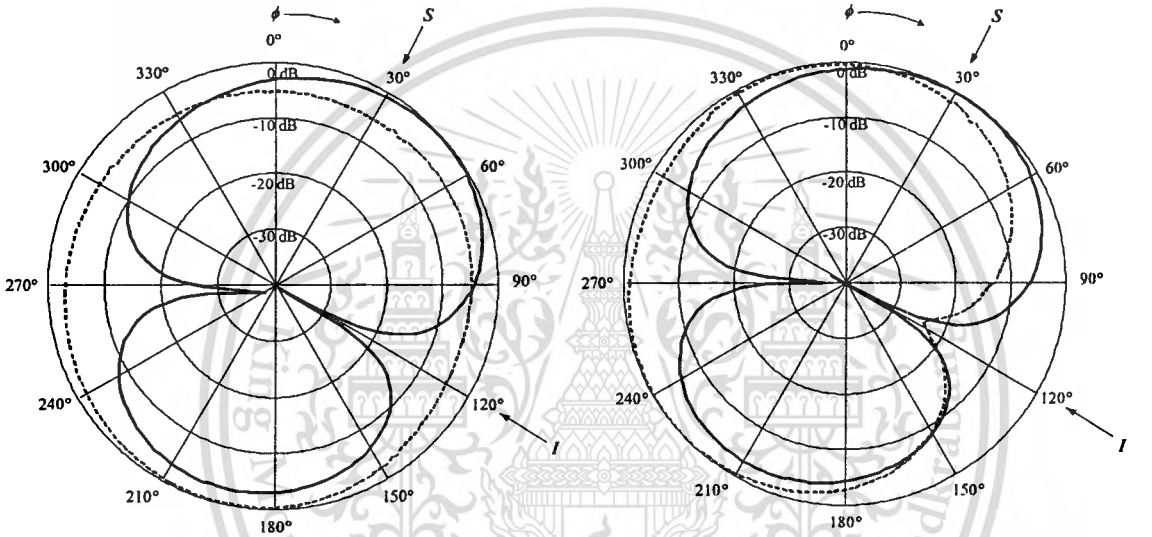

(a) (b)

Fig. 5.8 Radiation patterns after adaptation: (a) 500 iterations, (b) 1,000 iterations.
---- CMA, —— CMA with beam-switching initialization

5.4 Conclusion

This chapter has described the prospective applications of a phased array antenna of switched-beam elements for the future wireless communications systems. One of the envisaged applications concerns multiple-input multiple-output (MIMO) systems. The channel capacity of MIMO system using a phased array antenna of switched-beam elements has been investigated. It has been shown that the channel capacity of the switched-beam array antenna can substantially increase with the same number of antenna elements. The phased array antenna of switched-beam elements with various combinations of element patterns provides the channel capacity ranging from 14.0 to 17.0 bps/Hz at 20-dB SNR. The second application that has been described has concerned an

adaptive antenna system using the Constant Modulus Algorithm (CMA). In this case, the switched-beam array antenna has been applied to initiate the CMA adaptive algorithm so that the adaptive process can efficiently perform. The preliminary results have shown that the convergence rate is faster, i.e. the eye-pattern of signal constellation is opened after 500 iterations. The radiation patterns after adaptation have shown that the CMA algorithm can be improved with the beam-switching initialization.

CHAPTER 6
CONCLUSIONS AND DISCUSSIONS

The capability of a switched-beam antenna to eliminate the interference in the wireless communication systems can be improved by incorporating antenna elements with variable null pattern. The thesis has presented a new switched-beam antenna called a phased array antenna of switched-beam elements, which provides beam and null steering capability. It is a phased array antenna in which the main beam is switched using phase shifters, and switched-beam elements, two-beam switched elements, are applied as the array elements to change the null pattern.

Two types of switched-beam antennas, a switched-beam single patch antenna and a flat four-beam compact phased array antenna, have been presented in Chapter 2. They have been designed and developed to form the foundation to designing and developing a phased array antenna of switched-beam elements. The switched-beam single patch antenna has been proposed as the switched-beam element of the phased array antenna of switched-beam elements. The beam is switched using the PIN diodes to change the antenna operating modes between TM^{z}_{200} and TM^{z}_{020} modes. The corresponding beams are switched in azimuth directions. A flat four-beam compact phased array antenna has been designed to switch beam in four directions by using 1-bit phase shifters. Four directions of 45°, 135°, 225° and 315° have been selected in this design. In order to produce variable nulls these array incorporates single patch elements with two changeable beams.

Chapter 3 has presented the design and development steps of the phased array antenna of switched-beam elements and its simulated and measured characteristics. The developed phased array antenna of switched-beam elements shows the VSWR of less than 2:1 and radiation patterns with changeable null directions. There are 64 radiation patterns available.

Chapter 4 has shown the application of this array antenna to improve the quality of indoor wireless communication. The received signal improvement is described in terms of correlation coefficient and diversity gain. The minimum correlation coefficient of 0.37 is obtained, and the diversity gain of 8 dB is obtained when switched combining is applied under Ricean channel conditions. The performance in terms of signal-to-interference ratio improvement has also been investigated. The interference suppression

improvement is obtained by switching the beam of elements. In this way, the signal-to-interference ratio is improved more than 10 dB.

Chapter 5 addresses the prospective applications of a phased array antenna of switched-beam elements in future wireless communications systems. The antenna has been applied in the multiple-input multiple-output (MIMO) system to increase the channel capacity of the system. The channel capacity ranging from 14.0 to 17.0 bps/Hz at 20-dB SNR has been obtained using the phased array antenna of switched-beam elements with various combinations of element patterns. The advantage of using the switched beam antenna has also been demonstrated with respect to the CMA adaptive array antenna. It has been shown that the flat four-beam compact phased array antenna can improve the convergence rate of CMA algorithm by switching the beam and employing the maximum received signal of the switched-beam antenna as an initial value for CMA algorithm.

This thesis has presented the full design, development and test results of the phased array antenna of switched-beam elements. Its application has been demonstrated in a number of practical examples. However, there are many other interesting areas in which this antenna can be usefully applied. With respect to these new areas, further work may be required with regard to such issues as miniaturization of the antenna size and development of new signal processing algorithms and hardware.

REFERENCES

[1] N. Kuga and H. Arai, "A flat four-beam switched array antenna," *IEEE Trans. Antennas Propagat.*, vol. 44, no. 9, pp. 1272-1230, Sept. 1996.

[2] A. Sibille, C. Roblin, and G. Poncelet, "Circular switched monopole arrays for beam steering wireless communications," *Electron. Lett.*, vol. 33, no. 7, pp. 551-552, Mar. 1997

[3] J. Huang, "Planar microstrip Yagi array antenna," *Proceedings of the IEEE International Symposium on Antennas and Propagation and USNC/URSI Radio Science Meeting*, June 1989, vol. 2, pp. 894-897.

[4] D. Gray, J. W. Lu, and D. V. Thiel, "Electronically steerable Yagi-Uda microstrip patch antenna array," *IEEE Trans. Antennas Propagat.*, vol. 46, no. 5, pp. 605-608, May. 1998.

[5] S. L. Preston, D. V. Thiel, J. W. Lu, S. G. O'Keefe, and T. S. Bird, "Electronic beam steering using switched parasitic patch elements," *Electron. Lett.*, vol. 33, no. 1, pp. 7-8, Jan. 1997.

[6] R. G. Vaughan, "Switched parasitic elements for antenna diversity," *IEEE Trans. Antennas Propagat.*, vol. 47, no. 2, pp. 399-405, Feb. 1999.

[7] D. V. Thiel and S. Smith, *Switched Parasitic Antennas for Cellular Communications*. Norwood: Artech House, 2002.

[8] K. Gyoda and T. Ohira, "Design of electronically steerable passive array radiator (ESPAR) antennas," *Proceedings of the IEEE International Symposium on Antennas and Propagation and USNC/URSI Radio Science Meeting*, July 2000, vol. 2, pp. 922-925.

[9] N. C. Karmakar and M. E. Bialkowski, "A beam-forming network for a circular switched-beam phased array antenna," *IEEE Microwave Wireless Comp. Lett.*, vol. 11, no. 1, pp. 7-9, Jan. 2001.

[10] M. Krairiksh, P. Ngamjanyaporn, and C. Kessuwan, "A flat four-beam compact phased array antenna," *IEEE Microwave Wireless Comp. Lett.*, vol. 12, no. 5, pp. 184-186, May 2002.

[11] P. Ngamjanyaporn and M. Krairiksh, "Switched-beam single patch antenna," *Electron. Lett.*, vol. 38, no. 1, pp. 7-8, Jan. 2002.

[12] C. A. Balanis, *Antenna Theory: Analysis and Design*. 2nd ed. New York: John Wiley & Sons, 1997.

[13] C. A. Balanis, *Advanced Engineering Electromagnetics*. New York: John Wiley & Sons, 1997.

[14] J. Helszajn, *Microwave Engineering: Passive, Active and Non-Reciprocal Circuits*. Singapore: McGraw-Hill, 1992.

[15] http://www.semiconductors.philips.com/pip/BAP51-02.html

[16] *IE3D*, Zeland Software Inc.

[17] R. H. Clarke, "A statistical theory of mobile radio reception," *Bell Syst. Tech. J.*, vol. 47, pp. 957-1000, Jul.-Aug. 1968.

[18] W. C. Jakes, *Microwave Mobile Communications*. New Jersey: IEEE Press, 1994.

[19] A. A. Abu-Dayya and N. C. Beaulieu, "Switched diversity on microcellular Ricean channels," *IEEE Trans. Vehicular Tech.*, vol. 43, no. 4, pp. 970-976, Nov. 1994.

[20] J. P. V. Deursen and M. G. Jansen, "Switched antenna diversity within a DECT system." *Proceedings of the IEEE 2nd Symposium on Communications and Vehicular Technology*, 1994, pp. 141-148.

[21] P. Ngamjanyaporn, C. Phongcharoenpanich, P. Akkaraekthalin and M. Krairiksh, "Signal-to-interference ratio improvement by using a phased array antenna of switched-beam elements," *to be published in IEEE Trans. Antennas Propagat.*

[22] G. J. Foschini and M. J. Gans, "On limits of wireless communication in fading environments when using multiple antennas," *Wireless Personal Commun.*, vol. 6, pp. 311-335, 1998.

[23] T. Svantesson, "Correlation and channel capacity of MIMO systems employing multimode antennas," *IEEE Trans. Vehicular Tech.*, vol. 51, no. 6, pp. 1304-1312, Nov. 2002.

[24] P. Inthong, P. Ngamjanyaporn, C. Phongcharoenpanich and M. Krairiksh, "Simulation of channel capacity of MIMO communications system using switched beam antennas," *Proceedings of the 2003 International Symposium on Communications and Information Technology*, Sept. 2003, vol. 2, pp. 877-880.

[25] S. Haykin, *Unsupervised Adaptive Filtering*. New York: John Willey & Sons, 2000.

[26] D. N. Godard, "Self-recovering equalization and carrier tracking in two-dimensional data communication systems," *IEEE Trans. Commun.*, vol. 28, no. 11, pp. 1867-1875, Nov. 1980.

[27] A. Boonpoonga, P. Ngamjanyaporn, P. Sirisuk, C. Phongcharoenpanich and M. Krairiksh, "An adaptive phased array antenna using CMA and switched-beam initialization," *Proceedings of the first Electrical Engineering/Electronics, Computer, Telecommunications, and Information Technology (ECTI) Annual Conference*, May 2004, pp. 287-290.

RELATED PUBLICATIONS

1). P. Ngamjanyaporn and M. Krairiksh, "Switched-beam single patch antenna," *Electron. Lett.*, vol. 38, no. 1, pp. 7-8, Jan. 2002.

2). M. Krairiksh, P. Ngamjanyaporn, and C. Kessuwan, "A flat four-beam compact phased array antenna," *IEEE Microwave Wireless Comp. Lett.*, vol. 12, no. 5, pp. 184-186, May 2002.

3). P. Ngamjanyaporn, C. Phongcharoenpanich and M. Krairiksh, "Analysis of a flat compact phased array of switched-beam elements," *Proceedings of the Second International Symposium on Communications and Information Technology*, Oct. 2002, pp. 269-272.

4). P. Ngamjanyaporn, C. Phongcharoenpanich and M. Krairiksh, "A phased array antenna of switched-beam elements for wireless communications," *Proceedings of 2003 Asia-Pacific Microwave Conference*, Nov. 2003, pp. 941-944.

5). P. Ngamjanyaporn, C. Phongcharoenpanich, P. Akkaraekthalin and M. Krairiksh, "Signal-to-interference ratio improvement by using a phased array antenna of switched-beam elements," *to be published in IEEE Trans. Antennas Propagat.*

6). P. Ngamjanyaporn, M. Krairiksh and M. E. Bialkowski "Combating interference in an indoor wireless communication system with the use of a phased array antenna of switched-beam elements," *to appear in Microwave and Optical Technology Letters,* vol. 45, No. 5, June 2005 issue.

AUTHOR BIOGRAPHY

Phaisan Ngamjanyaporn was born on September 11, 1977 in Chonburi, Thailand. He received the B.Eng. degree in Telecommunications Engineering and the M.Eng. degree in Electrical Engineering from King Mongkut's Institute of Technology Ladkrabang, Bangkok, Thailand, in 1998 and 2001, respectively. Between 2002 and 2005 he was a Ph.D. student supported by a scholarship from the Thailand Research Fund through The Royal Golden Jubilee (RGJ) program. During the time period between September and November, 2004 he was a visiting scholar in the School of Information Technology and Electrical Engineering, the University of Queensland, Australia. His research interests concern antennas for mobile communication, phased array antennas and applications of microwaves.